Cervical Spine Segment Modeling at Traumatic Loading Levels for Injury Prediction

by

Jennifer Adrienne DeWit

A thesis

presented to the University of Waterloo

in fulfilment of the

thesis requirement for the degree of

Master of Applied Science

in

Mechanical Engineering

Waterloo, Ontario, Canada, 2012

AUTHOR'S DECLARATION

I hereby declare that I am the sole author of this thesis. This is a true copy of the thesis, including any required final revisions, as accepted by my examiners.

I understand that my thesis may be made electronically available to the public.

Abstract

Cervical spine injury can range from minor to severe or fatal, where severe injuries can result in incomplete or complete quadriplegia. There are close to 45,000 Canadians currently affected by paralysis due to traumatic spinal cord injury (tSCI) with an estimated 1700 new cases each year. The majority of tSCI occur in automotive collisions, and current methods for injury prediction are limited to predicting the likelihood for occupant injury but lack the detail to predict the specific injury and location at the tissue level. This research focused on major injuries associated with high impact automotive collisions such as rollover type collisions. Although whiplash is an injury commonly associated with automotive collisions, it was not considered for this study based on the low risk of neurological impairment. The goal of this study was to develop a cervical spine segment finite element model capable of predicting severe injuries such as ligament tears, disc failure, and bone fracture.

The segment models used in this study were developed from previous cervical spine segment models representative of a 50th percentile male. The segment models included the vertebrae, detailed representations of the disc annulus fibres and nucleus, and the associated ligaments. The original model was previously verified and validated under quasi-static loading conditions for physiological ranges of motion. To accomplish the objectives of this research, the original models were modified to include updated material properties with the ability to represent tissue damage corresponding to injuries. Additional verification of the model was required to verify that the new material properties provided a physically correct response.

Progressive failure was introduced in the ligament elements to produce a more biofidelic failure response and a tied contact between the vertebral bony endplates and the disc was used to represent disc avulsion. To represent the onset of bone fracture, a critical plastic strain failure criterion was implemented, and elements exceeding this criterion were eroded. The changes made to the material models were based on experimental studies and were not calibrated to produce a specific result. After verifying the modifications were implemented successfully, the models were validated against experimental segment failure tests. Modes

of loading investigated included tension, compression, flexion, extension and axial rotation. In each case, the simulated response of the segment was evaluated against the average failure load, displacement at failure, and the observed injuries reported in the experimental studies. Additionally, qualitative analysis of elevated stress locations in the model were compared to reported fracture sites. Overall, the simulations showed good agreement with the experimental failure values, and produced tissue failure that was representative of the observed tissue damage in the experimental tests.

The results of this research have provided a solid basis for cervical spine segment level injury prediction. Some limitations include the current implementation of bone fracture under compressive loads, and failure within the annulus fibrosus fibres of the disc should be investigated for future models. In addition to material model modifications, further investigation into the kinetics and kinematics of the upper cervical spine segment are important to better understand the complex interactions between the bone geometry and ligaments. This would give insight into the initial positioning and expected response in subsequent models. Future research will include integrating the current segment-level failure criteria into a full cervical spine model for the purpose of predicting severe cervical spine injury in simulated crash scenarios, with future applications in sports injury prevention and protective equipment.

Acknowledgements

Table of Contents

List of Figures

List of Tables

Chapter 1

Introduction

1.1   Motivation for Research

It is estimated that there are more than 1700 reported cases of traumatic spinal cord injury (tSCI) in Canada each year where motor vehicle accidents continue to be the leading cause (Farry and Baxter, 2010). It is important that research continue to focus on developments in injury prevention and occupant protection in the automotive industry, including understanding injury mechanisms and the ability to predict injuries. Etiological studies and reviews indicate that the highest incidence of injuries occurs at the upper and lower segments of the cervical spine (Cusick and Yoganandan, 2002). The injury severity ranges from minor to fatal, where severe injury cases may include spinal cord damage, and are often the result of multiple failures in both hard and soft tissues. Minor injuries could include whiplash, an injury commonly associated with automotive collisions, as well as singular damage to isolated areas of the cervical spine. Although whiplash is one of the most common injuries reported in automotive collisions, the focus of this study was on severe injuries with an associated higher risk of neurological impairment. Severe cervical spine injuries can result in complete or incomplete quadriplegia, seriously affecting the quality of life of the afflicted individual.

Automotive manufacturers are required to meet specific safety regulations mandated by the government, for example, the Canadian Motor Vehicle Safety Standards (CMVSS) in Canada and the Federal Motor Vehicle Safety Standards (FMVSS) in the United States. These guidelines require destructive crash tests to be carried out on each vehicle model to ensure the necessary safety standards are met. Anthropometric test dummies (ATD's) are used as human surrogates to evaluate the occupant response and have aided in the

development of many important safety devices. However, ATD's are limited in that they cannot predict local tissue response and injury. In addition, physical crash testing is expensive and time consuming. To address these limitations, advanced numerical modeling to simulate crash tests has been adopted by automotive manufacturers to help offset the cost of crash testing vehicles. There are limitations to what an ATD can predict during a crash test, and human volunteer testing must be kept to sub-injurious loads. Simplified numerical models have been used for several years but it has only been in recent years that there has been sufficient computing power to created detailed numerical models of humans that allow for developments in injury prediction.

From a developmental perspective, a numerical model must be validated for all injuries that may occur during a collision. Despite the fact that the incidence of severe cervical spine injury is relatively low compared to the incidence of severe injuries associated with the head and thorax, it is important that the model have the ability to predict all types of injury. The majority of numerical simulations regarding the cervical spine have been confined to quasi-static simulations to investigate the load-sharing behaviour of local tissue (Kumaresan et al. 1997; Teo and Ng, 2001; Ng et al. 2004; Panzer and Cronin, 2009). A small number of studies have used numerical simulations of full cervical spines to evaluate occupant injury risk during automotive collisions (Halldin et al. 2000; Meyer et al. 2004; Panzer, 2006), but these studies have been limited to low speed impacts and sub-catastrophic failure. To predict injury, it is important that the model be as biofidelic as possible and must include accurate geometry and material properties, as well as a variety of experimental data that can be used for model verification and validation.

1.2   Research Objective and Approach

The objective of this research was to develop a cervical spine segment finite element model capable of tissue level injury prediction. Using a fundamental approach, this research concentrated on developing both upper and lower cervical spine segment models capable of

predicting injuries under a variety of modes of loads. To accomplish this, segment models extracted from an existing cervical spine model were used as a starting point. The existing model was previously verified and validated under physiologic loads (Panzer, 2006; Panzer and Cronin, 2009), in frontal impact (Panzer et al. 2011), and in rear impact (Fice et al. 2011). This early research primarily focused on low level impacts and did not include catastrophic tissue damage. The original segment models required modifications to the material properties of bone, disc and ligaments enabling the representation of tissue damage. An iterative approach was used to verify that the individual tissues of the bone, disc and ligaments were capable of representing tissue damage associated with potential injuries. The changes made to the material models were based on experimental studies and were not calibrated to produce a specific result. Once the tissue models were verified, the models were then validated against experimental segment testing found in the literature. In keeping with a fundamental approach, the studies selected for validation were experiments that focused on testing cervical spine segments to failure under a single mode of loading. For each load case, the simulations were designed to replicate the load and boundary conditions of the experimental test and evaluated based on their response. All simulations were carried out as finite element analysis using the commercial code, LS-DYNA (LSTC, Livermore, CA) version 971 R3.1 using single precision calculations on a Linux workstation.

The goal of the simulations was to reproduce the results from the experimental tests including observed tissue damage as well as failure load and displacement. In all cases, the experimental failure values were reported as either an average value plus or minus a standard deviation (±SD), or an average value plus or minus a 95 percent confidence interval (95 % CI) that create a corridor where failure is most likely to occur. There are many variables that could affect the experimental corridors including but not limited to age, gender, condition and number of samples. Keeping this in mind, the experimental corridors were used as a guideline for the success of a simulation but were not the sole means of evaluation. Additional evaluation of the simulation was carried out by comparing the simulated tissue damage with the tissue damage reported experimentally, as well as

qualitative observations of areas of elevated stress in the simulation. Areas of elevated stress were compared to the location of reported injuries in the experimental tests as well as in clinical studies.

This approach of conducting verification and validation throughout the development of the model using material properties obtained from literature ensures that the model is diverse in its ability to predict injury under a variety of loading conditions. The ability of the segment model to predict injury under single modes of loading enables further investigation into combined loading scenarios. Additionally, future studies will be able to use the failure prediction methods developed for the segment model and apply them to a full cervical spine finite element model. The full cervical spine model can then be used to simulate larger scale tests to predict injury at the full cervical spine level.

1.3   Thesis Outline by Chapter

This thesis is organized to provide the reader with the necessary background to understand the process and the motivation behind this research. Chapter two focuses on the anatomy and physiology of the tissues of the cervical spine. It also introduces biomechanical terminology that will be used throughout the thesis to describe model features and development.

The focus of this thesis was to develop a cervical spine model capable of injury prediction. Chapter three is dedicated to describing cervical spine injury and the various areas of study surrounding the epidemiology and classification of injury. It also highlights key experimental studies important to the development of the numerical model for injury prediction.

Chapter four focuses on previous numerical models of spine segment models and the development of the model used in this research. There is a detailed description of the previously verified and validated cervical spine segment model developed by Matthew Panzer. The chapter continues with the modifications and enhancements made to the

previous model to represent injuries when subjected to a traumatic load. Each modification was discussed in detail to provide the reader with the motivation for the change as well as what injury each modification was intended to predict.

Once the modifications to the model were implemented, the new model underwent verification and validation against test cases to provide confidence in model accuracy. Chapter five goes through a detailed discussion of the experimental studies chosen to complete the validation and verification of the new model. It presents the results of the simulations for segment models of the upper and lower cervical spine followed by a discussion on how well the model performed as well as the current limitations.

The final chapter summarizes the work completed in this thesis while offering general conclusions and recommendations for future study.

Chapter 2

Anatomy and Physiology of the Cervical Spine

The following sections provide an overview of biomechanical terms and the anatomy of the cervical spine as it pertains to this research. Detailed anatomical descriptions of the features important to the segment models including the vertebral bodies, intervertebral disc, facet joints and ligaments are discussed. It should be noted that the musculature of the cervical spine has not been included as they were not investigated at the segment level. For a detailed description of the associated musculature, please refer to works by Fice (2010) and Panzer (2006).

2.1 Biomechanical Terminology

Anatomy refers to the structure of the cervical spine whereas physiology refers to the function of the components of the cervical spine anatomy. Function is not independent of anatomy. The following section describes the anatomy of the cervical spine and how the anatomical structures contribute to the overall function of the cervical spine.

To minimize the ambiguity when describing features of the body, anatomical terms are defined by dividing the human body into three planes; frontal, sagittal, and transverse (Fig. 2-1). The frontal plane divides the body into anterior and posterior sections. The sagittal plane separates the left and right sides of the body, and to describe features in this plane the terms medial (towards the midline) and lateral (away from the midline) are used. The transverse plane divides the body in to top and bottom sections. When describing features in the transverse plane, the terms superior (towards the head) and inferior (away from the head) are used. In addition to descriptors relating to the planes, other terms are used to describe anatomy.   The terms superficial (surface), intermediate (in between), and deep (below surface) are common injury descriptors.

6
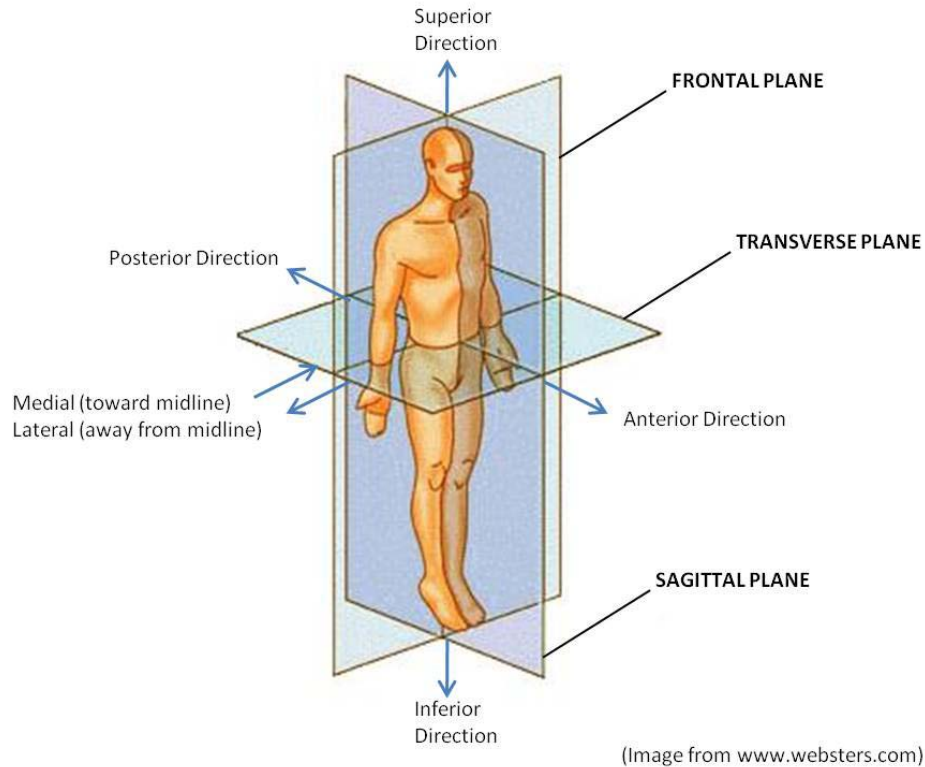
Figure 2 - 1: Anatomical Reference Planes and Directions

Specific anatomic terms related to the movement of the head and cervical spine are flexion, extension, axial rotation and lateral bending (Fig. 2-2). Flexion and extension are opposite motions describing the neck rotating about the lateral axis in the sagittal plane. Flexion can be thought of as "looking down" while extension can be thought of as "looking up." Axial rotation describes the motion of the neck as it rotates about the superior-inferior axis in the transverse plane, and can be visualized by thinking of a person looking over their left shoulder and then rotating their head to look over their right shoulder. Lateral bending refers to the motion of the neck as it rotates about the anterior-posterior axis in the transverse plane, or the action of bringing ones ear towards their shoulder on either side. Normal ranges of motion for the cervical spine in these motions are 40 – 60 degrees in flexion, 45 – 70 degrees in extension, 60 – 80 degrees in axial rotation and approximately 45 degrees in lateral bending.

FLEXION/EXTENSION   AXIAL ROTATION   LATERAL BENDING

(Images from www.howardnorthrup.com)
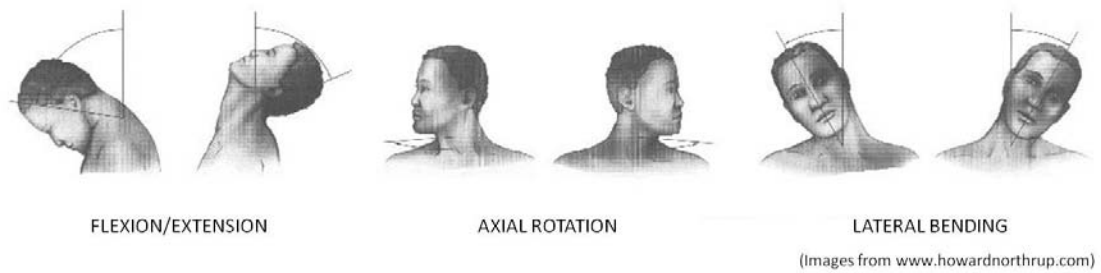
Figure 2 - 2: Head Ranges of Motion

2.2   Vertebrae

The human spinal column is composed of 26 bony structures called vertebrae. The column is subdivided into three regions (cervical, thoracic, and lumbar), as well as the sacrum and the coccyx (Fig. 2-3). The vertebral bodies in the spine are separated by intervertebral discs at each level beginning with the second vertebral body of the cervical spine down to the sacrum. The intervertebral discs create moveable joints between the vertebral bodies. The sacrum and coccyx are fused vertebrae forming one or two bones and are immovable. Before fusion, the total number of vertebrae in the spine totals 33 (Gray, 1918).
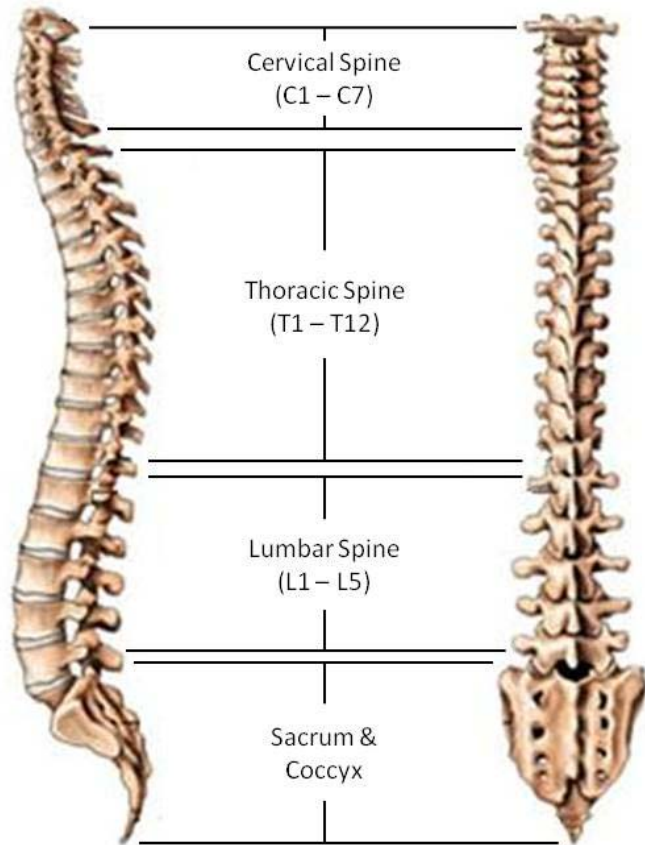
(Image from www.back.com)

Figure 2 - 3: Human Spinal Column Regions

The cervical spine is composed of seven vertebral bodies. It is also commonly divided into three regions (Fig. 2-4) including the upper (C1-C2), middle (C3-C5), and lower (C6-T1) cervical spine. The first thoracic vertebra is often included in cervical spine descriptions as it serves as the inferior attachment point for the C7 disc to form the lowest cervical spine joint.
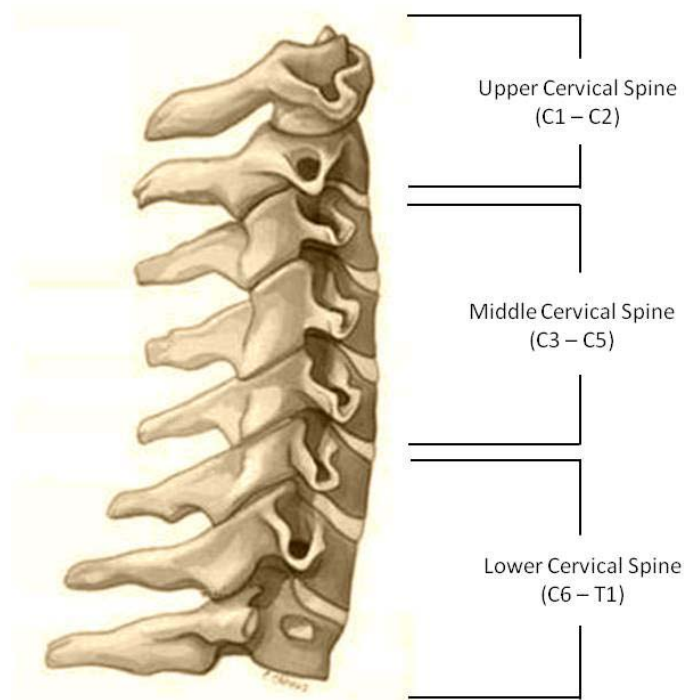
(Image from www. hughston.com)

Figure 2 - 4: Cervical Spine by Region

2.2.1 Vertebral Anatomy

The anatomy of the vertebrae from C2-C7 is very similar and can be thought of as having an anterior aspect and posterior aspect. The anterior aspect, or vertebral body, makes up the disc-shaped anterior portion of the vertebra and is the primary load bearing structure. The superior and inferior surfaces, or bony endplates, of the body serve as the attachment points for the intervertebral discs. The posterior aspect, or vertebral arch, is made up of the laminae, the pedicles, and seven processes. The pedicles extend posteromedially from the vertebral body and unite with the laminae to form the vertebral arch. Together with the posterior surface of the vertebral body, the vertebral foramen is created. The vertebral foramen of each vertebra forms the canal through which the spinal cord passes. The seven processes extending from the vertebral arch consist of four articular processes, two transverse processes and one spinous process. The four articular processes form joints with the adjacent vertebrae. The two inferior articular processes of the upper vertebra articulate with the two superior articular processes of the lower vertebra. These joints are referred to

10

as facets, or facet joints. The two transverse processes extend laterally from the intersection of the pedicle and lamina on either side of the vertebra while the spinous process extends posteriorly from the junction of the two laminae. These three processes function as muscle and ligament attachment points (Gray, 1918). These features are detailed in Fig. 2-5.

BODY
ANTERIOR TUBERCLE OF TRANSVERSE PROCESS
TRANSVERSE PROCESS
FORAMEN TRANSVERSARIUM
PEDICLE
POSTERIOR TUBERCLE OF TRANSVERS PROCESS
SUPERIOR ARTICULAR SURFACE
LAMINA
INFERIOR ARTICULAR SURFACE
SPINOUS PROCESS
VERTEBRAL FORAMEN

BODY
SUPERIOR ARTICULAR SURFACE
ARTICULAR PILLAR
SPINOUS PROCESS
ANTERIOR TUBERCLE OF TRANSVERSE PROCESS
POSTERIOR TUBERCLE OF TRANSVERSE PROCESS

(Images from www.ispub.com)

Figure 2 - 5: Lower Cervical Vertebrae Anatomy

The vertebrae of the upper cervical spine are unique to the rest of the vertebrae in the body (Fig. 2-6). The first cervical vertebra (C1) supports the head and is commonly called the atlas. It has the appearance of a ring of bone made up of anterior and posterior arches and large lateral masses on either side and does not have a vertebral body or a spinous process. The lateral masses form the superior articular surfaces that articulate with the occipital condyles of the head forming the atlanto-occipital joint. This joint enables the movement required in the action of nodding the head in a "yes" motion. The inferior surfaces of the lateral masses form the inferior articular surfaces that articulate with second cervical vertebra (C2). The second cervical vertebra is commonly called the axis. What makes this

vertebra unique is the protrusion of bone from the vertebral body called the dens, or odontoid process. The odontoid process passes through the vertebral foramen of the atlas to create a pivot for the head and atlas. This allows for side-to-side rotation as in the motion of the head that signifies "no." The joint formed between the atlas and odontoid process and between the articular surfaces of C1 and C2 is called the atlanto-axial joint (Gray, 1918).

ATLAS (C1)
SUPERIOR VIEW
INFERIOR VIEW

AXIS (C2)
ANTERIOR VIEW
POSTERIOR VIEW

ANTERIOR TUBERCLE
ANTERIOR ARCH
TRANSVERSE PROCESS
FORAMEN TRANSVERSARIUM
SUPERIOR FACET
POSTERIOR ARCH
POSTERIOR TUBERCLE
POSTERIOR ARCH
VERTEBRAL FORAMEN
LATERAL MASS
INFERIOR FACET
ARTICULAR FACET FOR ODONTOID PROCESS
ANTERIOR ARCH

ODONTOID PROCESS
ARTICULAR SURFACE FOR ARTICULAR FACET OF ATLAS
SUPERIOR FACET
PEDICLE
INFERIOR FACET
VERTEBRAL BODY
ARTICULAR SURFACE FOR TRANSVERSE LIGAMENT
VERTEBRAL BODY
TRANSVERSE PROCESS
FORAMEN TRANSVERSARIUM
LAMINA
SPINOUS PROCESS

(Images from www.spineuniverse.com)

Figure 2 - 6: Upper Cervical Vertebrae Anatomy

The bony structures of the vertebrae consist of a thin cortical bone shell surrounding a porous trabecular, or cancellous bone interior (Fig. 2-7). Relative to the other bones in the human body, the vertebrae are quite small. The vertebral bodies have a shape similar to an elliptical cylinder where the lateral width is slightly larger than the anterior-posterior depth. The lateral distance between the tips of the transverse process is slightly smaller than the distance from the anterior face of the vertebral body to the tip of the spinous process. The average height of the vertebral bodies is 14 mm with an elliptical cross-section of approximately 15 mm depth and 30 mm width (Panjabi et al. 1991b; Gilad and Nissan, 1986).The cortical bone thickness of the vertebral bodies and bony endplates are quite thin, ranging from 0.4 mm to 0.7 mm (Panjabi et al. 2001a). The cortical shell surrounding the

posterior elements of the cervical vertebrae is thicker than the cortical shell found on the vertebral bodies (Gray, 1918).

Cancellous Bone Core

Cortical Bone Shell

(Image from Gray, 1918)   Bony Endplate
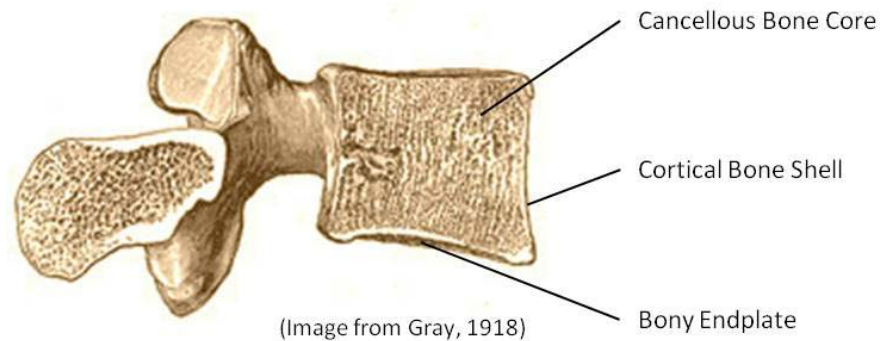
Figure 2 - 7: Vertebra Bony Structures

The trabecular bone contained within the cortical shell has a porous structure built up of vertical rods and columns supported by thinner horizontal trabeculae giving it a sponge-like appearance (Mosekilde et al. 1987; Kopperdahl and Keaveny, 1998). This architecture allows for strength in the primary loading direction (compression) with minimal bone mass (Cowin, 2001). Trabecular bone in the cervical spine has an apparent density between 0.1 g/cm^3 and 0.3 g/cm^3 (Kopperdahl and Keaveny, 1998), which is considerably less than the density of the trabecular bone in the other bones of the body (Keaveny et al. 2001). The porous space of the trabecular bone is filled with interstitial fluid, blood vessels, blood, marrow, nerve tissue and miscellaneous cells (Carter and Hayes, 1977).

2.2.2   Vertebral Function

The primary physiological loading on the cervical spine is axial compression where the majority of the load is transmitted through the trabecular bone (White and Panjabi, 1990). This differs from the rest of the bones in the body where the cortical bone bears more load. The compressive load is transmitted from the superior bony endplate of the vertebral body, through the trabecular bone or the cortical shell, to the inferior bony endplate. Because the thickness of the cortical bone is quite thin, the resulting cross-sectional area is relatively small so the majority of the load is transmitted through the trabecular bone (White and

Panjabi, 1990). Rockoff et al. (1969) showed that, in vertebrae 40 years old and younger, up to 55% of an applied compressive load was carried by the trabecular core.

The facet joints of the mid and lower cervical spine are also contributors in compressive load sharing offsetting the load borne by the vertebral body and intervertebral disc by approximately 10% under physiological loading (Goel and Clausen, 1998). The load carried by the facet joints increases under extension, axial rotation and lateral bending. As noted by Goel and Clausen (1998), the load sharing is increased to approximately 85%, 33% and 37% respectively for each mechanism. Under flexion loading, the facet joints are separated and bear no compressive load. The facets of the upper cervical spine bear 100% of the axial compressive load transferred from the head to the cervical spine.

2.3   Intervertebral Discs

The intervertebral discs are the most widely studied feature of the spine as it is the primary feature involved in spine mobility and often associated with spine injuries (White and Panjabi, 1990). The discs are a fibrocartilaginous structure that form strong joints between the vertebrae and absorb vertical shock (Fig. 2-8). Under compressive loads they compress and bulge from the intervertebral spacing.

INTERVERTEBRAL DISCS

VERTEBRAL BODIES

(Image from www.skillbuilders.patientsites.com)
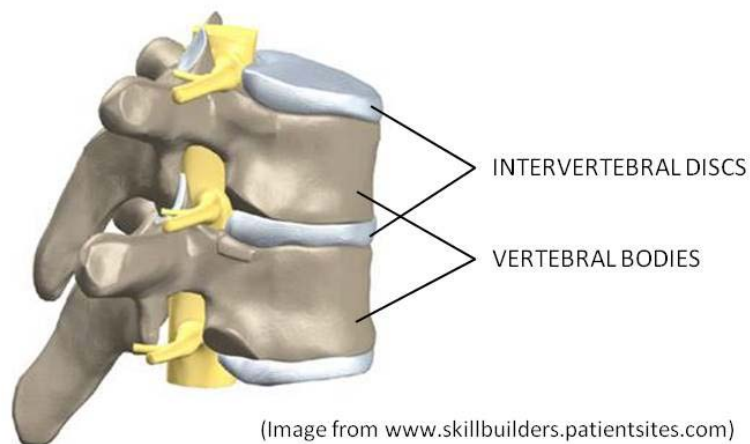
Figure 2 - 8: Intervertebral Disc between Adjacent Vertebral Bodies

14

2.3.1 Intervertebral Disc Anatomy

The intervertebral discs are made up of three distinct components, the annulus fibrosus, nucleus pulposus and the cartilaginous endplates. The annulus fibrosus is a set of concentric fibrous rings consisting of fibrocartilage that surround the nucleus pulposus and form the outer layer of the disc. The cartilaginous endplates are located on the superior and inferior surfaces of the disc, serving as attachment points for the annulus fibrosus and the bony endplates of the vertebral bodies.

The annulus fibrosus is a composite structure composed of collagen fibres within a gel-like substance called ground substance. The ground substance is a mixture of proteoglycans, water, and other proteins (Klisch and Lotz, 1999; Iatridis et al. 1998). The collagen fibres within the ground substance form concentric laminae. The fibre orientation between adjacent layers is offset by 90 degrees in each direction. Typically, fibre orientations in the adjacent layers near the outer lamina measure ±30 degrees from the transverse plane (Fig. 2-9) and gradually change to ± 45 degrees for the inner layers (Cassidy et al. 1989; Marchand and Ahmed, 1990; Wagner and Lotz, 2004; White and Panjabi, 1990). The type of collagen found in the annulus fibrosus vary from the outer laminae to the inner. A higher ratio of Type I collagen, the type found in ligaments, is found near the outer edges of the annulus fibrosus. Towards the inner layers of the laminae the collagen ratio changes to predominately Type II collagen which is a common building block of cartilage (Skaggs et al. 1994). The variation in collagen types is one of the primary propositions of the regional variation in the mechanical properties found in the annulus fibrosus.

(Image from Panzer, 2006)
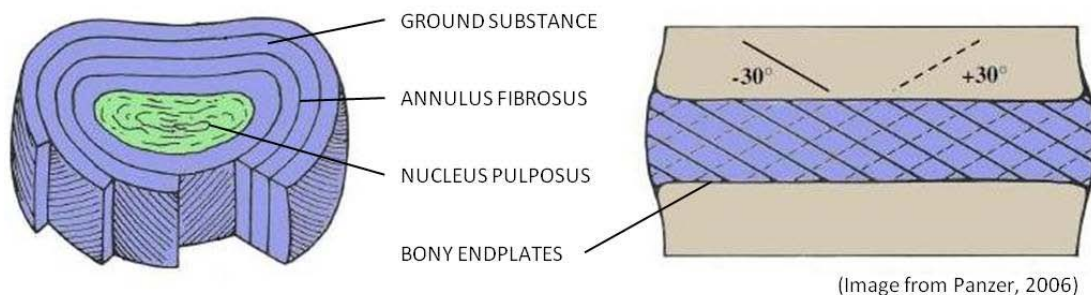
Figure 2 - 9: Intervertebral Disc Features

The nucleus pulposus is enclosed in the inner layers of the annulus fibrosus. It is made up of a loose matrix of proteoglycans and collagen. At birth, this matrix is approximately 90% water but decreases down to approximately 70% by the time a person is in their 50's (White and Panjabi, 1990; Iatridis et al. 1996). The high water content of the nucleus leads to the assumption that the tissue behaves similar to an enclosed fluid. The cartilaginous endplates bound the nucleus pulposus on its superior and inferior surfaces. As a person ages, the cartilaginous endplates calcify and, as a result, the fibres of the annulus fibrosus attach directly to the vertebral body via the bony endplates (Setton et al. 1993).

2.3.2 Intervertebral Disc Function

The majority of the physiological behaviour of the intervertebral disc is dependent on the annulus fibrosus tissue. Its composite structure and orientation guide the motions of the disc such that it functions as an intervertebral ligament (Bass et al. 2004). The intervertebral disc experiences a variety of loading, often subjecting the annulus to large, multidirectional loads (White and Panjabi, 1990). Because the annulus fibrosus lamina fibres considerably stiffer than those of the ground substance, they support the majority of the tensile stresses developed in the annulus (Iatridis and ap Gwynn, 2004; Pezowicz et al. 2005).

The presence of a healthy nucleus also contributes to the overall function of the intervertebral disc (White and Panjabi, 1990). It has been shown that the inner layers of the annulus fibrosus bulge inward in the absence of the nucleus due to a lack of internal pressure. The lack of internal pressure increases the shear stress between the lamina increasing the risk for disc injury (Meakin et al. 2001). An unhealthy or degenerated nucleus pulposus occurs with a decrease in water content over time. This degeneration affects the mobility of the spine and can increase the risk of spine injury (Ng et al. 2004).

The interactions between the nucleus pulposus and the annulus fibrosus are responsible for the function of the intervertebral disc under physiological loading. When loaded in compression, the disc experiences and increase in hydrostatic pressure and pushes against the inner layers of the annulus fibrosus (Fig. 2-10). This causes the layers to bulge in a radial

direction around the disc loading the fibres in tension (Holzapfel et al. 2005). The alternating fibre orientations of each lamina result in biaxial tension through the annulus fibrosus fibres. This behaviour resembles that of a pressure vessel where the annulus is the pressure vessel and the nucleus is the fluid or gas contained within the vessel (White and Panjabi, 1990).

(Image from Panzer, 2006)
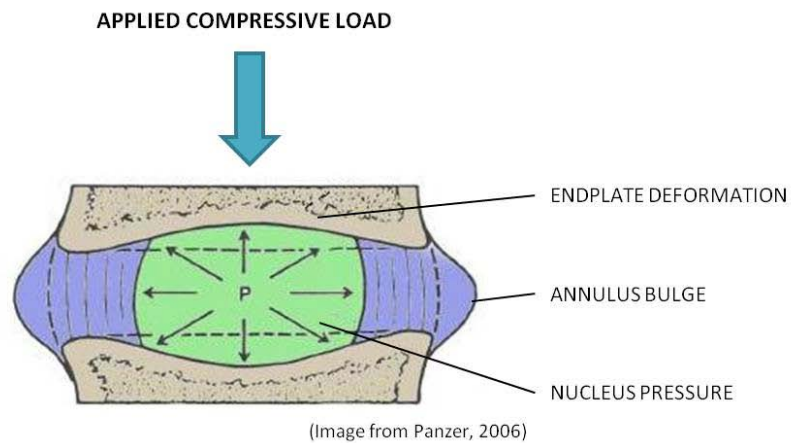
Figure 2 - 10: Intervertebral Disc Response under Compressive Load

Under bending loads the nucleus functions as a pivot for the vertebral body to rotate (White and Panjabi, 1990). For example, in flexion the vertebral body will pivot around the nucleus to induce a tensile load in the posterior section of the disc and a compressive load in the anterior section of the disc (Fig. 2-11). In both cases the annulus fibres are supporting a tensile load.

(Image from Panzer, 2006)
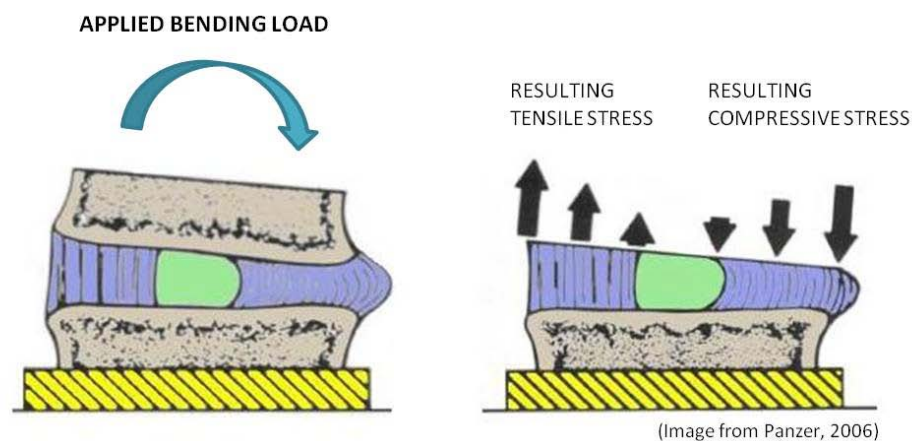
Figure 2 - 11: Intervertebral Disc Response under Bending Load

17

In axial tension, the annulus fibrosus support the entire tensile load since the nucleus pulposus behaves like a liquid. The orientations of the annular fibres are oriented away from the primary load direction, thus the resulting stiffness of the disc is lower in tension than in compression. Similarly, in axial torsion, only half of the fibres have the ability to support load while the others are in tension resulting in a low torsional strength in the disc.

2.4   Facet Joints

2.4.1   Facet Joints Anatomy

The facet joints are synovial joints formed between the articulating surfaces of adjacent vertebrae. A synovial joint is made up of cartilage, synovial fluid, and a synovial membrane (Fig. 2-12). The articular cartilage on the facets is an extremely strong yet elastic cartilage called hyaline cartilage. This forms the smooth, articulating surface of the joint. The synovial fluid is a viscous fluid made up of hyaluronic acid (Fung, 1993) that lubricates the joint allowing for smooth, low-friction motion. It also provides nutrients to the articular cartilage. The synovial fluid is contained within the joint by the synovial membrane, a dense connective tissue that surrounds the joint and secretes synovial fluid. In the cervical spine, the synovial membrane is surrounded by the capsular ligament providing strength in tension.
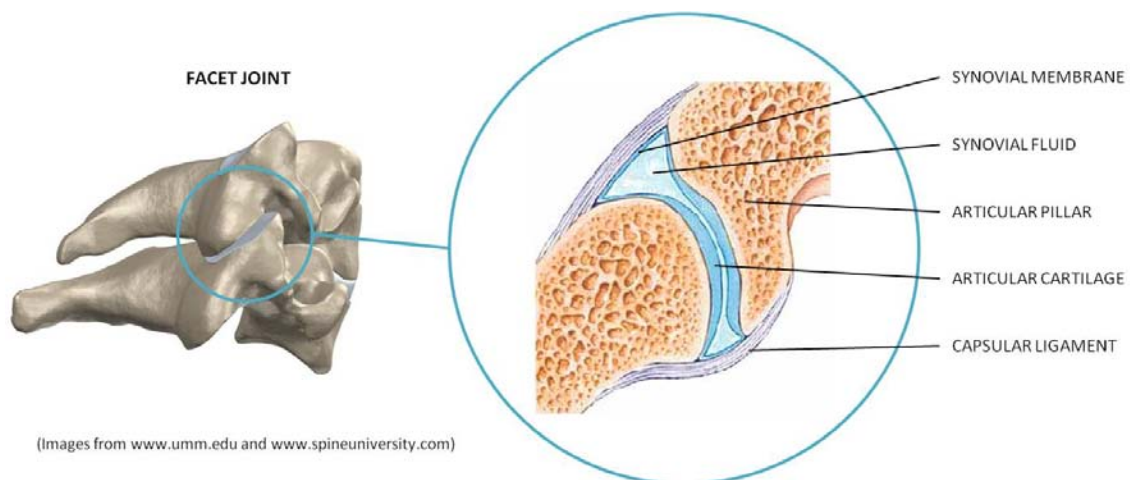
Figure 2 - 12: Facet Joint Anatomy

18

The facet joint surfaces are elliptical in shape with the lateral measurement slightly larger than the anterior-posterior measurement. The facets of the cervical spine are commonly oriented in the posterolateral direction. The average plane of their surfaces forms an angle between 30 and 65 degrees to the transverse plane and 0 to 15degrees to the sagittal plane (Panjabi et al. 1993; Pal et al. 2001).

2.4.2 Facet Joint Function

The facet joints of the cervical spine bear a significant amount of the compressive load acting on the spine (Goel and Clausen, 1998). Goel and Clausen, (1998) observed the load borne by the facet joints increased approximately 51% with the inclusion of extension to the load mechanism. Increases were also observed in one facet joint under lateral bending and axial rotation. In addition to the load bearing requirements of the facet joints, they also assist in controlling primary and secondary movements of the cervical spine (Boduk and Mercer, 2000). Axial rotation and lateral bending are a coupled motion in the facet joints (Boduk and Mercer, 2000). As the joint is axially rotated, the superior articular surface of the facet joint tracks up the inferior articular surface inducing lateral bending. Similarly, when undergoing lateral bending, the superior articular surface of the compressed facet joint tracks downwards and posteriorly inducing a rotation between the vertebrae.

2.5 Ligaments

2.5.1 Ligaments Anatomy

Ligaments are fibrous bands of tissue that connect bones to form joints. They are made up of Type I collagen and elastin, and support the joint under tensile loading along the fibre direction (Myklebust et al. 1988; Yoganandan et al. 2001).The ligaments of the middle and lower cervical spine are similar in structure to the ligaments found throughout the entire spine. The main ligament groups consist of the longitudinal ligaments, the accessory elements, and the capsular ligaments (Fig. 2-13).

The longitudinal ligaments consist of the anterior longitudinal ligament (ALL) and the posterior longitudinal (PLL). The ALL is a strong, continuous band of fibres extending along

the anterior surface of the vertebral body from the C2 (axis) down the length of the entire cervical spine. It has attachment points on each vertebral body and supports the intervertebral discs. The PLL extends through the vertebral canal along the posterior surface of the vertebral bodies. Similar to the ALL, it begins at the C2 and extends continuously along the full spine attaching to vertebral bodies and supporting the intervertebral discs.

The accessory ligaments include the ligamenta flava (LF), the interspinous ligament (ISL), and the nuchal ligament (NL). The LF connects the lamina of two adjacent vertebrae. They are a thin, wide band of tissue that form the posterior wall of the vertebral canal, and are present from the C2-C3 vertebral joint down the length of the spine. There are two portions to the LF each beginning on either side of the roots of the articular processes. They each follow along their respective lamina until it reaches the point where the lamina meets to form the spinous process. The ISL is a thin, weak ligament connecting the spinous processes of adjacent vertebral bodies. It extends the full length of the spinous process, meeting with the LF in the anterior and the NL at the posterior. The NL is found only on the cervical spine and is similar to the supraspinous ligament found on the thoracic and lumbar spines (Cross, 2003). It is a thick, fibroelastic membrane extending from the occipital protuberance on the skull to the spinous process of C7. There are attachment points for the NL on the spinous processes of each cervical vertebra up to C1 (atlas). Inferiorly, it is connected to the supraspinous ligament and to the ISL along the full length of the spinal column.

The last ligament group of the middle and lower cervical spine are the capsular ligaments (CL). The CL surrounds the facet joint attaching to the margins of the articular processes of adjacent vertebra providing stability to the facet joints.

Figure 2 - 13 diagram labels:

LIGAMENTA FLAVA (LF)

CAPSULAR LIGAMENT (CL)

INTERSPINOUS LIGAMENT (ISL)

POSTERIOR LONGITUDINAL LIGAMENT (PLL)

ANTERIOR LONGITUDINAL LIGAMENT (ALL)

(Image from www.spineuniverse.com)
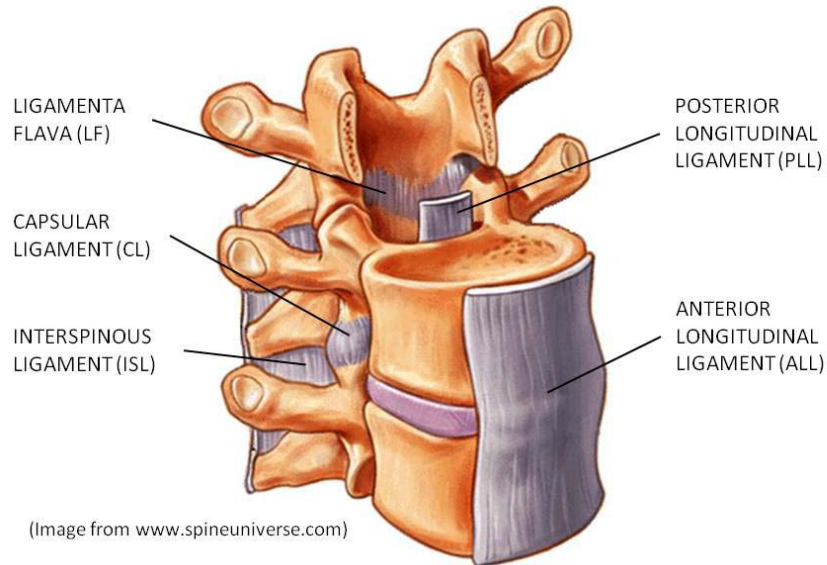
Figure 2 - 13: Ligaments of the Lower Cervical Spine

The upper cervical spine contains some of the same ligaments as the mid and lower cervical spine, but has additional unique groups of ligaments used in supporting the head and upper cervical spine. The upper cervical spine ligaments used to connect the atlas to the occipital bone are called the atlanto-occipital ligaments. Ligaments in this group consist of the anterior and posterior atlanto-occipital membranes, as wells as the capsular ligaments associated with the atlanto-occipital joints. The anterior atlanto-occipital membrane (AAOM) is a broad ligament attached the full length of the anterior arches of the atlas and extends to the anterior margins of the foramen magnum. The AAOM is reinforced down the middle by a strong, round cord attached at the basilar process of the occipital bone extending down to the anterior process of the anterior arch of the atlas (Gray, 1918). The posterior atlanto-occipital membrane (PAOM) is a broad ligament inserting at the posterior margins of the foramen magnum and extending to the medial part of the posterior arch of the atlas. When compared to the AAOM, the PAOM is a much weaker ligament (Gray, 1918). The capsular ligaments of the atlanto-occipital capsules surround the occipital condyles connecting them to the articular surfaces of the atlas with a thin loose membrane enclosing the synovial membrane of the joint (Gray, 1918).

The second group of unique ligaments in the upper cervical spine providing support for the relative movement between the atlas and the axis are the atlanto-axial ligaments. These ligaments include the transverse ligament (TL), the anterior and posterior atlanto-axial membranes (AAAM, PAAM), and the capsular ligaments. The TL is a thick, strong band that reaches across the ring of the atlas attaching on either side to the inner surface of the lateral masses. The TL is the largest and strongest ligament in the cervical spine (Panjabi et al. 1998), and serves to keep the odontoid process in contact with the anterior arch of the atlas. The area of the TL in contact with the posterior surface of the odontoid is broader and thicker than at the attachment points on either side (Gray, 1918). In addition to the TL, there are some smaller ligaments that support and stabilize the odontoid. From the middle of the TL where it crosses the odontoid, a small longitudinal band (superior crux) runs up from the upper edge posterior surface of the TL and inserts into the basilar process of the occipital bone. Similarly, a band (inferior crux) extends downward from the lower edge of the posterior surface of the TL attaching at the base of the odontoid process. These small longitudinal ligaments are closely situated along the tectorial membrane. The crossing of the longitudinal and transverse ligaments is known as the cruciate ligament of the atlas (Gray, 1918).

The AAAM and PAAM are similar to the AAOM and the PAOM of the atlanto-occipital ligaments. The AAAM is a continuation of the ALL in the mid and lower cervical spine. It is attached superiorly to the inferior edge of the anterior arch of the atlas, and inferiorly to the base of the odontoid process and the axis body. Similarly to the AAOM, there is a thick cord down the midline of the AAAM that provides additional strength the ligament. The PAAM is similar to the LF of the middle and lower cervical spine. It is attached to the lower edge of the posterior arch of the atlas and extends down to the upper edge of the lamina of the axis (Fig. 2-14).

The capsular ligaments between the atlas and the axis are similar to the other articular capsular ligaments. They surround the synovial membrane providing strength and stability to the joints.
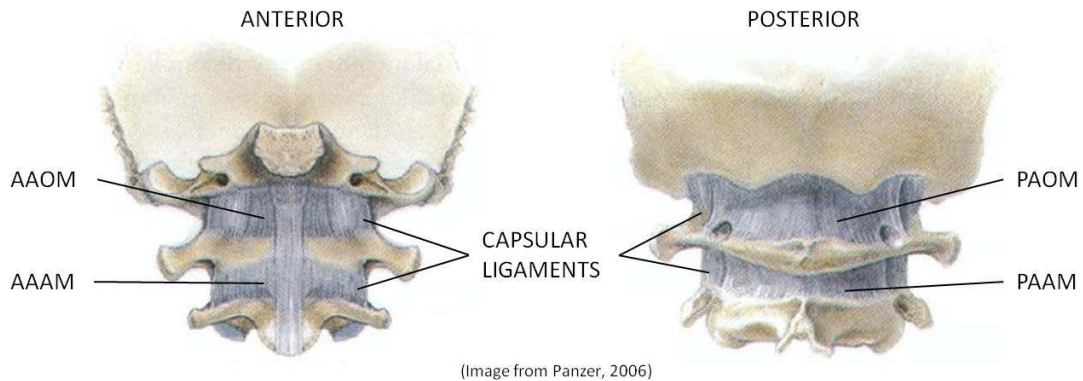
Figure 2 - 14: Outer Ligaments of the Upper Cervical Spine

The last group of ligaments unique to the upper cervical spine attaches the axis to the occipital bone (Fig. 2-15). These ligaments further stabilize the occipital-atlanto-axial complex under flexion, extension and axial rotation. The ligaments in this group are the tectorial membrane, the alar ligaments, and the apical odontoid ligament. The tectorial membrane (TM) has a similar anatomical position to the PLL found on the mid and lower cervical spine. Running through the vertebral canal, it inserts superiorly through the foramen magnum into the basilar groove of the occipital bone and attaches inferiorly to the posterior surface of the axis body covering the TL and its associated ligaments. The alar ligaments extend from either side of the odontoid process and attach to the medial sides of the occipital condyles, and the apical odontoid ligament extends from the tip of the odontoid process to the anterior margin of the foramen magnum (Gray, 1918).

APICAL
(not pictured)

UPPER CRUX

TL (cut)

LOWER CRUX

CAPSULAR
LIGAMENT

ALARS

TM (cut)

(Image from Panzer, 2006)
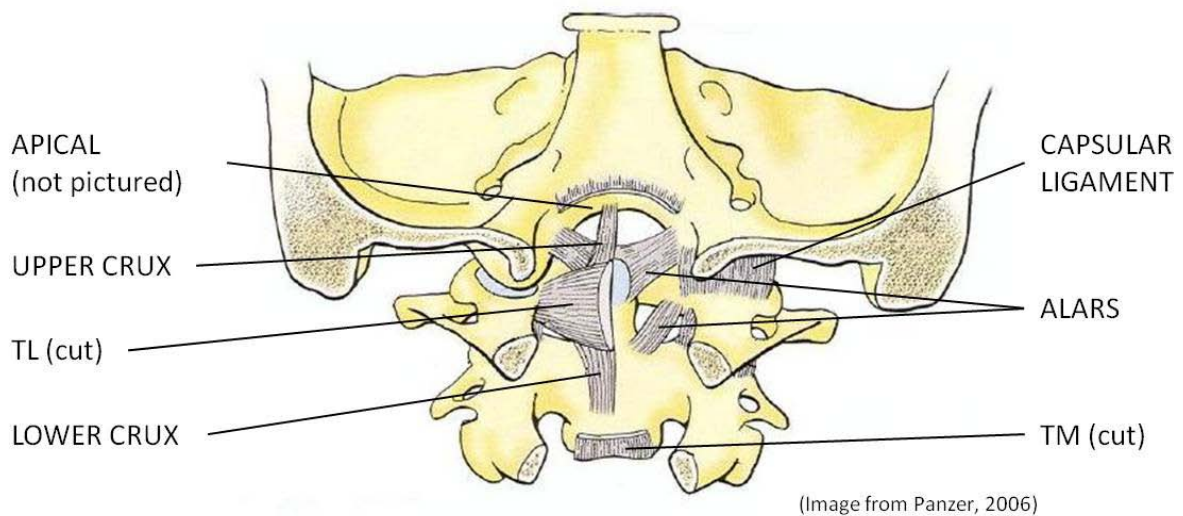
Figure 2 - 15: Internal Ligaments of the Upper Cervical Spine

2.5.2   Ligament Function

The primary function of a ligament is to provide joint stability by resisting or restricting its motion (White and Panjabi, 1990). In the cervical spine, ligaments connecting the vertebral bodies limit the mobility of the spine, particularly motion in the sagittal plane. Additionally, the ligaments provide resistance and stability under external tensile loading.

Through the different modes of loading, certain ligaments engage more than others. As mentioned above, the intervertebral discs serve as a pivot point for the vertebral bodies. When the vertebral bodies undergo an external flexion load, the ligaments in the posterior section of the vertebrae (PLL, LF, ISL and CL) engage to provide support and stability. Similarly, when loaded in extension, ligaments in the anterior portion (ALL) provide the support. The ability of each ligament to resist load is dependent on their relative stiffness and proximity to the pivot. For example, the ALL and PLL are significantly stiffer than the LF and ISL but based on their relatively close proximity to the pivot point, their contribution to overall joint stiffness in a bending load is minimal.

In the upper cervical spine, the ligaments constrain the motion of the head. Combined with the anatomy of the atlas and axis, the alars and transverse ligament provide the primary stability for the head to nod, rotate, and tilt (Gray, 1918; Panjabi et al. 1998). The alars are the

primary constraint in rotation (Panjabi et al. 1991a) with secondary support provided by the TM, AAAM, and the capsular ligaments (Dvorak and Panjabi, 1987). Smaller roles in maintaining stability are played by the atlanto-occipital ligaments. The AAOM resists the motion of extension, or "looking up", while the PAOM resists the motion of flexion, or "looking down." The TL functions to hold the odontoid process against the atlas minimizing translation, but still allowing for smooth rotation between the atlas and axis (Panjabi et al. 1998).

Chapter 3

Injury and Biomechanics of the Cervical Spine

The overall objective of injury biomechanics is to gain a better understanding of injury mechanisms and develop approaches to minimize or avoid functional or structural damages to the area of impact (Viano et al. 1989). The human body sustains an injury when a biological tissue is deformed beyond physiological limits, affecting the biomechanical properties or physiological function of that tissue. Injuries result in the loss of function of the associated tissue, where the severity and extent of the loss depends on the injury type. The type of injury incurred can vary based on the size and shape of the impacting object, as well as the rate at which the impact occurs (Viano et al. 1989).

Injuries to the cervical spine can result from impacts to the head and neck where injury severity can range from minor to fatal. Minor injuries include sprains and strains to the soft tissue as well as isolated fractures to a single area. Severe injury cases may include spinal cord damage which could result in complete or incomplete quadriplegia. These injuries are classified based on the loading scenario or a specific loading condition (Cusick and Yoganandan, 2002). The primary focus of this research was to develop a segment level numerical model that could predict severe cervical spine injuries. The following section provides an epidemiological review of major cervical spine injuries and how they are classified. Additionally, it contains a review of biomechanical studies investigating the mechanical response of cervical spine segments under various loading conditions.

3.1   Epidemiology of Cervical Spine Injuries

Injuries to the cervical spine are often associated with a high risk of disability or fatality. It is estimated that over 1700 new traumatic spinal cord injuries (tSCI) are reported each year in Canada adding to the nearly 45,000 Canadians currently affected by paralysis due to tSCI

(Farry and Baxter, 2010). Etiological studies and reviews indicate that the majority of cervical spine injuries occur in motor vehicle accidents (MVA), causing 40 – 65% of all spine traumas (Yoganandan et al. 1989b). The cervical spine was the most commonly injured spine area in automotive collisions accounting for 50.7% of all spine injuries (Robertson et al. 2002). For serious spine injuries of AIS 3 or greater, the cervical spine was the primary injury site (Fig. 3-1) with the highest incidences of injuries occurring at the upper and lower segments of the cervical spine (Yoganandan et al. 1989b; Cusick and Yoganandan, 2002). Note that various injury classifications including the Abbreviated Injury Scale (AIS) are further discussed in section 3.2.

- Thoracic Spine - 31%
- Cervical Spine - 44%
- Thoracic Cord - 1%
- Cervical Cord - 14%
- Cervical Respiratory - 5%
- Other - 5%

(Reproduced from Yoganandan et al. 1989b)
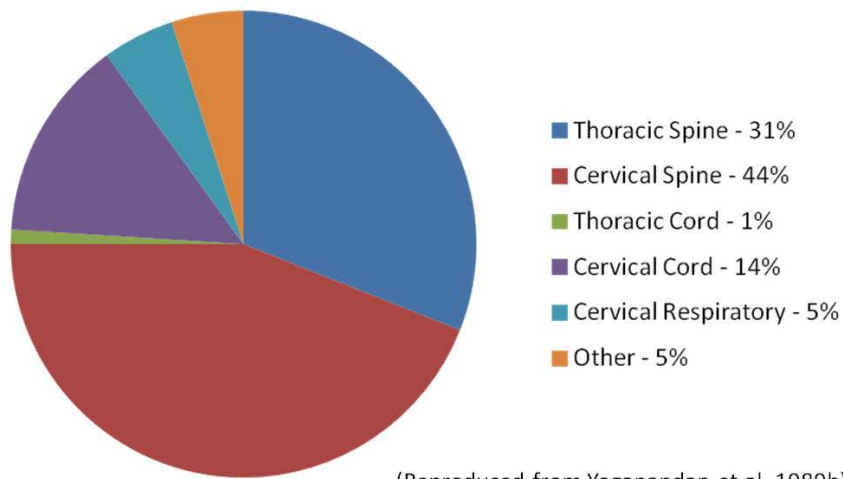
Figure 3 - 1: Distribution of AIS 3+ Injuries to the Spine from MVA

The type and severity of cervical spine injury is dependent on the type of MVA. Minor injuries, such as soft tissue injuries like whiplash, have the highest incidence of injury in rear impact collisions (Yoganandan et al. 1989b), while severe cervical spine injuries are much more likely to occur in a rollover type collision (Fig. 3-2, & Fig. 3-3). Even though the overall incidence for severe cervical spine injury is relatively low, it is still important to consider as the outcome to the individual could have a significant impact on their quality of life, especially in an injury resulting in complete or incomplete quadriplegia.
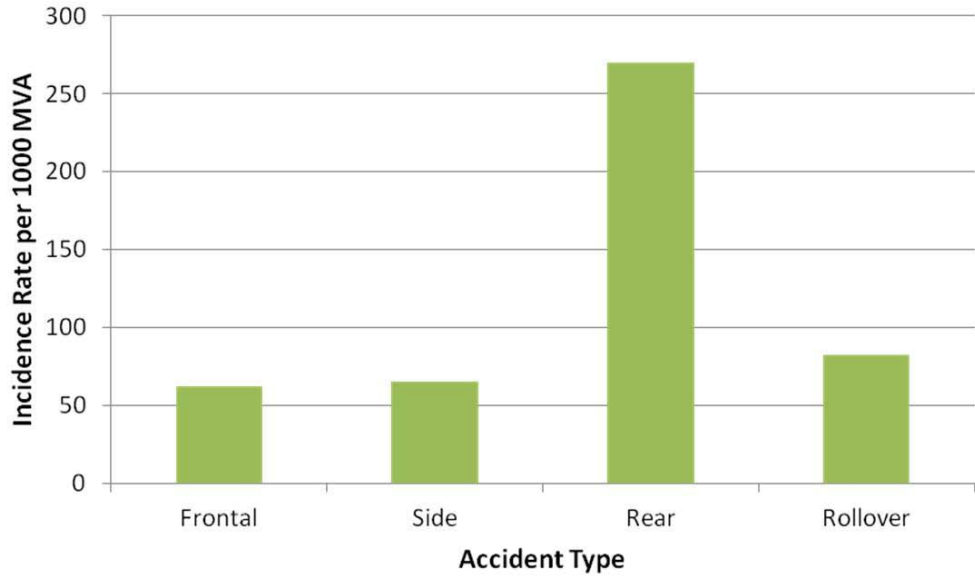
(Reproduced from Yoganandan et al. 1989b)

Figure 3 - 2: Incidence Rates per 1000 MVA by Collision Type for AIS 1 (Minor) Injury
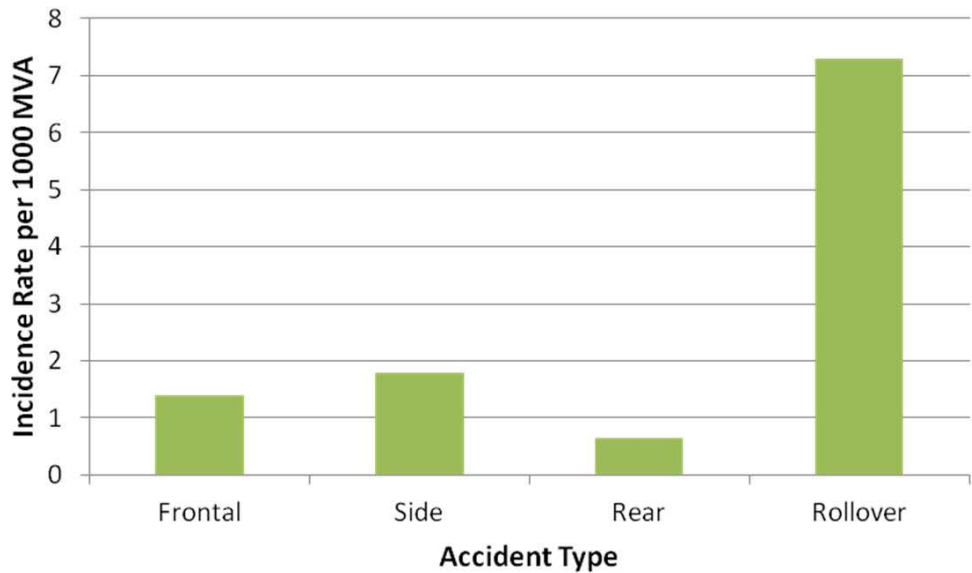
(Reproduced from Yoganandan et al. 1989b)

Figure 3 - 3: Incidence Rates per 1000 MVA by Collision Type for AIS 3+ (Major) Injury

The type of injury incurred is dependent on the applied loading scenario. Severe injuries AIS 3+ are most often associated with high impact scenarios such as those seen in high speed automotive collisions involving rollovers. Upper segment injuries are directly related

to the direction of the skull contact forces at the skull-atlanto-occipital junction while lower segment injuries are caused by forces directly applied to the vertebral body or through a lever arm of several adjacent segments (Cusick and Yoganandan, 2002). Similar conclusions were reached in studies by Robertson et al. (2002), and Daffner et al. (2006) showing a distribution of fractures at each vertebral level with the majority of fractures occurring in the upper and lower segments (Fig. 3-4). Robertson et al. (2002), conducted a review of car and motorcycle accidents finding that the most commonly injured spine region a in a car accident is the cervical spine (50.7%) while in a motorcycle accident, the cervical spine is the least commonly injured spinal region (17.4%). In a two year review of admitted trauma patients, Daffner et al. (2006) found that 297 of the admitted patients sustained fractures to the cervical spine. In a total of 309 observed fractures, it was found that the highest incidence of fracture was occurred at C2 and C7 with 30.1% and 20.1% of the total fractures respectively.
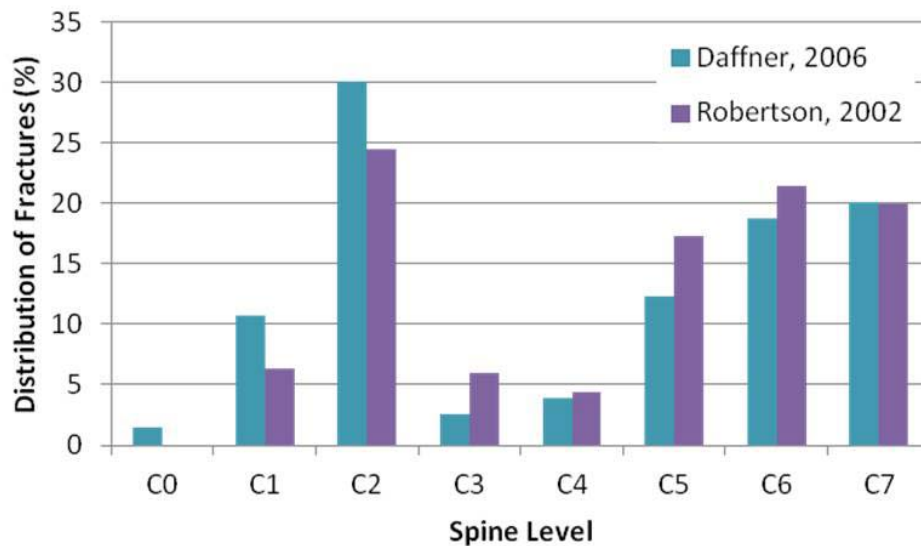
(Reproduced from Robertson et al. 2002; Daffner et al. 2006)

Figure 3 - 4: Clinical Observations of Fractures by Spine Level

Yoganandan et al. (1989b) conducted a clinical study to determine the most commonly injured anatomical area during motor vehicle accidents and relate the injury locations to the level of impairment. The findings from this study also highlight the high incidence of injury

occurring in the upper and lower cervical spine. The results showed that, in the upper cervical spine, injuries ranged from minor to fatal with the majority being minor (Fig. 3-5), whereas injuries to the lower cervical spine had the highest level of complete and incomplete quadriplegia, specifically at the C5-C6 segment level (Fig. 3-6). Additional studies by Burney et al. (1993), Myers and Winkelstein, (1995), and Riggins et al. (1977) also recognized that vertebral fractures have a high probability of leading to significant neurological impairment. The injuries most common at the segment level are compression-flexion injuries and burst (comminuted) fractures of the vertebral bodies.
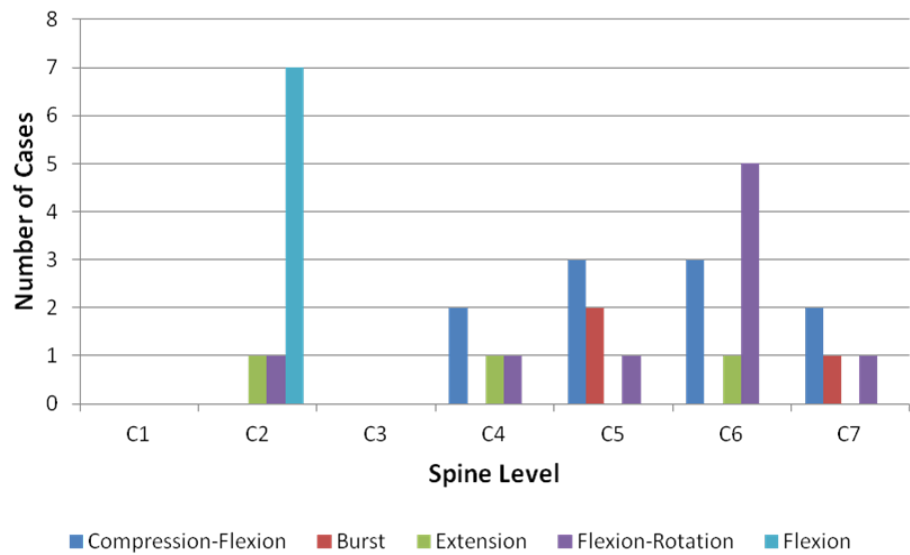
(Reproduced from Yoganandan et al. 1989b)

Figure 3 - 5: Cases of Minor Injury by Spine Level
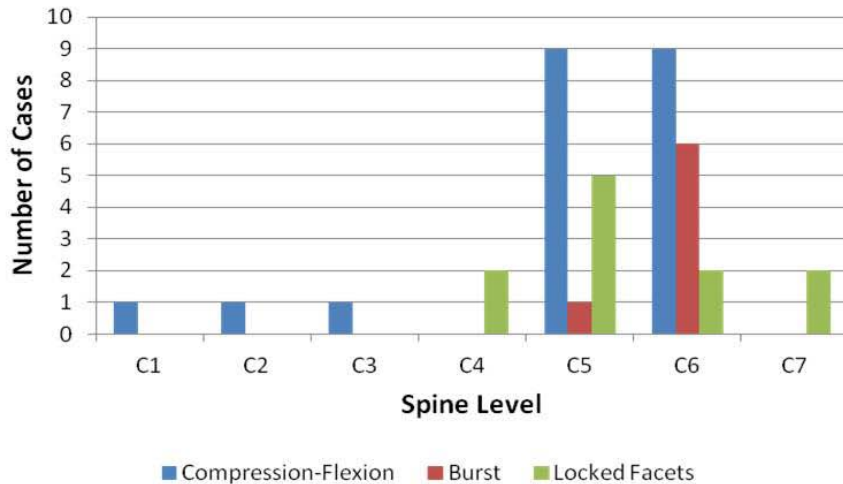
(A)
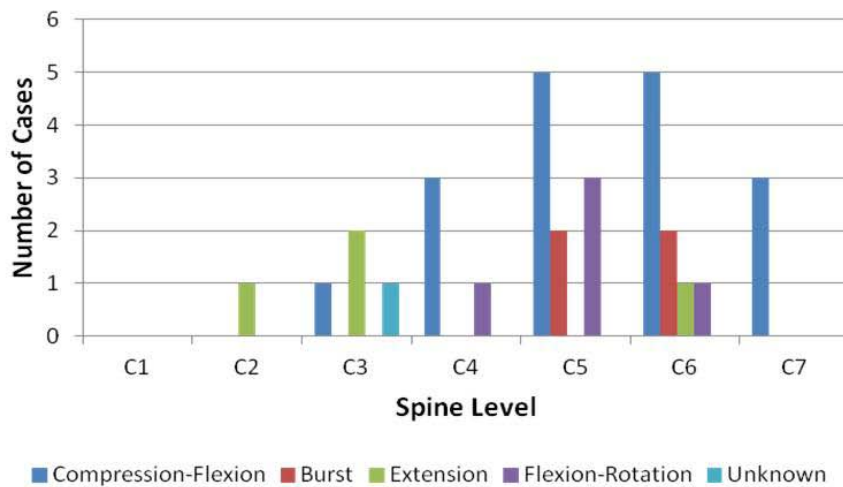
(B)   (Reproduced from Yoganandan et al. 1989b)

Figure 3 - 6: Cases of Complete (A) and Incomplete (B) Quadriplegia by Spine Level

In a similar review study of lower cervical spine trauma cases, Argenson et al. (1997), found that 33% of the reported trauma cases were compression injuries, 28% were flexion-extension injuries, and 39% were rotation injuries. It should be noted that although there is a high frequency of rotation injuries, they are generally associated with lower severity. To put this in perspective, 51% of the rotation injuries were considered the least severe (unifacet fracture) based on injury mechanism, whereas 70% of the compressive injuries were considered to be the most severe (tear-drop fracture) based on mechanism. Also, 50% of the

flexion-extension injuries were among the second most severe injury type (severe sprain). Tension loading scenarios such as airbag deployment could result in a load to the cervical spine in out-of-position occupants resulting in serious injury (Blacksin, 1993; Traynelis and Gold, 1993; Kleinberger and Summers, 1997; Sato et al. 2002).

3.2   Injury Classification

Injury classification of cervical spine injury mechanisms is an important resource for linking epidemiological, clinical and biomechanical research. In a review of major cervical spine injuries, Cusick and Yoganandan, (2002) investigated injury classification based on correlating certain biomechanical parameters and clinical factors associated with the cause and occurrence of traumatic cervical spine injuries. Developing a classification of injury patterns for major cervical spine injuries can vary widely based on different interpretations of biomechanical studies, mitigating circumstances such as predisposition to injury, as well as clinical limitations defining injury patterns. During the review process, Cusick and Yoganandan, (2002), put forth a table of mechanistic factors that could potentially influence injury type (Table 3-1) where the authors acknowledge the following table to not be totally inclusive of all injury mechanisms related to cervical spine injury. Further discussion also considered patient factors such as age, gender and history of degenerative disease.

Table 3 - 1: Mechanistic Classification of Injury

Load Mechanism	Resulting Injury
Axial Compression	Comminuted fracture of C1 (Jefferson)
	Vertical or oblique fractures (burst) of axis
	Comminuted fractures of vertebral bodies (burst)
Flexion – shear	Odontoid fracture with posterior displacement
	Atlanto-axial instability from the TAL compromise
Flexion – compression	Vertebral body fractures (wedge, tear drop)
	Compromise of posterior ligamentous complex
Flexion – distraction	Bilateral facet dislocation (PLL and capsule rupture, ALL stripping)
Flexion – rotation	Unilateral facet dislocation
Extension - distraction	Spondylolisthesis of C2
	Anterior C1 fracture
	Occipital-cervical (O-C) dislocation
	Hangman's fracture
Extension – compression	ALL and annular compromise
	Vertebral arch fracture (lamina, articular pillar, spinous process)
	Vertical vertebral body fracture
Extension – shear	Odontoid fracture (anterior displacement)
	Posterior atlanto-axial dislocation (without fracture)
Note: Rotation and lateral flexion injuries are not included because of the rare association with "major" injury situations	

(Adapted from Cusick and Yoganandan, 2002)

In 1997, Argenson et al. used data collected from trauma patients between 1980 and 1994 in France to develop a classification system first based on the dominant force vector and then sub-divided into three levels of severity. For the lower cervical spine, the dominant force vectors are Compression, Flexion-Extension-Distraction, and Rotation referred to as Type A, Type B, and Type C respectively, each with three levels of severity; Level I, Level II, and Level III, with Level III being the most severe injury (Fig. 3-7) (Argenson et al. 1997).

(Reproduced from Argenson et al. 1997)
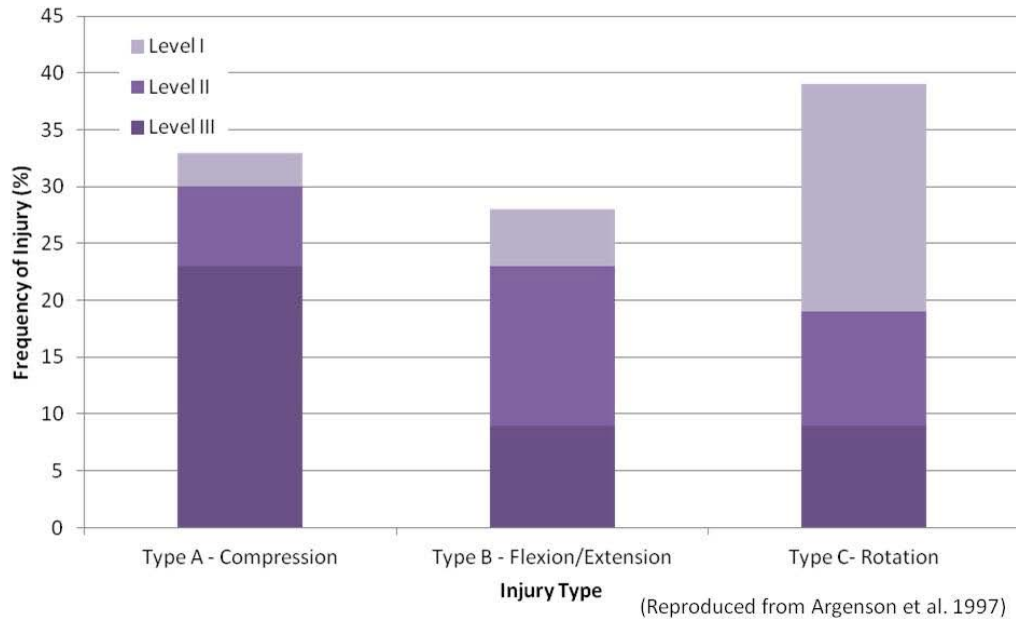
Figure 3 - 7: Cervical Spine Injury Frequency Based on Classification Scheme

Type A, or compression injuries were primarily marked by bone trauma (Fig. 3-8). Level I injuries relate to anterior vertebral body fractures or wedge fractures, Level II fractures were comminuted or burst fractures, and Level III fractures were tear-drop fractures which are influenced by a small flexion component to the dominant compression vector.

I – Anterior Wedge Fractures   **II – Comminuted Fractures**   **III – Teardrop Fractures**

(Panzer, 2006)
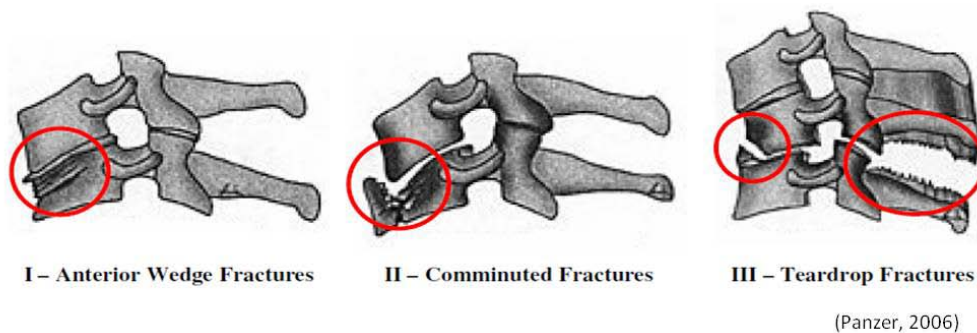
Figure 3 - 8: Levels of Type A Compression Injuries

Type B, or Flexion-Extension-Distraction injuries are primarily soft tissue injuries related to rotation in the sagittal plane and the inherent tension (distraction) resulting in the soft tissues (Fig. 3-9). Level I injuries correspond to moderate sprains including whiplash, while Level II injuries are severe sprains defined by the disruption of the PLL and can incur

34

fractures to the vertebral bodies. Level III injuries are defined by bilateral fracture dislocations.

I – Moderately Sprains   II – Severe Sprains   III – Bilateral Fracture-Dislocation

(Panzer, 2006)
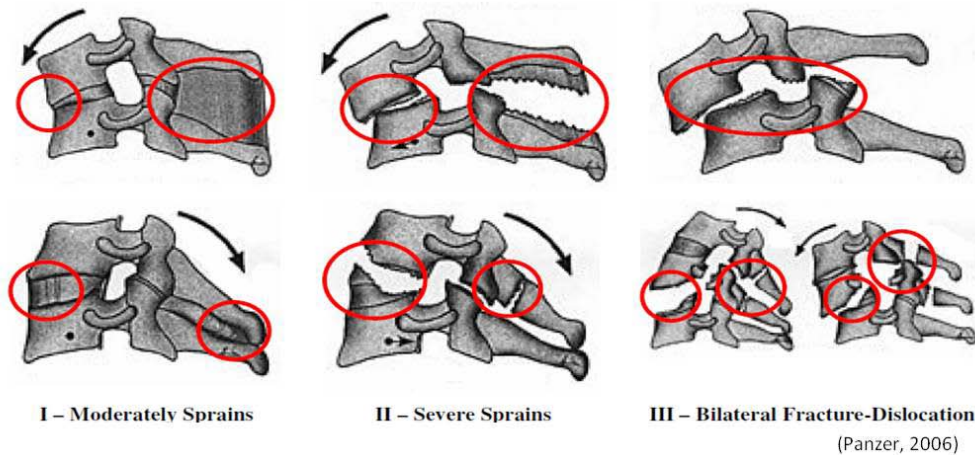
Figure 3 - 9: Levels of Type B Flexion-Extension-Distraction Injuries

Type C, or Rotation injuries involve axial rotation, inducing some lateral bending due to the anatomical restrictions on the mechanical behaviour of the cervical spine (Fig. 3-10) (White and Panjabi, 1990). Level I injuries involve a single facet fracture, while Level II injuries include the fracture of the articular pillars resulting in separation from the vertebral bodies. Level III injuries consisted of unilateral dislocation of a facet joint.

I – Unifacet Fracture   II – Fracture Separation   III – Unilateral Dislocation

(Panzer, 2006)
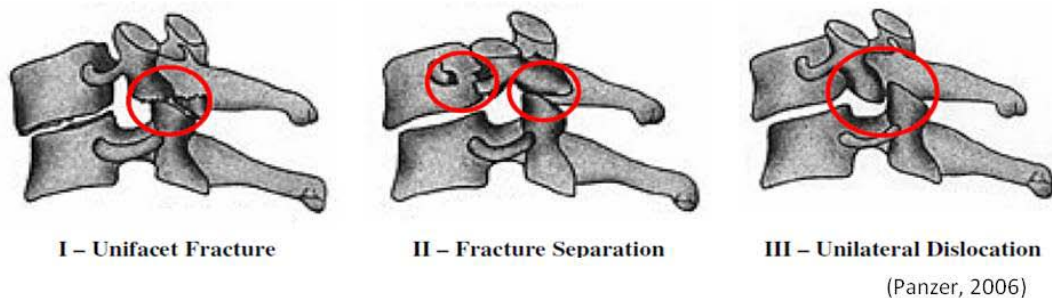
Figure 3 - 10: Levels of Type C Rotation Injuries

The previously mentioned classification methods focused primarily on the correlation between injury mechanism and location. The Abbreviated Injury Scale (AIS), developed by the Association for the Advancement of Automotive Medicine (AAAM), focused on classifying injuries based on severity. First introduced in 1977, the AIS has been universally

accepted as the foundation of injury severity scaling systems and is used extensively to classify the severity of injuries at different locations of the human body by trauma clinicians and data managers, injury researchers, and public health policy professionals. The AIS ranks injuries on a scale of one through six with six representing a fatality. The AIS for the cervical spine is shown below in Table 3-2.

Table 3 - 2: Abbreviated Injury Scale for the Cervical Spine

AIS Score	Description	Possible Injuries
1	Minor	Minor strain with no fracture or dislocation (Whiplash)
2	Moderate	Compression fracture C1-C7 <20% loss of height in vertebral body
		Fracture and/or dislocation/subluxation of the spinous process, transverse process or atlanto-occipital joint
		No spinal cord injury
3	Serious (non life-threatening)	Compression fracture/subluxation
		Spinal cord contusion/compression with or without transient neurological signs (weakness, paralysis, loss of sensation)
		Disc rupture/herniation with nerve root damage
		Fracture and/or dislocation/subluxation of the lamina, body, facet, pedicle, or odontoid process
4	Severe (life-threatening)	Lesion (incomplete cord syndrome with preservation of some sensation or motor function)
5	Critical	Vertebral crush (C4 or below)
		Cord laceration (C4 or below)
		Complete cord syndrome (quadriplegia or paraplegia with no sensation) (C4 or below)
		Total transaction (C4 or below)
6	Fatal	Vertebral crush (C3 or above)
		Cord laceration (C3 or above)
		Complete cord syndrome (quadriplegia or paraplegia with no sensation) (C3 or above)
		Total transaction (C3 or above)

(Adapted from Abbreviated Injury Scale, 2005)

For the purpose of this study; the major injuries identified to be important for cervical spine failure in the simulations were based on frequency under each mode of loading (tension, compression, flexion, extension, and axial rotation) and then cross-referenced with the expected injuries found in the experimental tests for each mode of loading.

3.3   Injury Prediction in Automotive Collisions

Current methods of injury prediction in the automotive industry rely primarily on the use of anthropomorphic test dummies (ATD's). ATD's are used as human surrogates during vehicle crash tests to evaluate potential occupant injuries. They are instrumented to record information such as impact forces and deflection, and the results are then compared to Injury Assessment Reference Values (IARV) for injuries to specific body regions developed from experimental testing on cadavers. The results of the comparison offer a likelihood of injury type and severity that a human could incur given their involvement in a similar collision. The most commonly used neck injury criteria is the Nij criteria. The Nij criterion is currently used in Federal Motor Vehicle Safety Standard 208 as the occupant neck load limit in frontal crash (National Highway Traffic Safety Administration, 2002). This criterion is only valid for neck motion in the extension/flexion direction, and assumes that no lateral force or bending moment is present (Eppinger et al. 1999). The Nij criterion considers the combination of extension/flexion moment and the tension/compression load on the neck (Eppinger et al. 1999). The resulting neck loading is plotted on a graph, where neck loads within the critical intercepts are considered safe. The critical intercepts for the 50th percentile male are 6160 N in compression, 6806 in tension, 310 Nm in flexion, and 135 Nm in extension. The intercepts form a diamond where the area inside the diamond is considered safe. A Nij value of 1 corresponds to a probability of 22% for an AIS 3 injury to occur (Eppinger et al. 1999).

In addition to using ATD's to predict occupant injury, implementation of numerical modeling to simulate crash tests has been adopted by automotive manufacturers to improve their understanding of collisions, as well as to help offset the cost of crash testing vehicles by allowing for more initial design iterations. Though the prediction of injury in these

simulations is still in early stages of development, it offers the opportunity for a wide variety of scenarios to be tested that may have been previously unavailable experimentally. The introduction of a biofidelic human model has the potential to increase the level of detail in the injuries predicted during a collision test by representing injury at the tissue level.

3.4   Cervical Spine Segment Studies

Cervical spine segments used in experimental testing often consist of two vertebral bodies, an intervertebral disc, and the associated ligaments. In some cases there are three vertebral bodies with two intervertebral discs and the associated ligaments. This type of segment is referred to as a functional spinal unit (FSU), and is used in compressive tests. For testing, the above mentioned segments were stripped of the related musculature leaving all the ligamentous structures left intact. The upper cervical spine segment typically contains the OC, C1, and C2 vertebrae. It is still considered a spine segment due to the complex interactions and interdependency at the levels even though there is no intervertebral disc. A wide range of experimental testing has been conducted on cervical spine segments under a variety of loading conditions. The studies highlighted below relate directly to verification and validation work carried out in the development of the original model by Panzer (2006); however, it should be noted that there are several other groups that have also contributed significant results to the field. An inclusive list is provided in Table 3-3 at the end of this section.

Panjabi et al. (1986), conducted experiments to evaluate the cervical spine under translational loading. The three-dimensional response of the segment in tension, compression and shear were observed. It was noted that the compression response was coupled with extension and similarly, the tension response was coupled with flexion. The anterior and posterior shear also had flexion and extension motions coupled. The results showed that the cervical spine segments were most flexible under anterior shear loads and least flexible under compressive loads. The results for the remaining motions produced approximately equal stiffness values.

In a study by Goel et al. (1988a), the upper cervical spine segment (C012) was tested under small bending moments of 0.3 Nm; a relatively small load application that resulted in large rotations. This supports the idea that the ligaments in the C012 segment are minor contributors in comparison to the muscle activity in supporting the head. It should also be noted that the results showed the majority of the axial rotation of this segment occur between C1-C2.

Shea et al. (1991) examined the load-displacement relationship of the cervical spine using functional spinal units (three vertebral bodies). Eighteen cervical spines were tested in compression, tension, shear, and flexion-extension. Results were reported as linear stiffness values and then compared to previous single segment studies by doubling the results of the single stiffness segments.

In two studies, Nightingale et al. (2002, 2007) looked at the flexion and extension response of the cervical spine over a range of applied moments including loading to failure. The two studies were a gender comparison to determine if there was a significant difference in the flexion and extension response between female (2002) and male (2007) spines. Results indicated that there was not a significant difference in tolerance between the two studies but did suggest a significant difference in stiffness.

Table 3 - 3: Summary of Cervical Spine Segment Range of Motion Experimental Studies

Study	Mode of Loading
Liu et al. 1982	Tension, Compression, Anterior/Posterior Shear
Goel et al. 1984	Flexion/Extension, Axial Rotation, Lateral Bending
Panjabi et al. 1986	Tension, Compression, Lateral Shear, Anterior/Posterior Shear
Goel et al. 1988a	Flexion/Extension, Axial Rotation, Lateral Bending
Goel et al. 1988b	Flexion/Extension, Axial Rotation, Lateral Bending
Moroney et al. 1988	Flexion/Extension, Axial Rotation, Lateral Bending, Compression, Lateral Shear, Anterior/Posterior Shear
Panjabi et al. 1988	Flexion/Extension, Axial Rotation, Lateral Bending
Schulte et al. 1989	Flexion/Extension, Axial Rotation, Lateral Bending
Panjabi et al. 1991a	Axial Rotation
Panjabi et al. 1991c	Flexion/Extension, Lateral Bending
Shea et al. 1991	Tension, Compression, Anterior/Posterior Shear
Chang et al. 1992	Axial Rotation
Wen et al. 1993	Flexion/Extension, Axial Rotation, Lateral Bending
Camacho et al. 1997	Flexion/Extension
Richter et al. 2000	Flexion/Extension, Axial Rotation, Lateral Bending
Van Ee et al. 2000	Tension
Winkelstein and Myers, 2000	Flexion/Extension, Axial Rotation, Lateral Bending
Panjabi et al. 2001b	Flexion/Extension, Axial Rotation, Lateral Bending
Nightingale et al. 2002	Flexion/Extension
Nightingale et al. 2004	Tension
Puttlitz et al. 2004	Flexion/Extension, Axial Rotation, Lateral Bending
Wheeldon et al. 2006	Flexion/Extension
Nightingale et al. 2007	Flexion/Extension
Dibb et al. 2009	Tension

3.5   Cervical Spine Segment Failure Studies

To predict injury, it is important that the model be as biofidelic as possible. This requires accurate geometry and material properties, as well as a variety of experimental data used to verify and validate the model. To evaluate soft and hard tissue failure at the segment level, the cases considered in this study included direct tensile and compressive loading, as well as flexion, extension and axial rotation. These are fundamental modes of loading which are necessary to be validated individually before moving on to combined loading scenarios. The experimental studies chosen as verification and validation cases were selected based on the level of detail and quality of data, statistical significance of the results and reproducibility of the test boundary conditions for model validation. Cases selected for the verification and validation of the segment model under injurious loading are detailed below. Again, it should be noted that other groups have conducted similar experimental studies and are listed in Table 3-4 at the end of this section.

3.5.1 Tension

Segment testing to failure under tensile loading was reported in experimental studies by Dibb et al. (2009). Dibb et al. (2009) expanded on the experimental testing work conducted by Van Ee et al. (2000) using a similar test procedure and fixation for the segments. Tension testing was initially performed on full cervical spines to compare the results for load tests aligned with the head center of gravity (CG) and aligned over the occipital condyles (OC). Following full spine testing, a similar procedure was repeated for cervical spine segments C012, C45 and C67. The superior end of the segment was fixed according to the determined alignment of the head CG or the OC. The segments were mounted an apparatus designed to pull the segment in tension from the bottom vertebra. An eccentricity bracket was used for the lower segments to maintain the lordotic orientation of the segment to represent in vivo conditions (Fig. 3-11). For initial quasi-static tests, both the upper and lower vertebral bodies of the segment were held in a fixed position allowing for no relative translation or rotation. Under failure conditions, the superior end of the segment was held to the apparatus such that it was able to translate in the anterior-posterior direction and rotate into the sagittal

41

plane, while the lower end was fixed, unable to translate or rotate in any direction. For failure testing, each spine segment was loaded at a rate of 1000 N/s with the resulting failure force recorded by a six-axis load cell.
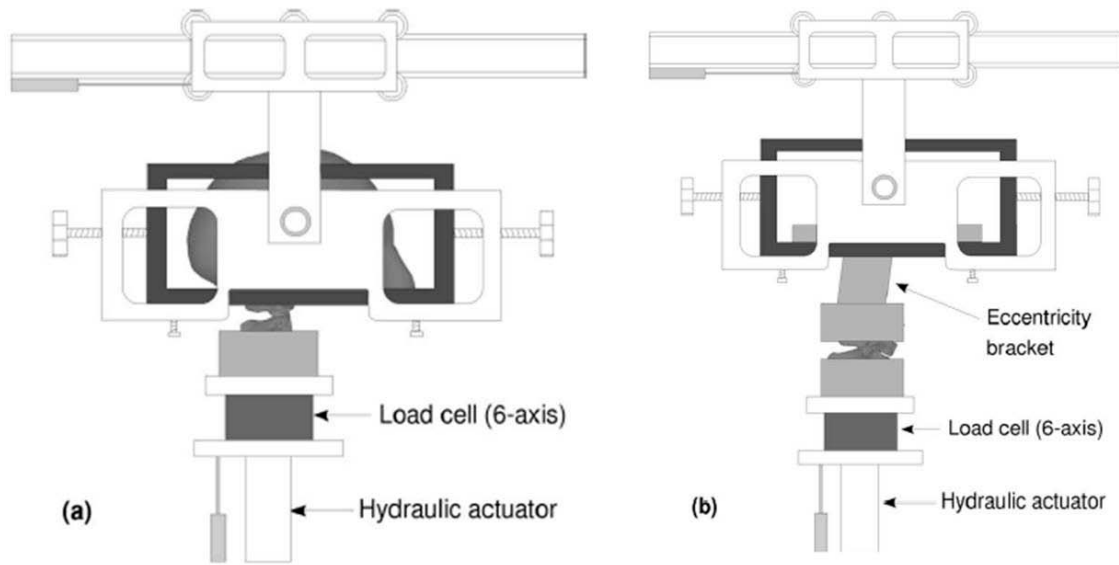
(Dibb et al. 2009)

Figure 3 - 11: Testing Apparatus for Upper (a) and Lower (b) Cervical Spine Segments

For the purpose of this research, only the results of tests carried out aligned with the head CG were considered for simulation comparison. The previous model was developed taking the head CG into consideration, therefore it was an appropriate place to begin failure testing. The C45 segments had a measured mean failure force plus or minus one standard deviation (±SD) of 1700 ± 199 N at an axial displacement of 7.7 ± 2.0 mm, while the C012 segment tests resulted in a higher mean failure force of 2417 ± 215 N at a failure displacement of 10.8 ± 3.9 mm (Fig. 3-12). The results shown below include a digitization of an experimental test of a C012 segment from Dibb et al. (2009).
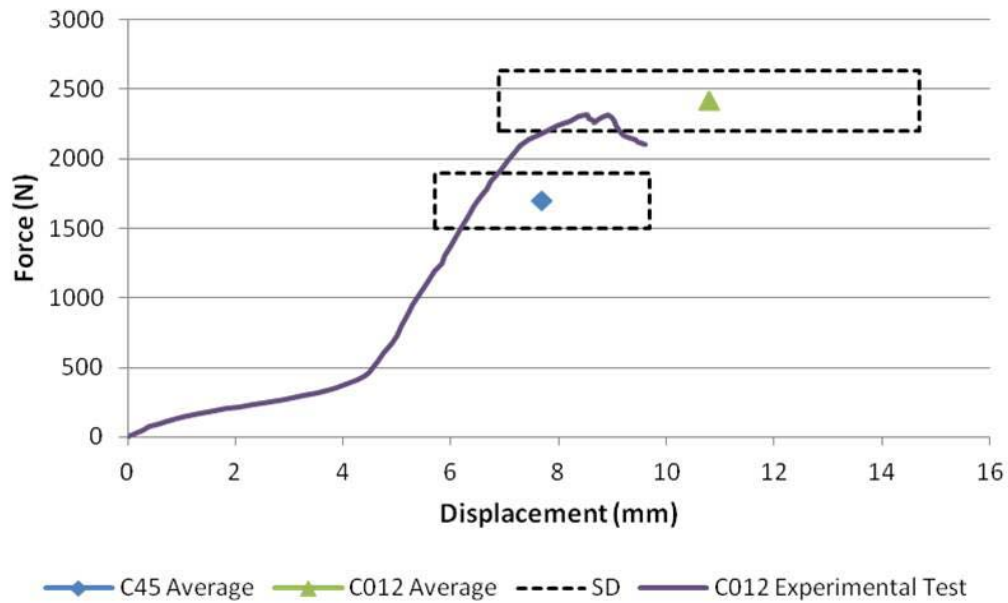
Figure 3 - 12: Experimental Averages (±SD) for C45 and C012 Segment Tests from Dibb et al. (2009)

Injuries produced to the lower cervical spine during the failure testing were classified as complete joint disruption. This included tearing of all ligamentous structures between the vertebral bodies as well as the intervertebral disc. Some vertebral body and spinous process fractures were observed, but it was noted that they originated near the fixation. Failures of the upper cervical spine segment included similar joint disruptions between C0-C1, C1-C2, or both, with severe ligament tearing. The failure testing also produced fractures of the odontoid, basilar skull, occipital condyles, and vertebral bodies.

3.5.2 Flexion and Extension

Flexion and extension tests to failure were studied by Nightingale et al. (2002, 2007). In 2002, Nightingale et al. focused on flexion and extension testing for range of motion and failure limits using an exclusively female sample group. The results were then used for comparison in a follow-up study in 2007 consisting of an exclusively male sample group. The lower cervical spine segments were fixed from the lower vertebral body and the moment was applied to the upper vertebral body (Fig. 3-13). The upper cervical spine segments were inverted such that the cephalad end was secured using a halo fixation, and the moment was

43

applied to the casting of the C2 vertebral body. The apparatus and test procedures for the 2007 tests were almost identical to those of the 2002 study so comparisons could be made between them (Nightingale et al. 2007). Initial quasi-static tests were performed on each of the segments to determine an average range of motion for each segment level. A counterbalance was used in the quasi-static tests to ensure that each segment had the same initial starting position. The failure simulations were loaded at an approximate rate of 90N/s with the counterbalance removed. It was necessary to remove the counterbalance during the failure tests in order to minimize the shear and tensile loads due to the dynamic nature of the tests (Nightingale et al. 2007).

(Nightingale et al. 2002)
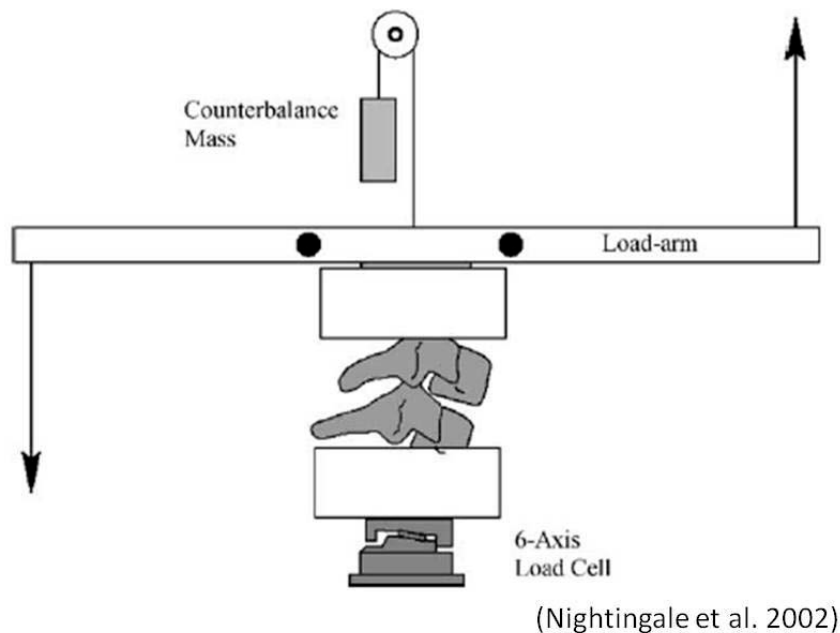
Figure 3 - 13: Testing Apparatus for Flexion and Extension (Lower Segment Shown)

For this research, only the experimental results from Nightingale et al. (2007) were considered as the numerical model used was representative of a 50th percentile male subject; however, the 2002 study was considered as a cross-reference for expected injuries. The 2007 results reported mean failure moments and rotational displacements (±SD) for the lower segment (C45) of 19.2 ± 2.8 Nm at 13.1 ± 3.4 deg in flexion and 15.6 ± 3.3 Nm at 13.0 ± 7.5 deg in extension. For the upper segment (C012), mean failure moments and rotational

44

displacements (±SD) were 39.0 ± 6.3 Nm at 58.7 ± 5.1 deg in flexion and 49.5 ± 17.5 Nm at 42.4 ± 8.0 deg in extension. The results plotted below (Fig. 3-14 & Fig. 3-15) are separated into flexion results and extension results for clarity. The flexion results include two experimental tests, one for C45 and one for C012, digitized from Nightingale et al. (2007). The upper cervical spine segment test has an offset of approximately 22 degrees due to the mass of the casting and the moment arm after the counterbalance was removed for the failure simulations. Note that the extension values are plotted as negative values only to differentiate the direction of the applied load and displacement.
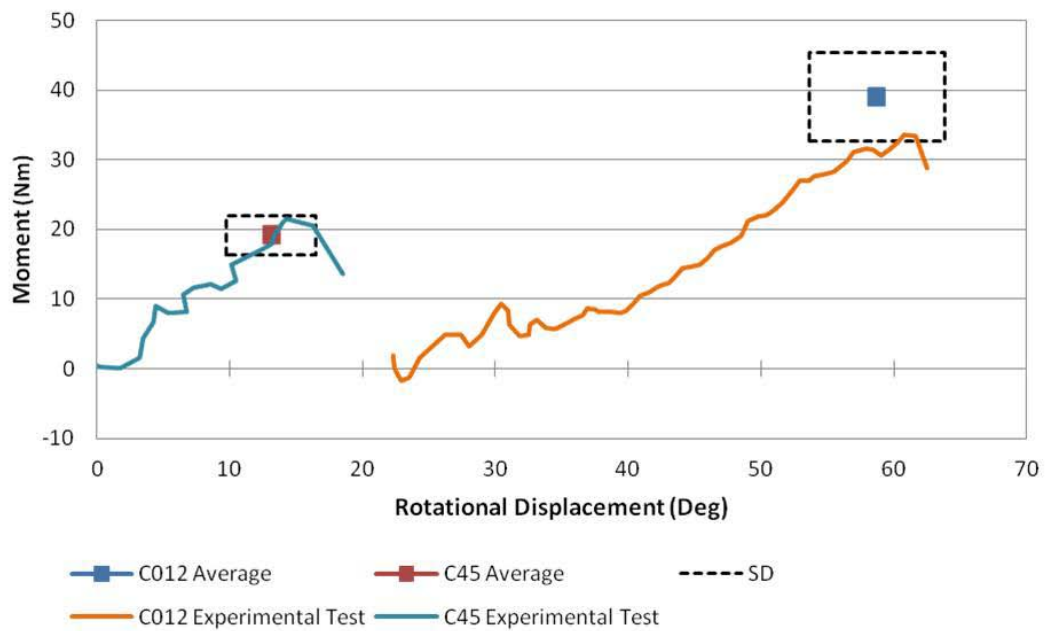
Figure 3 - 14: Experimental Averages (±SD) for C45 and C012 Segment Tests in Flexion from Nightingale et al. (2007)
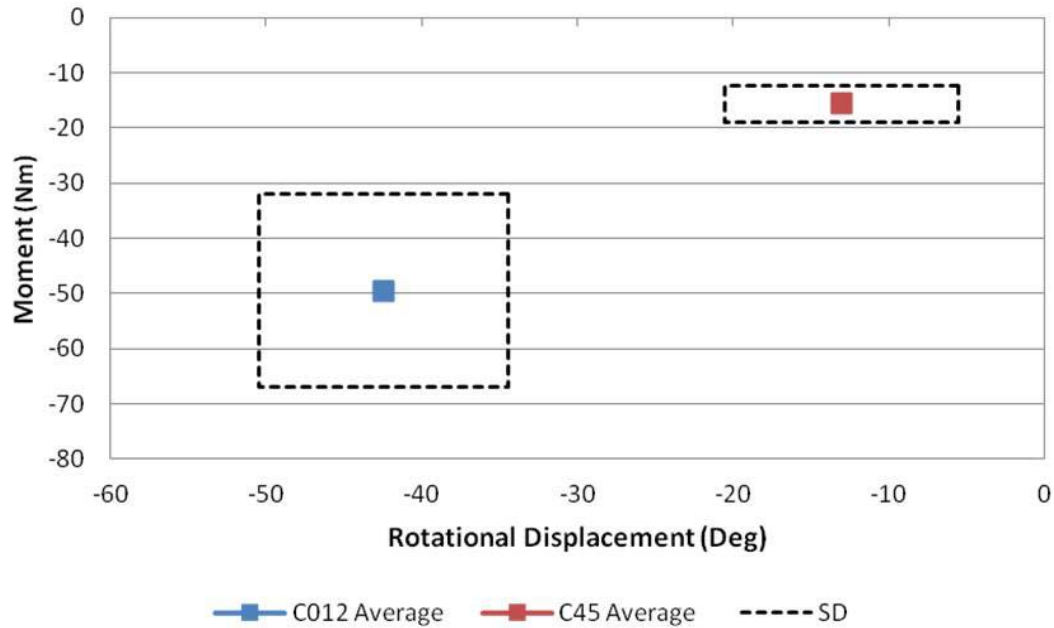
Figure 3 - 15: Experimental Averages (±SD) for C45 and C012 Segment Tests in Extension from Nightingale et al. (2007)

Injuries produced in the lower cervical spine segments in both flexion and extension were primarily dislocations which included complete disruptions of the ligamentous structures and disc between the vertebral bodies. Approximately one third of the segments tested had minor fractures of the spinous process, anterior body, or facets, where only two of the fractures were associated with the fixation. The observed fractures were not discussed with respect to loading mode (flexion/extension). For the upper cervical spine segments, injuries included Type III odontoid fracture (fracture at the base into the vertebral body), C0-C1 and C1-C2 dislocations, as well as, injuries to the alar, transverse, crux, and apical ligaments. The majority of the fractures occurred in extension failure testing, in contrast to, flexion failure testing, where the observed injuries were primarily soft tissue. In two flexion cases there was no discernable injury during joint dissection, only a notable laxity in the joint suggesting non-catastrophic ligament injury.

3.5.3 Compression

Segment compression tests to failure were carried out in an experimental study conducted by Carter et al. (2002). The purpose of this study was to test the impact of eccentricity in

46

compressive loading. Twenty-four functional spinal units (FSU) containing three vertebral bodies and two intact discs were randomly assigned to three groups: compression, compression-flexion, and compression-extension. The FSU's were taken from cervical spines at various levels between C2-C4 to C6-T1. Each FSU was mounted to a fixture that was set up to apply a load in one of the three modes and was then compressed based on the assigned loading mode. The fixture was designed such that the FSU could be potted in a manner that maintained the lordicity of the segment. Once potted, the mold containing the FSU was fit into the fixture (Fig. 3-16) and tested. In all cases for this study, both the superior and inferior vertebral bodies were subject to fixed end conditions. The FSU was initially preloaded to a level of 40N to represent the load of the head and then was loaded by a ram displacement of between 8mm and 15mm over a 16ms pulse length.
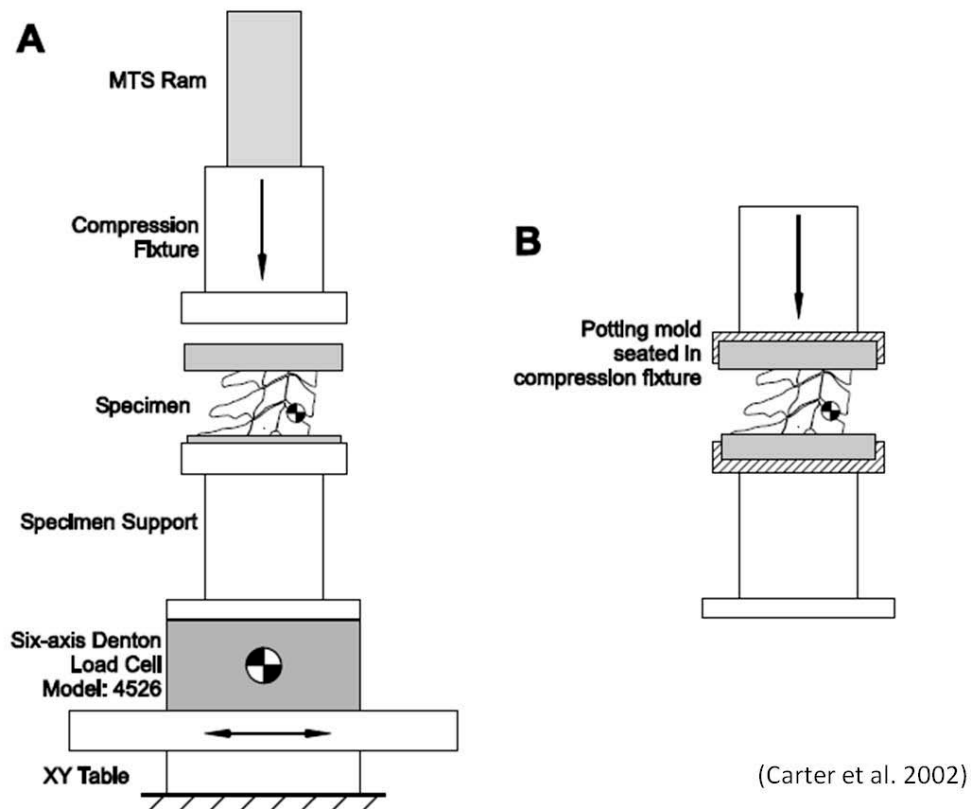
Figure 3 - 16: Testing Apparatus for Compression (Pure Compression Setup Shown)

For the purpose of this research, only the results from the FSU's loaded in pure axial compression were considered. Again, pure axial compression seemed an appropriate starting point for failure simulations before moving on to combined loading scenarios. Four out of eight FSU's tested in pure axial compression consisted of C5-C7 leading to the development of a C5-C7 FSU numerical model. Mean compressive force at failure was 3260.9 N with a 95% confidence interval (CI) of 707.7 N at a displacement of 2.91 mm with a 95% CI of 0.48 mm for FSU's tested in pure axial compression (Fig. 3-17). The failure force was measured using a load cell at the centroid of the inferior intervertebral disc.
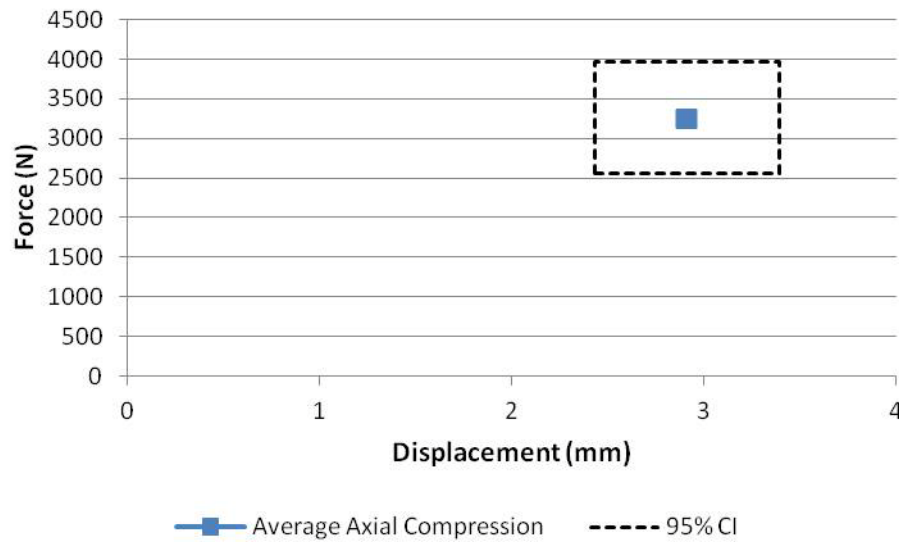
Figure 3 - 17: Experimental Averages (±95% CI) of Pure Axial Compression Tests from Carter et al. (2002)

This study primarily focused on comparing failure values to existing neck injury criteria and did not report observed injuries. However, in a clinical study of over 400 spinal injuries conducted by Denis, (1983), it was noted that compression and burst fractures where among the most common vertebral fractures. A compression fracture is confirmed when only the mid to anterior portion of the vertebral body is fractured while a burst fracture also includes fractures to the posterior of the vertebral body and into the laminae. Denis, (1983), observed that 62.4% of the 256 compressive fracture cases initiated at the superior bony endplate and,

for burst fractures specifically, 49.2% of fractures initiate at the superior endplate in the middle to anterior portion of the vertebral column.

3.5.4 Axial Rotation

Segment testing to failure under axial rotation was conducted by Goel et al. (1990) using only upper cervical spine segments (C012). The purpose of their study was to use load-to-failure tests to provide range of motion data to determine an allowable load range prior to failure. Additionally, they show what structures (bony or soft tissue) are most likely to fail and what structures provide joint stability. The segments were prepared for testing by dissecting the C012 structure from the full cervical spine. The skull was trimmed down to a smaller portion approximately three inches wide, four inches long, and one inch deep. All additional surrounding tissues and musculature were removed to create a ligamentous spine segment. For testing, the segments were fixed to the apparatus such that C2 was constrained in all directions but axial rotation. The skull portion of the segment was attached to allow for all motions (flexion, extension, and lateral bending, as well as translation axially, laterally and anterior/posterior) except for axial rotation (Fig. 3-18). The segments were tested at a rate of approximately 4 deg/s in the transverse plane (axial rotation).
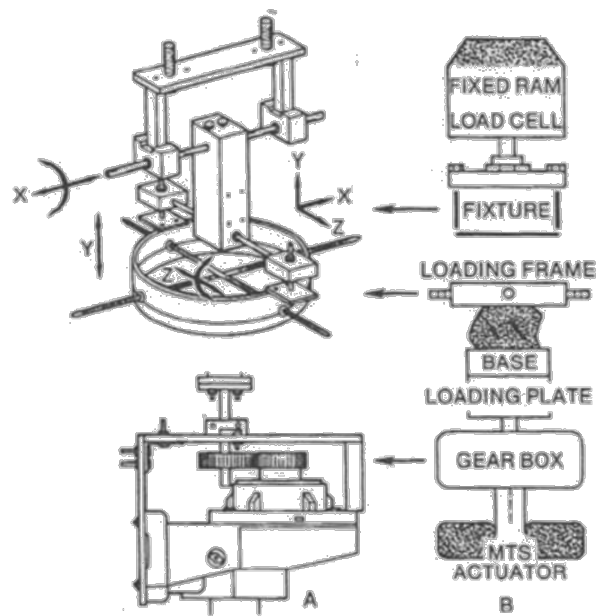
(Goel et al. 1990)

Figure 3 - 18: Upper Cervical Spine Segment Test Apparatus for Axial Rotation

The experimental results give mean failure values of 13.6 ± 4.5 Nm at 68.1 ± 13.1 deg. The digitized results from Goel et al. (1990) show a significant amount of rotation occurs before the segment engages and starts to bear a load (Fig. 3-19). This agrees with an earlier range of motion study conducted by Goel et al. (1988a) that showed very small moments produced significant axial rotation. The initial lag in engagement is likely caused by laxity in the ligaments of the upper cervical spine segment indicating that the majority of the joint stability can be attributed to surrounding musculature.
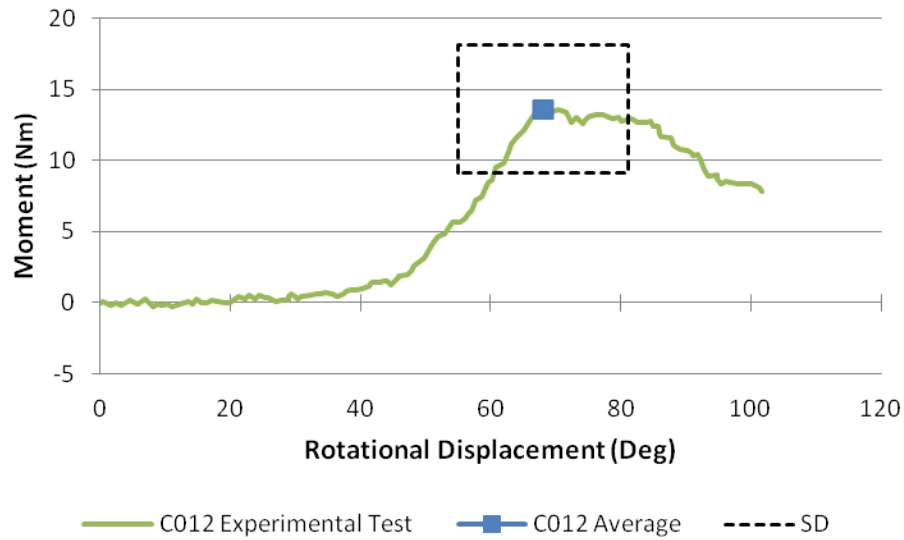
Figure 3 - 19: Experimental Averages (±SD) for C012 Segment Tests in Axial Rotation from Goel et al. (1990)

The observed tissue damage for all segments during failure testing included rotary subluxation of the C1-C2 facet joints with a bilateral rupture of the associated capsular ligaments, and rupture of the PAAM. Ligaments not damaged in the tests included the TL, C0-C1 joint capsules, AAOM, PAOM, apical, and AAAM. It should be noted; however, that there was some associated weakening of the apical and AAAM in one of the cases. Other isolated injuries observed in the segment tests were fractures at the odontoid process including apical avulsion, Type I (superior most portion of the odontoid), and Type II (at the base of the odontoid) odontoid fractures.

Table 3 - 4: Summary of Experimental Cervical Spine Segment Failure Studies

Study	Mode of Loading
Moroney et al. 1988	Flexion/Extension, Axial Rotation, Lateral Bending, Compression, Lateral Shear, Anterior/Posterior Shear
Goel et al. 1990	Axial Rotation
Van Ee et al. 2000	Tension
Carter et al. 2002	Compression, Compression-Flexion, Compression-Extension
Nightingale et al. 2002	Flexion, Extension (all female specimen)
Ivancic et al. 2007	Bilateral Facet Dislocation
Nightingale et al. 2007	Flexion, Extension (all male specimen)
Dibb et al. 2009	Tension

Chapter 4

Methods and Model Development

Numerical models of the spine can be used to predict the mechanics of the spine for occurrences that are difficult to investigate experimentally using physical models. Specifically, numerical models can determine internal loads, stresses, and strains in the spine tissue which is something that physical models are unable to predict (Panjabi, 1998). Simulation results of a numerical spine model allow researchers to investigate the inner workings of the cervical spine that could indicate the onset of injury as well as potential effects of that injury on the behaviour of the spine (Yoganandan et al. 1996). The following chapter discusses previously developed segment models, covering in detail the previously verified and validated model enhanced for this study. It will cover the model modifications required to evaluate severe injuries to the cervical spine as well as the experimental studies used to validate and verify the new model.

4.1   Early Segment Models

Cervical spine segment models can be made up of any section of the cervical spine but typically contain two vertebrae with the associated disc. In some cases, the segment models include three vertebrae and the associated discs representing a functional spinal unit (FSU). The models developed are compared against experimental data similar to the intended simulation. In the past, the majority of cervical spine segment models have been used to simulate quasi-static range of motion at various spinal levels. There are limited numerical models of cervical spine segments that have been used to investigate distractions to injurious levels. The intent of this research was to investigate loads beyond the physiologic range of motion into injurious levels. Some notable earlier works that include cervical spine segment models are summarized below.

53

Yoganandan et al. (1996) developed a C4-C6 segment model using geometric data obtained from CT scans. The model featured the cortical bone, trabecular bone, and the bony endplates of the vertebrae, and the AF ground substance and nucleus of the disc representing them with linear solid elements. The AF laminae were not represented in this model. Additionally, all the ligaments were represented using linear spring elements. The total number of elements in the segment model was 10371. Once developed, the segment model was evaluated in compression, flexion, extension, bending and rotation.

Clausen et al. (1997) also used CT scans to obtain the geometric data when developing a C5-C6 segment model. Linear solid elements were used to represent the various components of the vertebrae using gap elements to model the facet joints. The discs used linear solids to represent the AF ground substance and linear truss elements to represent the AF laminae. The nucleus was modeled as a fluid. In this model the ligaments were modeled using bilinear spring elements bringing the total number of elements to 5577. The cases run for this model included flexion, extension, bending and rotation.

Similar to the previous model Kumaresan et al. (1999) also developed at C5-C6 segment model based on CT scan geometry. This model contained a total of 10371 elements consisting of linear solids, linear truss, and non-linear spring elements. The components of the vertebrae were represented with linear solids as was the AF ground substance of the disc while the AF laminae were represented with linear truss elements. Both the facet joints and the nucleus of the disc were modeled as fluids and the ligaments were represented with nonlinear spring elements. This model was evaluated under direct axial compression as well as compression with eccentricity.

Nataranjan et al. (2000) developed a C5-C6 segment model for evaluation under flexion, extension, bending and rotation. The geometric data was taken from CT scans to include representations of the vertebrae, facets, disc and ligaments. Linear solids were used to represent the components of the vertebrae as well as the AF ground substance and nucleus. To model the facets, moving-contact surface elements were used. The AF fibres were

modeled using linear truss elements, and the ligaments were modeled with bilinear spring elements. The total number of elements in this segment model was 2323.

Ng and Teo (2001) developed a C4-C6 segment model using geometric data obtained from CT scans. This model contained 7628 elements consisting of linear solid and linear spring elements. Linear solids were used to represent the components of the vertebrae as well as the AF ground substance and nucleus of the disc. The AF laminae were not represented in this segment model. Linear springs were used to model the ligaments. This model was evaluated under compression, flexion, and extension.

The previous models described above have some deficits regarding mesh size and overly simplified, linear material models. Even though the models contained representations of the individual tissues of the vertebrae and disc, the low element count in each segment suggest a coarse finite element mesh relative to the scale of the tissue. Additionally, the simplified, linear material models may not accurately predict tissue level response. To address these issues, a biofidelic numerical model of the human cervical spine was developed by Panzer (2006). The development of this model focused on accurate representations of the cervical spine geometry and tissue-level material properties. Each segment level of the cervical spine was modeled and incorporated into a full cervical spine model. This model was chosen as the base model for this study. The details surrounding the development of this cervical spine and segment model are outlined below.

4.2   Previous Model Description

The full cervical spine model (Panzer, 2006) and subsequent segment models (Panzer, 2006; Panzer and Cronin, 2009) underwent a rigorous development process. All segment models were previously verified and validated under physiological loads (Panzer, 2006). The C45 segment model underwent additional verification and validation in a follow-up study by Panzer and Cronin, (2009). The full cervical spine model was also verified and validated under physiologic loads (Panzer, 2006), in frontal impact (Panzer, 2006; Panzer et al. 2011), and in rear impact (Fice, 2010; Fice et al. 2011). The segment models are an explicit finite

element model representative of a 50th percentile male. For the lower cervical spine segments, the model included a detailed disc (modeled using solid and shell elements), ligaments (modeled using 1D discrete elements) and the vertebral bodies (modeled using solid and shell elements) with an average overall mesh size of 1mm deemed appropriate through a mesh convergence study by Panzer, (2006) (Fig. 4-1).
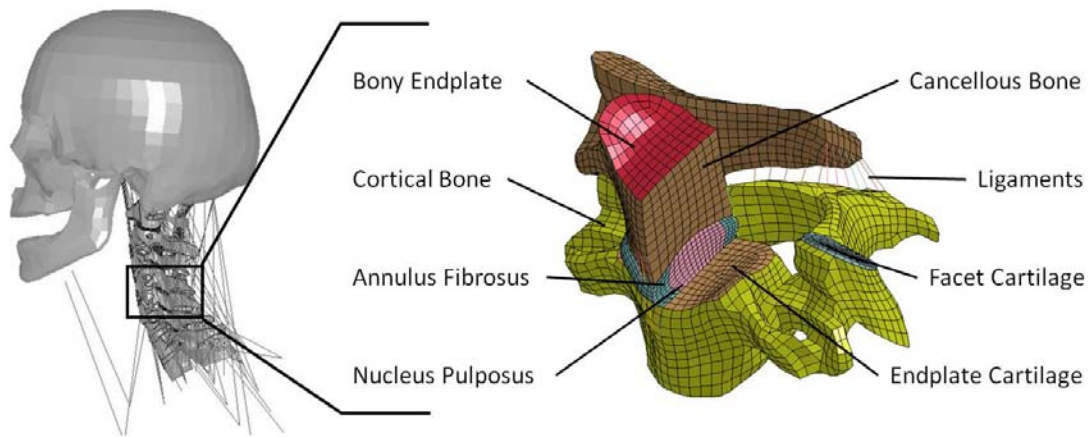
Figure 4 - 1: Lower Cervical Spine Segment (C45)

For the upper cervical spine segment (C012), the vertebral bodies and ligaments were modeled using similar methods to those used in the lower segment. Additionally, it included a representation of the skull modeled using shell elements. The primary function of the skull was for boundary condition application which justified the use of rigid shell elements to improve computational efficiency (Fig. 4-2). Again, the overall mesh size of approximately 1mm was confirmed via mesh convergence study by Panzer, (2006).
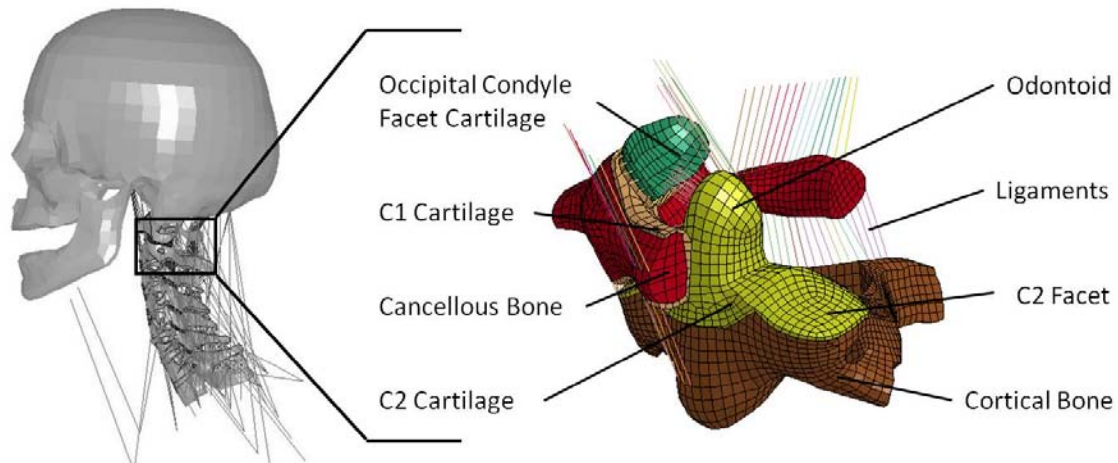
Figure 4 - 2: Upper Cervical Spine Segment (C012) (skull removed for clarity)

Material properties for the model were derived from experimental results in literature and applied to appropriate constitutive models. The constitutive models were not manipulated in any way to improve the response of the model during injury prediction simulations. The following sections highlight some of the key features in the development of this model. For a more in-depth discussion on the base model development refer to Panzer (2006).

4.2.1 Vertebral Bodies

The vertebral body geometry used in the model was originally extracted by Panzer (2006) from a cervical spine model developed by Deng et al. (1999). Using this geometry, Panzer (2006), developed the current vertebral bodies which were modeled using separate elements for the cortical bone, cancellous bone, and the bony endplates. The bulk of the vertebra was modeled using solid elements to represent the cancellous bone where the mass properties for the vertebral bodies were taken from Walker at al. (1973), and Robbins, (1983). A layer of shell elements was used to represent the cortical shell and the bony endplates of the vertebra (Fig. 4-3). The thickness of the cortical shell varied with each vertebral body based on values determined in an experimental study by Panjabi et al. (2001a).
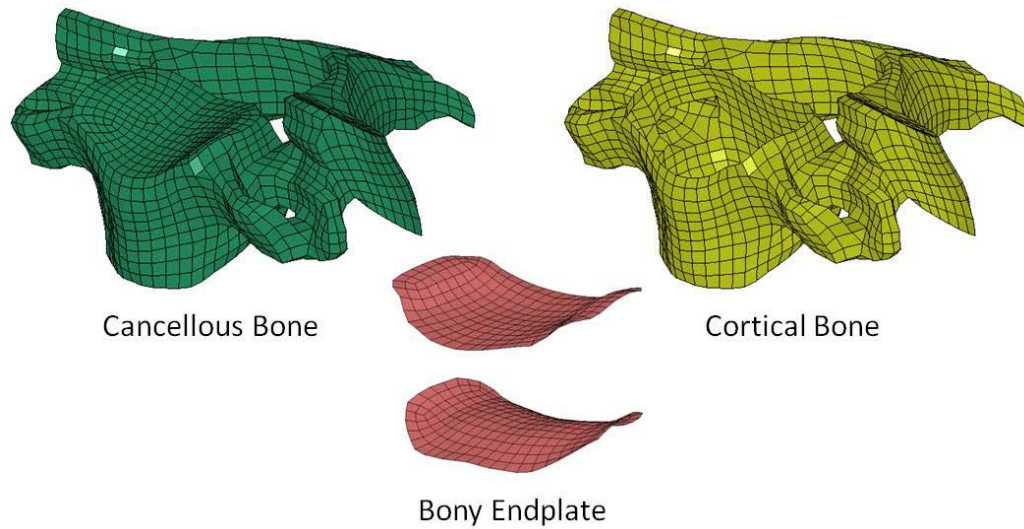
Figure 4 - 3: Vertebral Body Components

Three types of constitutive models were used for the vertebral bodies at the segment level

based on the applied loading. Some of the bony features where modeled as rigid bodies for

boundary condition application and to improve computational efficiency. In cases where

injury was expected, the bony features were modeled as elastic and elastic-plastic. Material

properties for the vertebral bodies were taken from a variety of experimental studies that

tested the mechanical properties of both the cortical and cancellous bone in tension and

compression, as well as at different rates (Table 4-1) (Keaveny et al. 2001; Kopperdahl and

Keaveny, 1998; Lindahl, 1976; McElhaney, 1966). The material properties for the bony

endplates were taken as one third the material properties of the cortical bone as assumed by

Panzer, (2006) producing results comparable to Denoziere and Ku, (2006).

Table 4 - 1: Summary of Experimental Studies of Bone Mechanical Properties

Study	Bone	Test	Results
McElhaney, 1966	Cortical	Compression	E=18.4GPa, e_{ult}=1.78%, σ_{ult}=190MPa
Lindahl, 1976	Cancellous	Compression	E=55.6MPa, e_y=6.7%, σ_y=4.0MPa, e_{ult}=9.5%, σ_{ult}=4.6MPa
Kopperdahl and Keaveny, 1998	Cancellous	Compression	E=291MPa, e_y=0.8%, σ_y=1.9MPa, e_{ult}=1.5%, σ_{ult}=2.2MPa (C)
		Tension	E=301MPa, e_y=0.8%, σ_y=1.8MPa, e_{ult}=1.6%, σ_{ult}=2.2MPa (T)
Keaveny et al. 2001	Cancellous	Compression	E=442MPa, e_y=0.77%, σ_y=2.4MPa

The facet cartilage and C1-C2 cartilage were modeled using solid elements attached to the vertebral bodies using different contact algorithms. In general, the constitutive model used was a deformable elastic model. For a full, detailed description of cartilage model development and implementation, the reader is encouraged to refer to Panzer, (2006).

4.2.2 Intervertebral Disc

The intervertebral disc model used in the simulation (Fig. 4-4) was developed by Panzer (2006) to evaluate physiological load ranges and for loading scenarios where the disc, ligaments and vertebral bodies were not damaged. It was developed based on a structural annulus fibrosus model using shell element layers for the annulus fibrosus (AF) laminae embedded in solid elements representing the annulus fibrosus ground substance. Additional solid elements were used to represent the nucleus pulposus. The segment model focused on the material properties of the annulus fibrosus laminae, ground substance and nucleus pulposus separately.
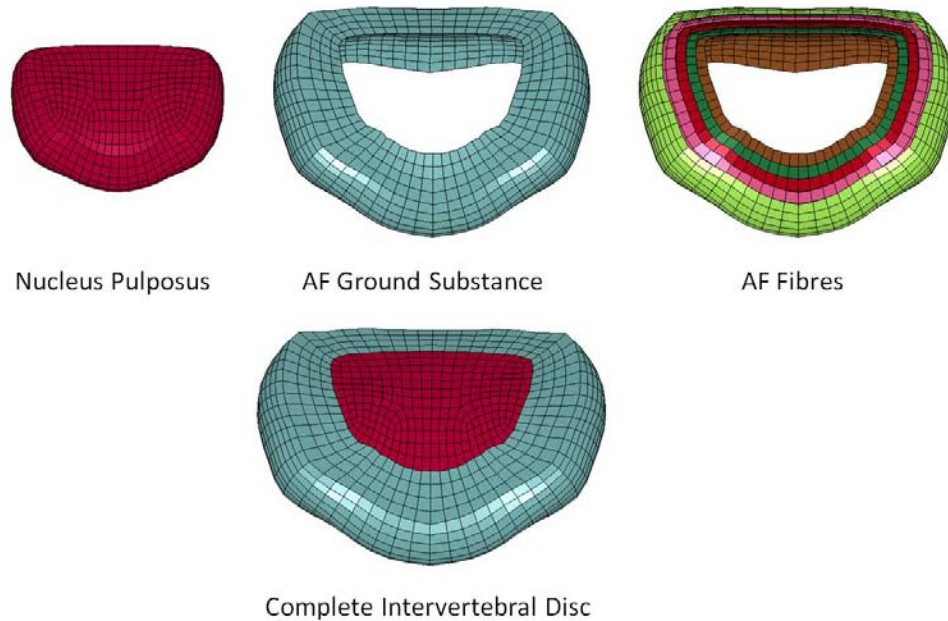
Figure 4 - 4: Intervertebral Disc Components

Five pairs of concentric shell layers (ten in total) were embedded within the solid ground substance layers. The fibres of the AF laminae in the cervical spine were oriented at angles between ±25 degrees in the outer layers to ±45 degrees in the inner layers (Cassidy et al. 1989; White and Panjabi, 1990; Wagner and Lotz, 2004). The mechanical properties of the annulus fibrosus are known to be non-linear and anisotropic. To develop the model, the material properties for the AF were taken from experimental results from Holzapfel et al. (2005) where single lamina samples were taken from cadavers, then tested along the fibre direction. Average stress-strain curves for the inner and outer layers of lamina were developed up to 4% by Holzapfel et al. (2005) which were then extrapolated by Panzer, (2006) to include higher strains based on data obtained from Skaggs et al. (1994) (Fig. 4-5). For the intermediate lamina, Panzer, (2006) interpolated curves using the results for the inner and outer layers found by Holzapfel et al. (2005). Due to the similarities between the mechanical responses of ligaments and the annulus fibrosus laminae, the material for the non-linear behaviour of the AF laminae was modeled using the mathematical model by Quapp and Weiss, (1998) for the fibre portion of a ligament. For a detailed description of how the mathematical model was applied, refer to Panzer, (2006).
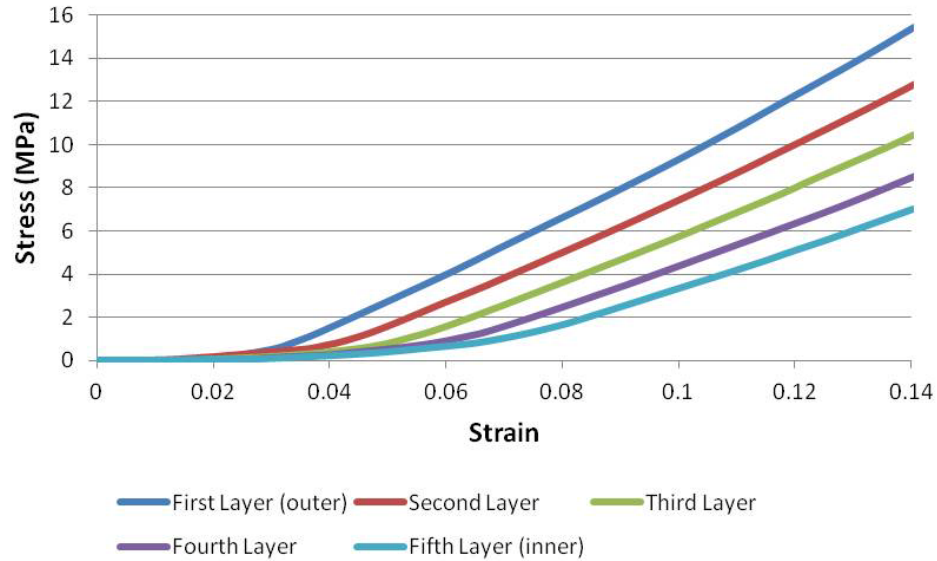
Figure 4 - 5: Stress-Strain Response of the AF Fibres along Fibre Direction

The material properties for the ground substance were found using a similar testing method to the AF lamina but to test the ground substance, specimens were tested perpendicular to the fibre direction to eliminate any influence from the fibres (Iatridis et al. 1998; Fujita et al. 1997). Testing in various directions revealed that the ground substance behaves in an isotropic manner (Iatridis et al. 1998; Klisch and Lotz, 1999). At lower strain rates (<10/s), ground substance is highly viscoelastic due to fluid-transport mechanisms (Iatridis et al. 1998; Iatridis et al. 1999), but at higher strain rates, viscoelastic property data for the ground substance is not available. Using the available experimental data, Panzer (2006) used the method of least squares to fit an Ogden-Rubber constitutive model to represent the material properties of the ground substance (Fig. 4-6) used in the segment model.
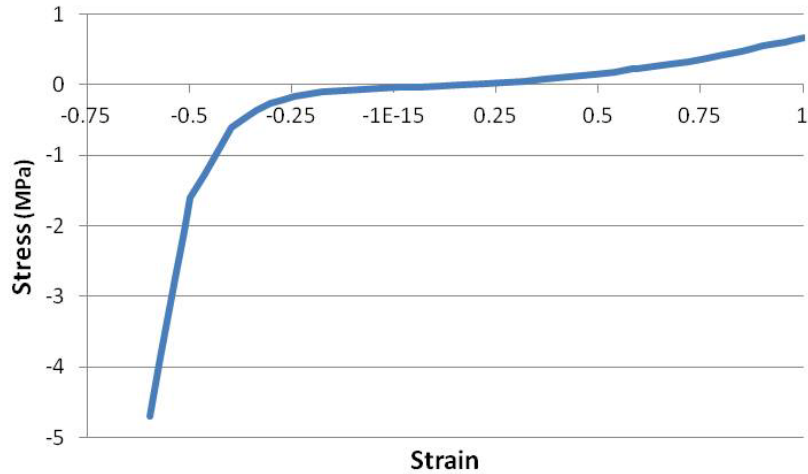
Figure 4 - 6: Uniaxial Stress-Strain Response of the AF Ground Substance

The nucleus pulposus was represented in the model using solid elements enclosed within the elements of the annulus fibrosus (Panzer, 2006). The nucleus pulposus exhibits fluid-like characteristics and was modeled using a general viscoelastic model. The parameters (Table 4-2) for the viscoelastic material model were obtained from a curve fit by Panzer (2006) based on experimental data by Iatridis et al. (1996) who looked at the stress relaxation of the nucleus.

Table 4 - 2: Model Parameters for the Nucleus Pulposus

Parameter	Value
K	1.720GPa
G_1, β_1	5.9300E-4 MPa, 1.4770E-3 1/s
G_2, β_2	6.7630E-4 MPa, 6.1524E-2 1/s
G_3, β_3	9.5160E-4 MPa, 1.018 1/s
G_4, β_4	2.0384E-3 MPa, 13.200 1/s

The cartilaginous endplates of the disc complex were modeled using shell elements. They attach to the disc using sharing nodes, and connect the disc to the adjacent vertebral bodies through a tied contact interface enabling load transfer and connectivity between the finer mesh of the discs and the coarser mesh of the vertebral bodies.

4.2.3 Ligaments

The primary concern for ligament response is tensile loading. The ligaments in the cervical spine model were modeled using sets of 1D, axial elements. The decision to use axial elements instead of shell elements to model the ligaments was based on the available experimental data for the ligaments. The data was primarily represented as force-displacement curves which is an unsuitable application for shell elements. The number of axial elements used per ligament varied with the geometry of the individual ligament and was selected to distribute the force along the attachment point. The axial elements were attached to the vertebral bodies using shared nodes at their anatomic locations (Fig. 4-7).
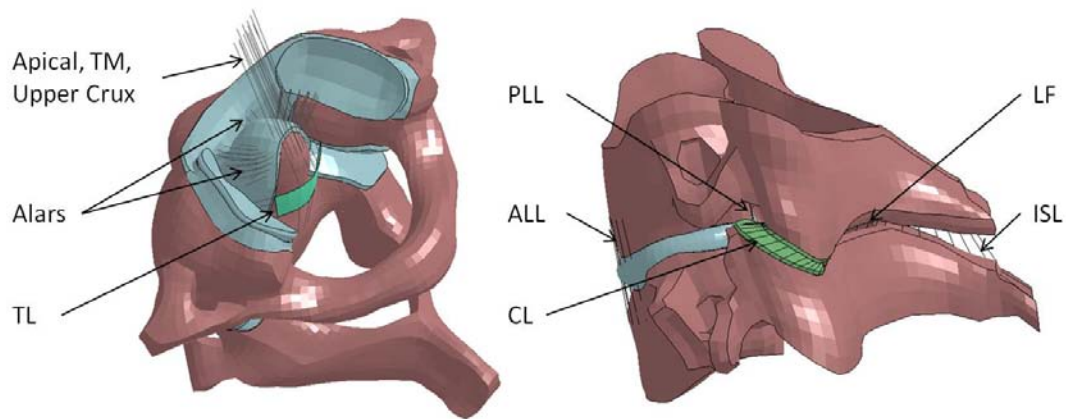
Figure 4 - 7: Ligament Model Examples in the Upper and Lower Segments (some ligaments removed for clarity)

The material model applied to the ligaments throughout the cervical spine model was a discrete non-linear elastic spring model. This material model determined the force in each element using quasi-static force-displacement curves developed for each ligament (Fig. 4-8 & Fig. 4-9) based on a variety of experimental studies that looked at the uniaxial response of cadaver ligaments under tensile loading (Mattucci, 2011; Yoganandan et al. 2001; Panjabi et al. 1998; Myklebust et al. 1988; Dvorak and Panjabi, 1987; Chazal et al. 1985).
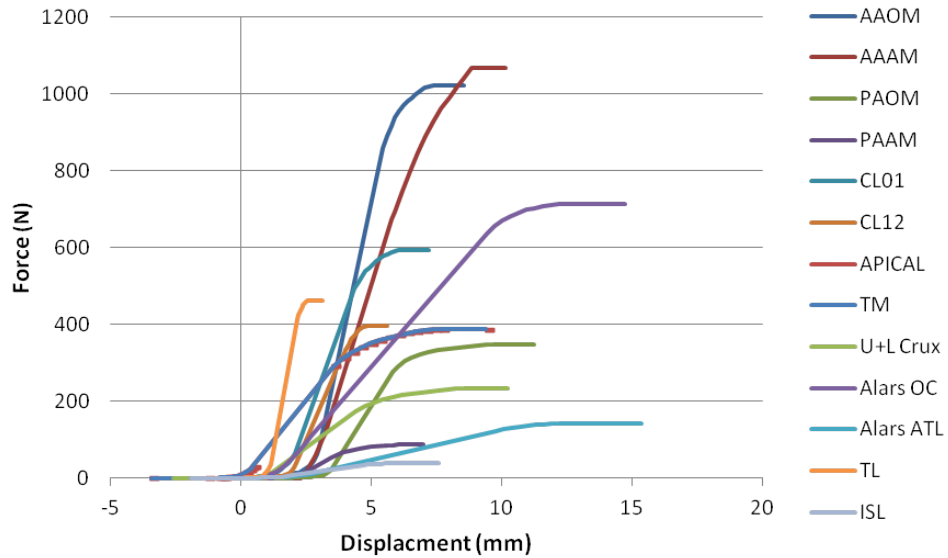
Figure 4 - 8: Upper Cervical Spine Ligament Curves (With Laxity and Pretension)
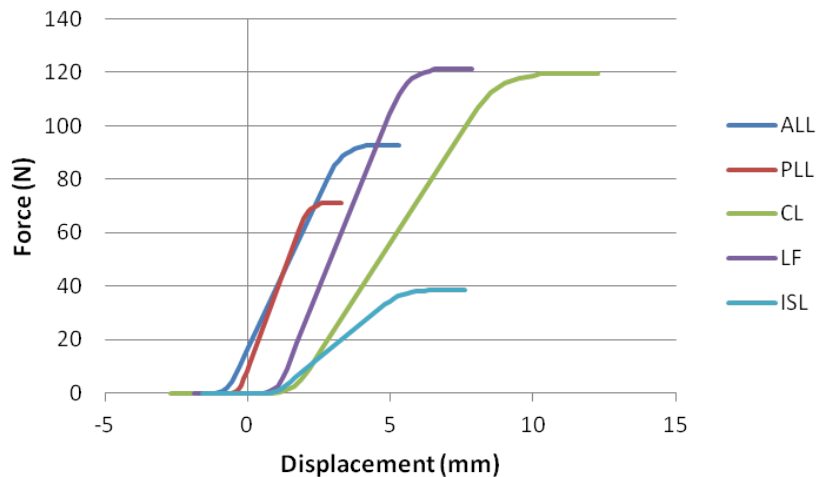
Figure 4 - 9: Lower Cervical Spine Segment Ligament Curves (With Pretension)

Each of the force displacement curves for the lower cervical spine segments had an applied pretension developed by Fice, (2010) based on experimental tests by Heuer et al. (2007), showing that the ligaments in the spinal column are under a preload in-vivo. Unlike the lower cervical spine where pretensions were calculated for the ligaments using the disc as the counterforce (Fice, 2010), there is no disc in the upper cervical segment to perform similar calculations. Pretensions, and in some cases, laxities were inferred for the upper

cervical spine ligaments based on results for the other segments, as well as information obtained in observation of experimental testing conducted by Mattucci, (2011). The pretensioned ligaments of the upper cervical spine segment include the Apical, TM, and the Alars OC. These ligaments were chose to have a preload based on results in literature describing their function and response under experimental quasi-static and failure tests by Goel et al. (1988a, 1990); Nightingale et al. (2002, 2007), and Dibb et al. (2009). The corresponding force values to the pretension ranged from approximately 0-5 N. The ligaments with applied laxity included the AAOM, AAAM, PAOM, PAAM, CL01, and CL12. Similar to how the pretension was determined; the laxities were applied based on the above mentioned literature describing the function and response of these ligaments under experimental testing. Descriptions of joint ranges of motion in various directions also assisted in determining appropriate laxities. Additionally, when simulations without laxity were compared to experimental results it could be inferred that adding ligament laxity to specific ligaments would improve the model response.

In addition to quasi-static loading, the ligament constitutive model was able to account for rate dependent loading by applying a dynamic scaling factor corresponding to a specific rate to the quasi-static force at a given displacement based on the above mentioned curves. The dynamic scale factor for the model was determined by Panzer, (2006), fitting a curve (Fig. 4-10) to experimental tests conducted by Yoganandan (1989a) where the ALL and LF were tested at rates of 9, 25, 250, and 2500 mm/s.
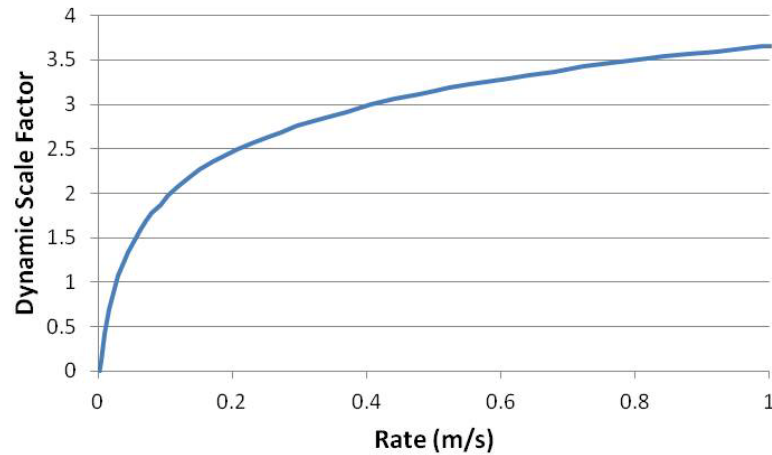
Figure 4 - 10: Dynamic Scale Factor Applied to Ligaments under High-Rate Loading

4.3   Tissue Response and Failure Implementation

The segment models used in this study were developed from the original models from Panzer (2006) and Panzer and Cronin (2009). The original models primarily focused on physiological range of motion and on low severity injury in frontal and rear impact. Those cases required using material models that reflected those goals. In order to obtain the correct response outside the physiological range, some changes and adaptations to the original segment model were required. Specifically, failure criteria needed to be introduced to the constitutive models such that the model could represent the location where an injury occurred and the associated threshold. The aspects of the model chosen for modification as well as the associated changes to achieve this goal are outlined in the following sections.

While the majority of the lower segment simulations could be conducted with the previously validated C45 segment model, the compression simulations required a segment containing three vertebral bodies and two discs. Using the existing cervical spine model developed by Panzer, (2006), a C5-C7 segment was extracted (Fig. 4-11). The segment was run under the compression validation cases used by Panzer, (2006) and a mesh convergence study, detailed in a later section, was conducted to ensure the response matched earlier validation results.
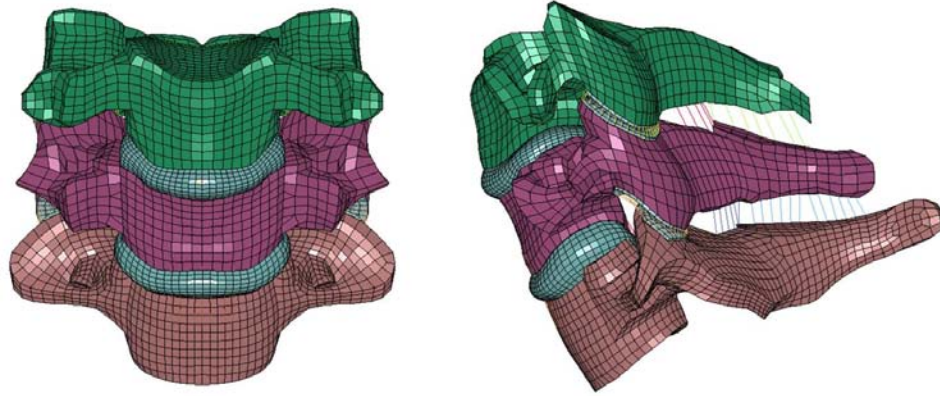
Figure 4 - 11: Lower Cervical Spine Segment (C567)

4.3.1 Ligament Failure

Ligament damage was one of the most commonly observed injuries when testing cervical spine segments at traumatic levels in tension, flexion, extension, and axial rotation (Dibb et al. 2009; Nightingale et al. 2002, 2007; Van Ee et al. 2000; Goel et al. 1990). Additionally, the ligaments have been reported in literature as a common injury location during automotive collisions (Yoganandan et al. 1989b; Argenson et al. 1997). It was important that the model be able to capture injury to the ligaments during the failure simulations.

As mentioned previously, the ligaments in the original model were represented using axial elements. This decision was based on the ability of axial elements to best represent the force-displacement results reported in literature. For failure implementation, there was consideration of modifying the ligaments to shell elements where element erosion could be used to represent ligament tearing under failure loads. Further investigation into this implementation resulted in similar conclusions to Panzer (2006). The use of shell elements to represent the ligaments had the potential to work well under tensile loading but when subjected to compressive loading, the shell elements exhibited high levels of deformation resulting in significant hourglassing and subsequent numerical instabilities. Based on this conclusion, the elements representing the ligaments under failure conditions would remain as axial elements.

Additions to the existing material model applied to the ligaments allowed the implementation of ligament failure. The force-displacement curves obtained from literature provided an average failure force and displacement value for each ligament tested. Preliminary failure simulations were conducted after applying the failure displacement value to the constitutive model as a critical value for failure under tensile loading. Ligament failure was modeled by removing, or failing, the associated discrete elements when the critical value was reached. Under this implementation, each ligament was considered a single part with an assigned number of discrete elements. This meant that when a ligament reached the critical displacement for failure, all associated elements failed simultaneously resulting in an instantaneous release of energy. After some initial simulations, it was observed that simply adding a displacement to failure to the entire ligament resulted in numerical instabilities that stemmed from the instantaneous release of energy as the elements were simultaneously deleted. Ligament failure tests conducted by Mattucci, (2011) demonstrated that, most often, ligaments do not fail abruptly but gradually tear; reducing the load they are able to carry down to zero (Fig. 4-12).

(Image courtesy of S. Mattucci)
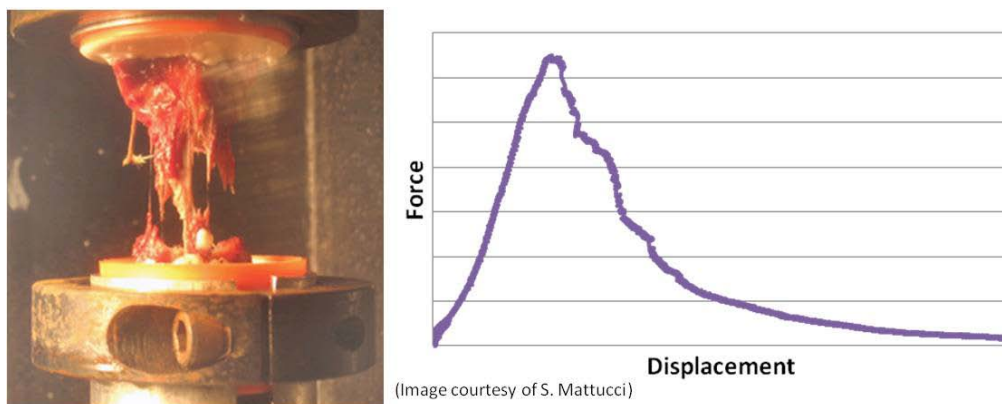
Figure 4 - 12: A Ligament Gradually Failing during Tensile Test

Implementing a force-displacement curve that included the post-failure response was not possible from a computational perspective. To address this need, the introduction of progressive failure to each ligament was required. Through progressive erosion of the multiple beam elements representing the ligament, the release of energy from the deleted elements could be drawn out reducing the likelihood of numerical instabilities. The

68

experimental observation by Mattucci (2011) showed that most ligament failures initiated on the outer edges of the ligaments, tearing inwards until the last fibrous strands failed near the center of the ligaments. To implement this into the model, each ligament part was broken down into a subset of elements of the original part (Fig. 4-13). Each subset was assigned a critical displacement value beginning with the original critical value reported in literature applied to the outer subset, and continuing with progressively larger critical values as the subsets moved towards the center.

Initial Ligament Failure Implementation

Progressive Ligament Failure Implementation
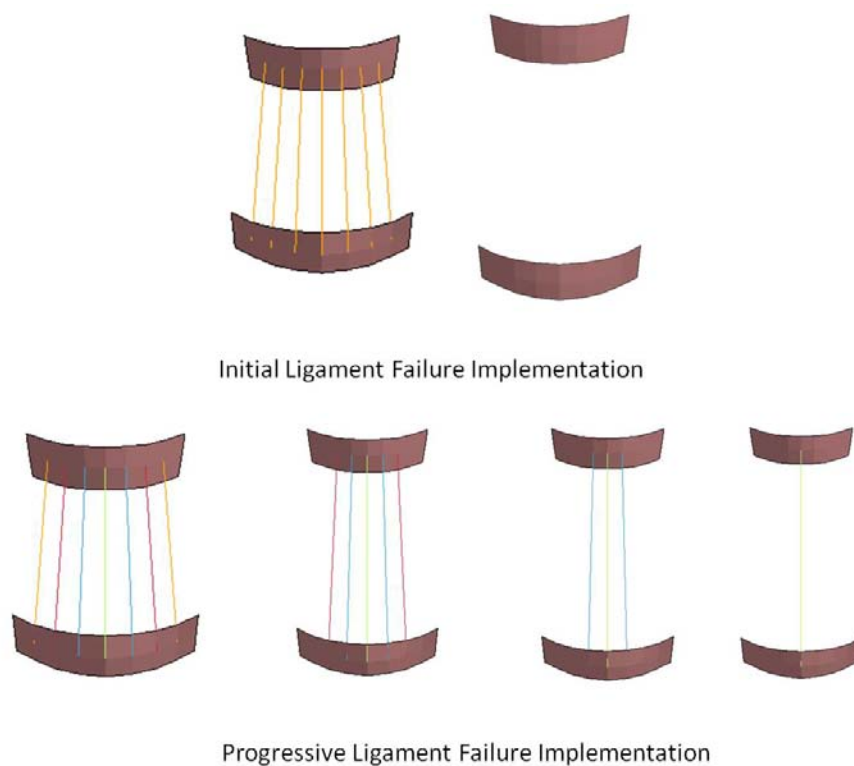
Figure 4 - 13: Evolution of Progressive Failure in the Ligaments

The application of progressive failure to the capsular ligaments was not quite as straight forward as the other ligaments due to the circular nature of their geometry. Initially, the 32 elements representing a single capsular ligament were randomized into four groups of eight. Each group of eight was given a displacement failure value beginning with the experimental failure and then three additional critical values progressively larger than the experimental value. The result for a single capsular ligament was duplicated for the adjacent ligament to ensure balance in the model. A preliminary test was conducted on the

randomized ligaments and it was found that the failure was scattered and unstable. A more structured approach was applied splitting the capsule into quadrants where each quadrant was treated like an eight element ligament where failure began at the edges of the ligament and progressed to the centre (Fig. 4-14). When tested, this produced a considerably more stable progressive failure.

ANTERIOR

- ● Fails last (longest)
- ● Fails third
- ● Fails second
- ● Fails first (shortest)

POSTERIOR
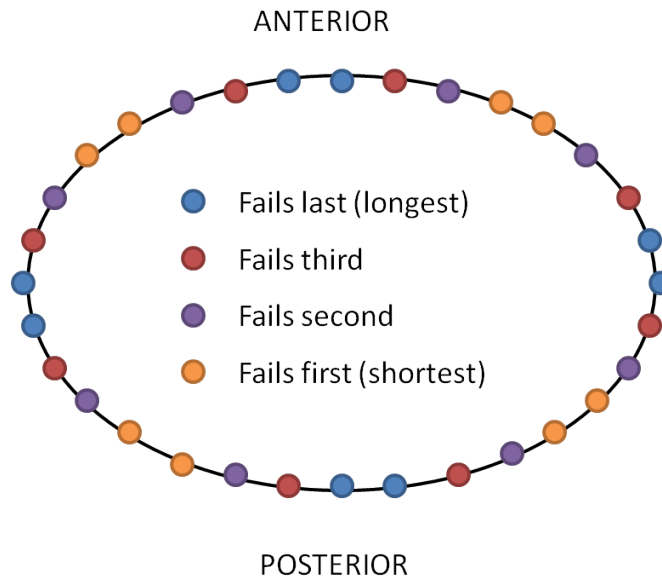
Figure 4 - 14: Progressive Failure Implementation for Capsular Ligaments

The critical values for each subset of elements was developed using the average post-failure experimental data from Mattucci, (2011). For most ligaments, the experimental post-failure response occurred in a stepwise manner gradually reducing the transmitted force down to zero. In order to model the stepwise nature of the failure, a curve fit was completed on the experimental post-failure region using a regression fit analysis with a sigmoidal function. The initial failure displacement value for each ligament was held constant to the value given in literature while the curve fit calculated the additional failure displacements. The results produced in the regression fit had the potential for variability. The current implementation of the ligaments evenly distributed the force between the total number of axial elements used for each ligament. The variability lay in the number of elements allowed to fail at each displacement. In an attempt to control this variability, the number of elements allowed to fail at each displacement was symmetric, moving from the outer elements to the center.

70

Four or five displacement values were calculated depending on the total number of axial elements in the ligament. Fig. 4-15 provides an example of the post-failure regression fit showing the original ligament model and the new post-failure response plotted with an experimental average.
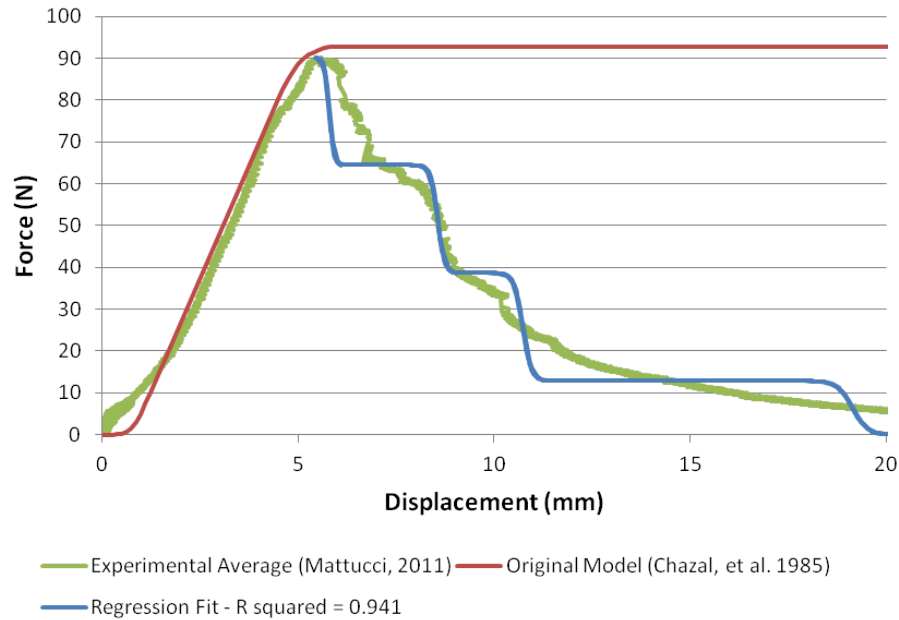
Figure 4 - 15: Post-Failure Regression Fit for the ALL

This procedure was carried out for all ligaments in the in the lower cervical spine segment, and key ligaments in the upper cervical spine segment. The results for the remaining ligaments are summarized in Table 4-3. The addition of progressive failure to the ligaments added a biofidelic failure response to the model and was successful in addressing some of the minor numerical instabilities in the model.

Table 4 - 3: Summary of Post-Failure Regression Values

Lower Segment Ligaments	R-squared Value	Upper Segment Ligaments	R-squared Value
ALL	0.941	AAOM	0.975
PLL	0.920	AAAM	0.851
LF	0.955	PAOM	0.940
ISL	0.912	PAAM	0.904
CL	0.925	TM COMPLEX	0.978
--	--	CL-01	0.990
--	--	CL-12	0.969

4.3.2 Disc Failure

The disc is another area of the cervical spine commonly injured under traumatic loading. Implementing failure into the disc model was initially more challenging than the ligament implementation. Disc failure is less straightforward and warrants a review of some of the important mechanical properties associated with the different parts of the disc and their response under a traumatic load. In an experimental test conducted by Pezowicz et al. (2005), it was found that, much like the ligaments, the fibres of the annulus fibrosus do not fail catastrophically but in a gradual progression (Fig. 4-16). Observed failure was noted as shear between adjacent AF layers as well as avulsion at the bone insertion site. Experimental results by Fujita et al. (1997) showed that the ground substance did not contribute significantly to the joint stability under tensile loading. These experimental results provided direction on implementing failure properties to the disc. The AF fibres failed in a similar manner to the ligaments, suggesting methods for a similar type of progressive failure be investigated; however, the material model used for the AF fibres was somewhat more complex. The AF fibre layers were modeled as shell elements using a fabric material model to account for the different fibre directions found on each layer. There was some consideration of modifying the material model of the AF fibres to axial elements similar to the ligaments. After careful consideration, the decision was made to keep the material

model of the AF fibres as they were in the original model by Panzer (2006). Changing to axial elements would no longer account for the fibre orientation and reduce the complexity of the material model. Furthermore, the original disc model had undergone extensive verification and validation therefore any changes to the material model would require the verification and validation work to be repeated. Using the previous implementation a similar method of progressive failure was not an options so different implementations were considered.

(Reproduced from Pezowicz et al. 2005)
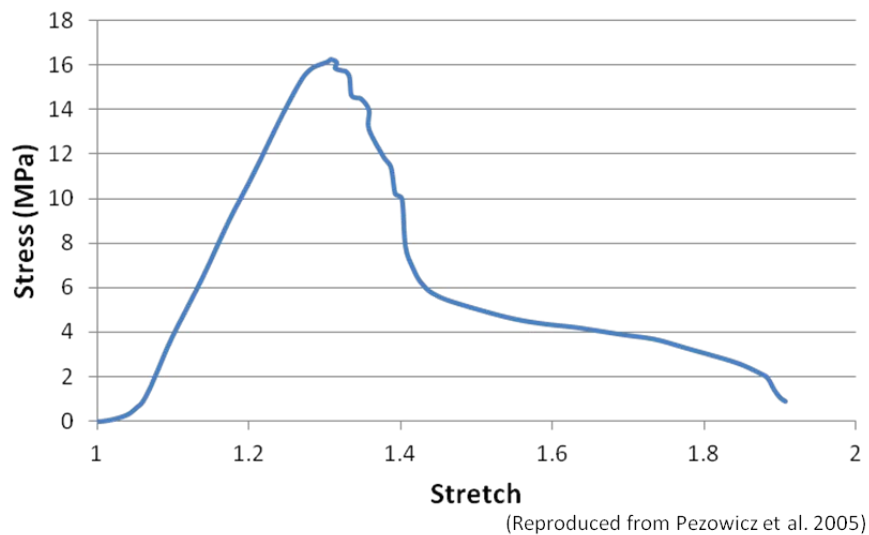
Figure 4 - 16: Stress-Strain Response of a Single Lamina along the Fibre Direction in Tension

Experimental data extending beyond the physiological range of the cervical spine was limited making it challenging to incorporate failure into the disc model. Data from Skaggs et al. (1994) indicate average failure stresses for individual layers along the fibre direction of 7.95 MPa at 10.95% strain for the outer layers and 4.70 MPa at 13.35% strain for the inner layers. The existing curves in the model were modified to plateau at these strain values for the outer and inner-most layers. The maximum strains for the three intermediate layers were linearly interpolated between the values presented by Skaggs et al. (1994). While this did not introduce physical failure into the model, it provided a point where the stress in the AF fibres would plateau at the failure values. Additional limitations in the material model used to represent the AF fibres were that it did not allow for direct failure and element

73

erosion could not be applied to the shell elements representing the AF layers. As mentioned earlier, changing the material model for the AF fibres would result in additional verification and validation therefore other methods of failure implementation were pursued.

A study conducted by Kasra et al. (2004), indicated that the majority of failures in tensile testing of bone-disc-bone specimens occurred at the endplate cartilage-AF interface at an average stress of 4.708 ± 2.18 MPa. Since a tie-break contact was used to represent this interface in the model, failure was introduced through a critical stress approach to represent disc avulsion once the critical stress was reached (Fig. 4-17).
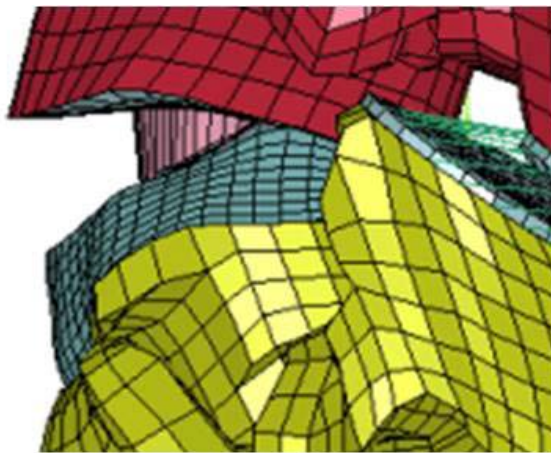
Figure 4 - 17: Tie-Break Contact Separating to Represent Disc Avulsion

Based on the failure stress presented by Kasra et al. (2004) and the surface area of the current disc, failure of the disc was predicted to occur at a force of approximately 1280 N. Dibb et al. (2009) reported that complete disruption (ligament and disc failure) of a C45 segment occurred at 1700 ± 199 N. Using the data from Yoganandan et al. (2001), it was determined that the ligaments account for approximately 450 N suggesting that the balance of the load on the disc should be 1250 N. This agrees with the results calculated from the values reported by Kasra et al. (2004). In order to apply this to our model, consideration needed to be taken into how the contact between the disc and the vertebral body was defined. The shell elements of the fibres were unable to bear load directly so their load was transferred to the discrete nodes of each annular ring; therefore, the failure stress of 4.70 MPa could not directly be applied as a failure stress to the tied contact. An average surface

area was calculated for the five AF layers and was used in conjunction with the failure force calculated from the experimental results for failure stress from Kasra et al. (2004). From this, an average failure stress for AF layers at the endplate cartilage-AF interface was determined (Table 4-4).

Table 4 - 4: Calculated Values for Disc Avulsion Implementation

	Average Stress (MPa)	Average Force (N)	Cross-sectional Area (mm^2)
Full Disc	4.70 (Skaggs et al. 1994)	1280	272.3
AF Layers	53.33	1280 (Kasra et al. 2004)	23.9 (5 layer average)

4.3.3   Bone Failure

During experimental testing, bone failure, or fracture, was most often reported when the vertebral bodies were subjected to a compressive load (Carter et al. 2002; Nightingale et al. 2002, 2007); however, fractures were also reported under tensile loading caused by soft tissue avulsion at the bone-tissue interface (Dibb et al. 2009; Nightingale et al. 2002, 2007). Additional literature on cervical spine injuries site specific locations where fracture was most likely to occur under different loading conditions. It was important that the model accurately represent the location of the fracture at the appropriate failure value.

The original model developed by Panzer (2006) represented the vertebrae using a rigid material model. This implementation was a reasonable representation for the original model as the work did not consider the potential for vertebral fracture. Additionally, it was an acceptable method for improving the computational efficiency of the simulations. For the current study, the vertebral body material model was selected to include failure based on plastic strain, using an elastic-plastic constitutive model. Although bone tissue only displays a limited response beyond yield, this was a realistic and numerically stable approach to model failure. Failure was predicted to occur once the effective plastic strain reached a critical value, based on reported values from the literature (Table 4-5).

75

Table 4 - 5: Summary of Failure Strains Used in the Model

Bone Type	Failure Strain (%)
Cortical	1.78
Cancellous	9.5
Bony Endplate	1.78

Post-failure response was simulated through element erosion and the location of element deletion was taken into consideration as the location for fracture onset. This is an effective method of visually representing failure (Fig. 4-18) but it is understood that there is a level of mesh dependency associated with this approach. Further, this approach may not accurately capture the post-failure response of fractures occurring under a compressive load. In compressive fractures of trabecular bone, tissue damage is progressive initiating quickly but slows as porosity is reduced. Element erosion removes material as the fracture propagates and does not account for reduced porosity. For fractures that occur under tensile loading, the element erosion provides a more realistic post-failure response.
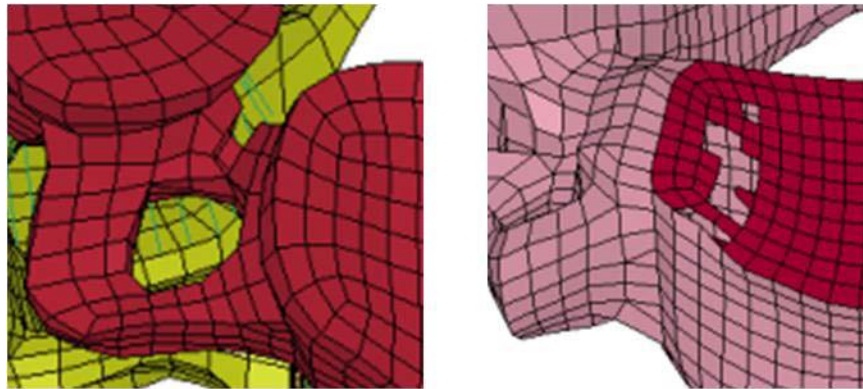
Figure 4 - 18: Examples of Element Erosion Representing Fracture Onset

In addition to using element erosion to predict the onset of bone fracture, it was observed that a qualitative investigation into areas of high stress allowed additional insight into potential fracture locations (Fig. 4-19).
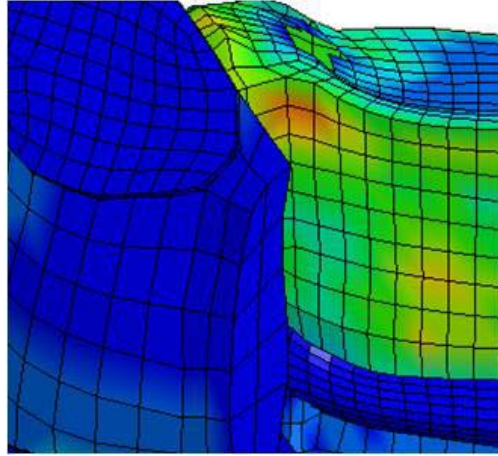
Figure 4 - 19: Areas of High Stress (red) Showing a Potential Fracture Location

These qualitative results can assist in assessing the validity of the model. Future studies will include investigations of more advanced methods to predict fracture.

4.4   Simulations Methods

For each validation case, the simulations were designed such that the boundary conditions were representative of the conditions imposed by the experimental apparatus. The experimental boundary conditions required some level of fixation of the superior and inferior vertebral bodies. To fix the vertebrae in the simulations, rigid body material properties were applied to the bony endplates at the superior end of the superior vertebral body and the inferior end of the inferior vertebral body. Making the endplates rigid allowed boundary conditions to be enforced that could represent fixed-fixed or include various modes of translation and rotation as required. A comparable approach was used for the upper cervical spine segment. In this case, the skull was implemented as a rigid body along with the inferior bony endplate of the C2 vertebral body. Another advantage to using rigid bodies to apply the boundary conditions was the binary outputs that recorded resultant forces, moments and displacement. This allowed for efficient data processing providing force-displacement or moment-rotational displacement curves that were comparable to the experimental results.

The loading was applied to each simulation using a velocity-time curve or a displacement-time curve depending on the case. The experimental data provided straightforward descriptions of the load time allowing for the creation of velocity-time curves. The data from the flexion and extension cases was more readily converted into a displacement-time curve. In both situations, the load curves were applied to the rigid bodies of the appropriate vertebral body depending on the simulation case. The compression simulation required an additional displacement-time curve to account for a 40 N preload used in the experiment conducted by Carter et al. (2002).

Simulations were solved using the commercial finite element software LS-DYNA (LSTC, Livermore, CA) version 971 R3.2.1 using single precision calculations on a Linux workstation. For the lower cervical spine, the tension, flexion, and extension model contained 15829 nodes and 22700 elements with a simulation time of approximately 4 hours using eight 2.2GHz processors. The compression model contained 32147 nodes and 46599 elements with a simulation time of approximately 45 minutes using eight 2.2 GHz processors. The upper cervical spine segment model used in tension, flexion, extension and axial rotation contained 21423 nodes and 22365 elements. In flexion and extension the model had a simulation time of approximately four hours using eight 2.2 GHz processors while the axial rotation cases had a simulation time of approximately 12 hours using eight 2.2 GHz processors. The tension cases were the most computationally expensive, taking approximately 40 hours using eight 2.2 GHz processors. The discrepancy in the simulation time can be accounted for in the variation between the experimental studies. The duration of the simulated tension tests case required a longer overall computation time than the simulated axial rotation, flexion and extension cases.

 A mesh convergence study was conducted on the compression simulation to determine an acceptable element size. Mesh sizes of 1, 0.5, and 0.25 mm were compared. Larger mesh sizes were not considered since they did not accurately represent the vertebral body geometry. The results from each simulation converged to a similar value and a final mesh size of 1 mm was chosen. While a smaller mesh size is ideal for smoother transitions over

complicated geometry, the computational expense is very high. Decreasing the mesh size to 0.5 mm increased the run time by approximately 4 times, approximately 17 hours versus 4 hours, which was undesirable for the scope of this study.

Chapter 5

Cervical Spine Segment Model Validation

5.1 Failure Validation Cases

Once the model was updated to include material properties capable of representing tissue damage and failure, the model required verification and validation under injurious loading conditions. The segments were evaluated under tension, compression, flexion, extension, and axial rotation. The experimental studies chosen as verification and validation are detailed below as an introduction to the simulated results presented for each mode of loading.

To validate the segment models in tension to failure, the experimental study conducted by Dibb et al. (2009) was chosen. In this experiment, tensile tests were conducted on the full cervical spine, as well as three spine segment levels; C012, C45, and C67. In this validations case, only the segment level results from C45 and C012 were considered. To test the specimen, the apparatus pulled the inferior vertebral body loading the segment in tension. An eccentricity bracket was used for the lower segments to maintain the lordotic orientation of the segment to represent in vivo conditions. Segments from each level were then tested to failure at a rate of 1000N/s. Under failure conditions, the superior end of the segment was held to the apparatus such that it was able to translate in the anterior-posterior direction and rotate into the sagittal plane, while the lower end was fixed, unable to translate or rotate in any direction.

The detailed descriptions of the boundary conditions used in the experimental testing making it an ideal case to use for validation. The loading was explicit and reproducible as a numerical load. It also provided average failure forces and displacements for each segment level as wells as a plotted example of the failure response of each segment level. The

80

important failure values used in the validation included the C45 segments with a measured mean failure force (±SD) of 1700 ± 199 N at an axial displacement of 7.7 ± 2.0 mm, and the C012 segment tests resulted in a higher mean failure force of 2417 ± 215 N at a failure displacement of 10.8 ± 3.9 mm. Additionally, the injuries observed in the testing were well documented for easy comparison against the numerical results. The most widely recognized injuries for C45 included complete joint disruption of the ligaments and disc, and for C012, also reported complete joint disruption of the ligaments and in some cases, odontoid fracture.

Flexion and extension validation was carried out using the experimental results from Nightingale et al. (2002, 2007). In 2002, Nightingale et al. focused on flexion and extension testing for range of motion and failure limits using an exclusively female sample group which were then used for comparison in a follow-up study in 2007 consisting of an exclusively male sample group. For this validation, only the experimental results from Nightingale et al. (2007) were considered since the numerical model used was representative of a 50th percentile male subject. Similar to the tension case, Nightingale et al. (2007) tested three cervical spine segment levels; OC2, C45, and C67. The lower cervical spine segments were fixed from the inferior vertebral body and the moment was applied to the superior vertebral body, and the upper cervical spine segments, the specimen were inverted such that the cephalad end was secured using a halo fixation, with the load was applied to the casting of the C2 vertebra. The failure simulations were loaded at an approximate rate of 90 N/s. The test procedure documented enabled accurate boundary conditions to be implemented into the material model. Detailed accounts of the injuries observed at each segment level allowed for direct comparison with the numerical results. The notable injuries included severe soft tissue damage in flexion and extension in C45 and C012. Additionally, the extension tests produced some associated bone fractures in both the C45 and C012. Average failure moments and angular displacements were recorded for each segment level. The results of interest reported mean failure moments and rotational displacements (±SD) of 19.2 ± 2.8 Nm at 13.1 ± 3.4 deg in flexion and 15.6 ± 3.3 Nm at 13.0 ±

7.5 deg for C45, and 39.0 ± 6.3 Nm at 58.7 ± 5.1 deg in flexion and 49.5 ± 17.5 Nm at 42.4 ± 8.0 deg in extension for C012.

Compression validation was carried out in an experimental study conducted by Carter et al. (2002). In order to understand the response under compressive loading, function spinal units (FSU) containing three vertebral bodies and two discs were tested. This type of segment allows for the response of the middle vertebral body of the segment to be observed whereas in a segment containing only two vertebral bodies the response of the bone can be affected by the experimental mounting. A variety of different FSU's were tested ranging from C2-C4 to C6-T1 where each was mounted to a fixture and compressed. The study tested pure axial compression, as well as eccentric loading with compression-flexion and compression-extension. During the experiment, both the superior and inferior vertebral bodies were subject to fixed end conditions. The FSU was initially preloaded to a level of 40N to represent the load of the head and then was loaded by a ram displacement of between 8mm and 15mm over a 16ms pulse length. The failure force was measured using a load cell at the centroid of the inferior intervertebral disc. For this validation case, only the results from the pure axial compression test were considered. The detailed account of the testing conditions and apparatus made it an ideal case for validation, and the segment model used in the compression simulations was C567 segment because four out of the eight FSU's tested in axial compression were made up of C567. The experimental results showed a mean compressive force at failure was 3260.9 N with a 95% CI of 707.7 N and a displacement of 2.91 mm with a 95% CI of 0.48 mm. This study primarily focused on comparing failure values to existing neck injury criteria and did not have as detailed account of observed injuries. However, other clinical studies, specifically Denis (1983), provided insight into injuries expected under compressive loading. The most frequently observed compression injuries include compression fractures and burst fractures to the middle vertebral body. It should be noted that the upper cervical spine was not validated under compression due to lack of experimental data.

Geol et al. (1990) studied the response of the upper cervical spine segment (C012) in axial rotation until failure. The testing procedures were well documented and the results were inclusive with detailed plots and concise injury descriptions making it an ideal validation case. For testing, the segments were fixed to the apparatus such that C2 was only allowed to move in axial rotation. The skull portion of the segment was attached to allow for all motions (flexion, extension, lateral bending as well as, translation axially, laterally and anterior/posterior) except for axial rotation. Segments were tested by applying an axial rotation at a rate of approximately 4 deg/s. There was a small initial preload of approximately 2.7 N caused by the apparatus. Each segment was tested to failure and the resulting angular displacement and load at failure was recorded. The experimental results give mean failure values of 13.6 ± 4.5 Nm at 68.1 ± 13.1 deg. The average response of the segments was graphed to show the progressive response of the segment up until failure noting that there was a significant amount of rotation before the segment engaged and bore a load. Following each test, the segment was dissected to assess the quality of the segment and the integrity of the ligaments and report any observed injuries. The most frequent injuries reported were capsular ligament tears at the C1-C2 level.

5.2   Lower Cervical Spine Segment Validation

The simulation results for all four loading cases produced failure values that fell within the corridors of the experimental data. The simulated responses also produced tissue failures representative of the injuries observed in the experimental studies. Results are presented based on the applied load case with an additional section presenting qualitative fracture results for flexion, extension and compression.

5.2.1   Tension

The average results presented by Dibb et al. (2009) are represented in the plot as a red square with the standard deviations for displacement and force represented as a box around the average. The simulated results fell outside the corridors for failure force and just inside for ultimate failure displacement (Fig. 5-1). The soft tissue failure represented in the simulation was dominated by the failure of the disc. As the disc avulsion progressed, failure

was observed in both the ALL and PLL, initiating with the PLL. The injuries observed in the simulations show good agreement with the injuries described in the results of the experimental testing.
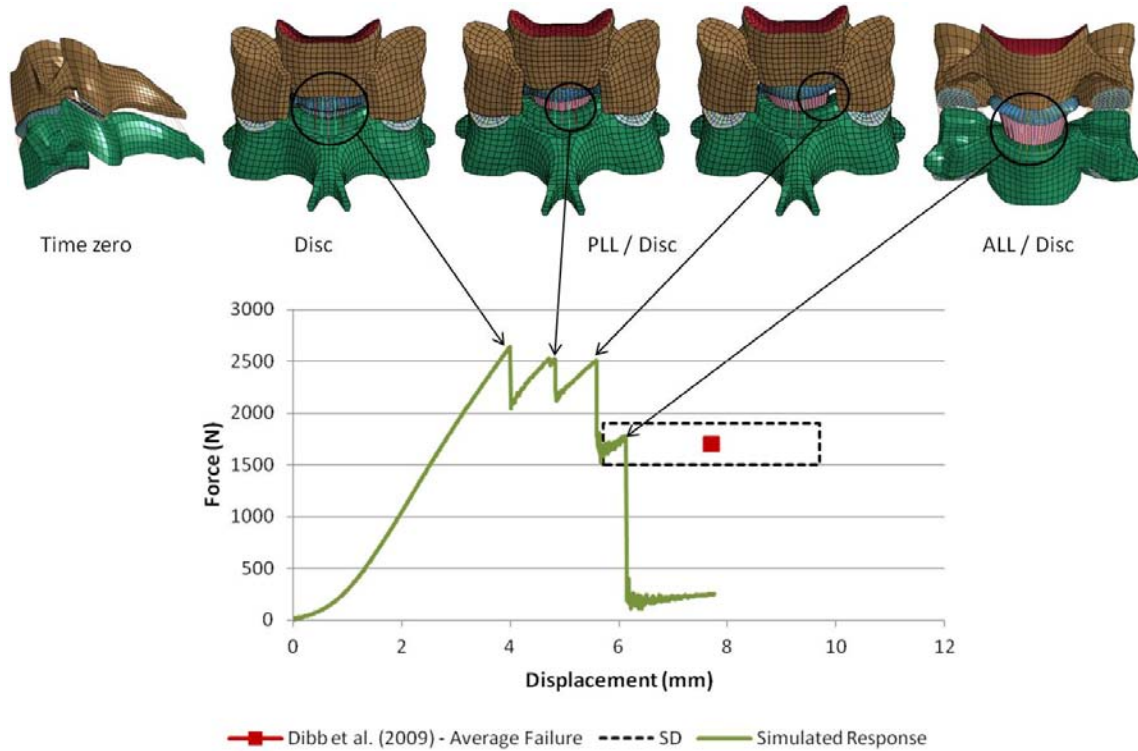
Figure 5 - 1: Tension Simulation Results (C4 Spinous Process Removed for Clarity)

5.2.2   Flexion and Extension

Similar to the tension case, the average experimental result is denoted with a red square with the standard deviations for rotational displacement and moment represented by the box around the average value (Fig. 5-2). Also plotted is an experimental flexion result of a C45 segment tested by Nightingale et al. (2007). In this case, the simulation represented the experimental data extremely well falling within the corridors for both failure moment and rotational displacement. The flexion simulation showed failure initiating with the ISL and LF at the posterior of the segment. As the segment continued to flex, failure progressed to the posterior interface of the lower vertebral body and the disc, culminating with disc avulsion and PLL failure. The failure moment was determined as the peak moment before a

significant drop in force occurred, and rotational displacement at failure was taken as the displacement at the aforementioned moment.
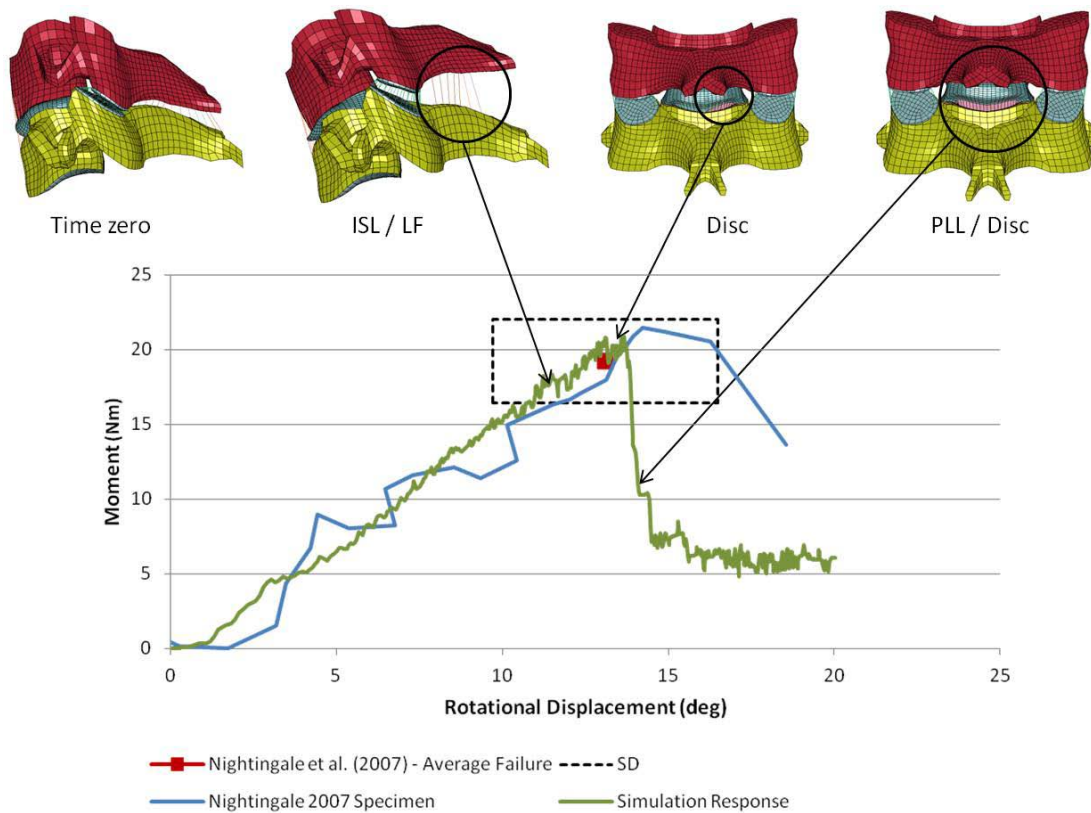
Figure 5 - 2: Flexion Simulation Results

Failure in extension initiated with the onset of fracture at the posterior pedicles of the facets in the upper vertebral body (Fig. 5-3). As the segment extended further, the anterior-lateral interface of the disc and upper vertebral body began to tear. The moment and rotational displacement of ultimate failure was recorded when the disc avulsed and the ALL failed completely causing a significant drop in the resultant moment. Ultimate failure of the simulated test occurred within the bounds for rotational displacement and just outside the bounds for the final failure moment.
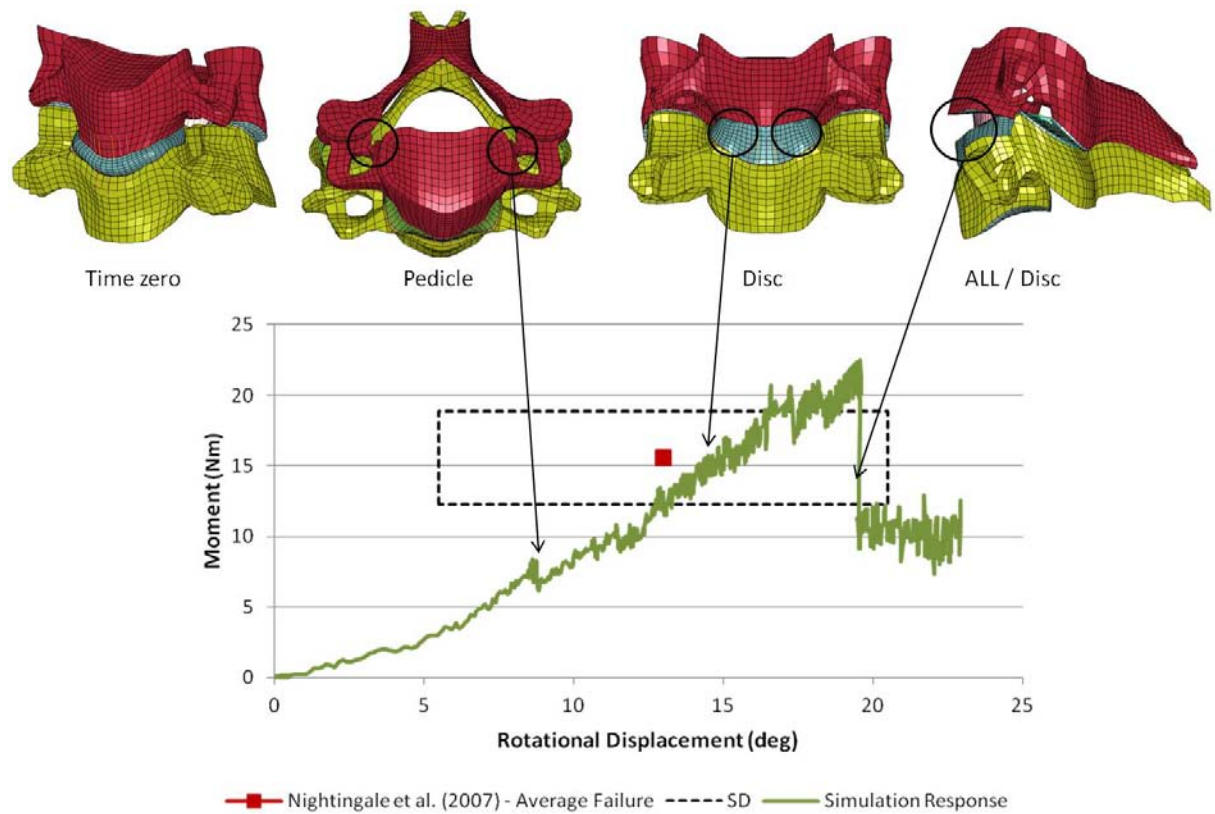
Figure 5 - 3: Extension Simulation Results

5.2.3 Compression

In compression, the failure observed occurred in the cortical and cancellous bone of the middle vertebral body. The simulation showed the failure location to be primarily at the superior bony endplate from the midline to the anterior portion of the column. Similar to the tension case, the peak failure force was determined by a significant drop in the load (Fig. 5-4). The peak failure occurs within the corridors for failure force falling just outside the failure displacement corridors. The simulation results for all four loading cases in comparison with their respective experimental studies are presented in Table 5-1.
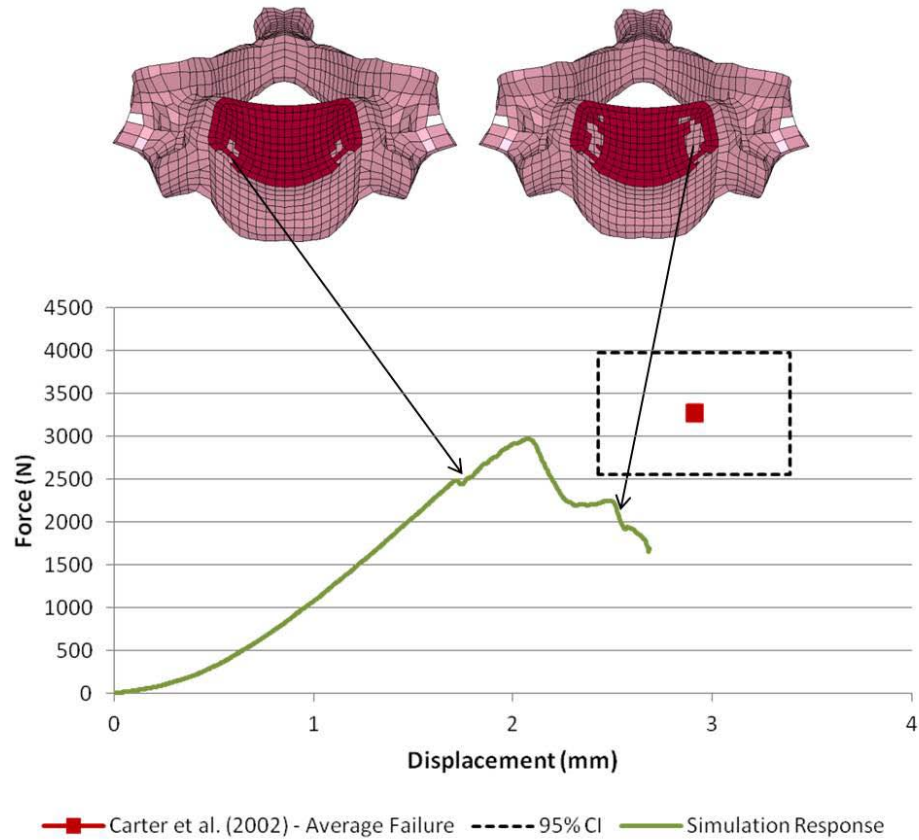
Figure 5 - 4: Compression Simulation Results

Table 5 - 1: Summary of Lower Segment Results

Load Case	Experimental Study	Failure Details		Simulation Results
Tension	Dibb et al. (2009)	Force (N)	1700±199	2639
		Disp. (mm)	6.8±2.0 (major)	3.9 (major)
			7.7±2.0 (ultimate)	5.7 (ultimate)
Flexion	Nightingale et al. (2007)	Moment (Nm)	19.2±2.8	20.9
		Rotational Disp. (deg)	13.1±3.4	13.7
Extension	Nightingale et al. (2007)	Moment (Nm)	15.6±3.3	22.4
		Rotational Disp. (deg)	13.0±7.5	19.6
Compression	Carter et al. (2002)	Force (N)	3261±708	2971
		Disp. (mm)	2.9±0.48	2.1

5.2.4 Qualitative Results – Lower Cervical Spine

In addition to quantitative failure results, the simulations were also able to provide insight into potential fracture locations for flexion, extension and compression by observing areas of elevated stress. The areas of elevated stress are helpful in depicting potential injuries as multiple tissues may be close to failure at the same time. In the extension case, fracture initiated at the posterior pedicle of the facets. Just prior to this fracture the model showed a significant elevation in stress at this location (Fig. 5-5).
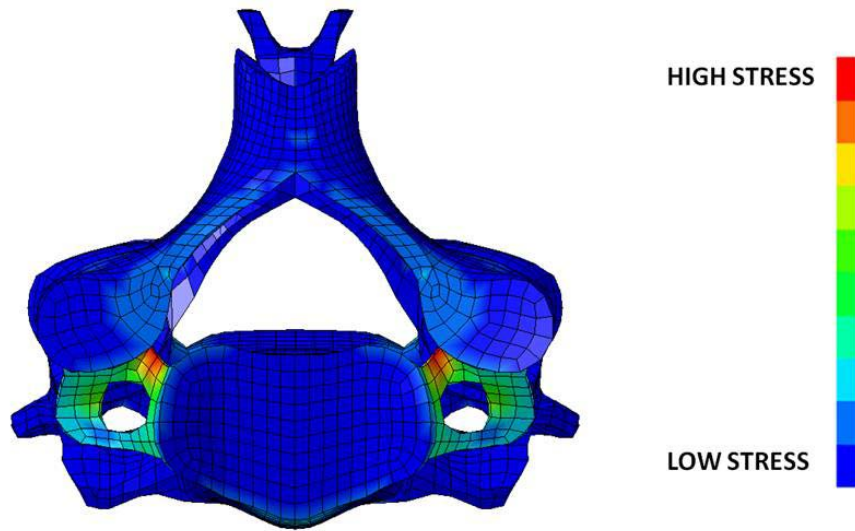
Figure 5 - 5: High Stress Level at Pedicles Immediately Prior to Fracture

In addition to the facet area, other fracture locations (Fig. 5-6) reported in flexion and extension were the spinous process, and anterior body.
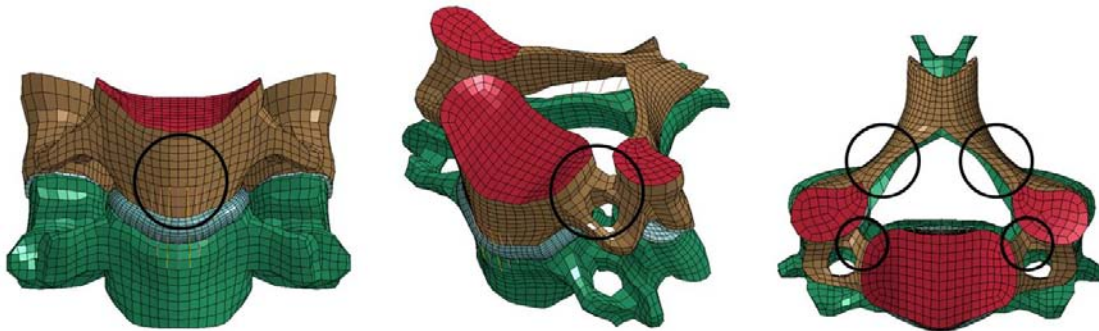
Figure 5 - 6: Reported Fracture Locations in Flexion and Extension

Both the flexion (Fig. 5-7) and extension (Fig. 5-8) simulations showed elevated stress levels in these areas prior to and immediately following the reported failure.
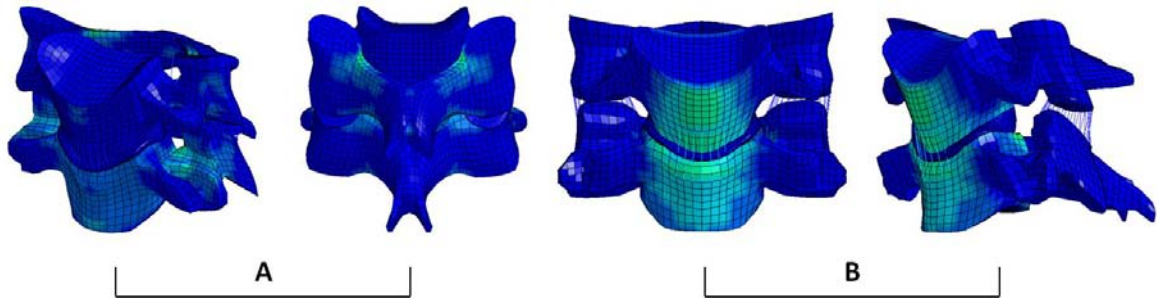
Figure 5 - 7: Stress Levels Before (A) and After (B) Observed Failure in Flexion
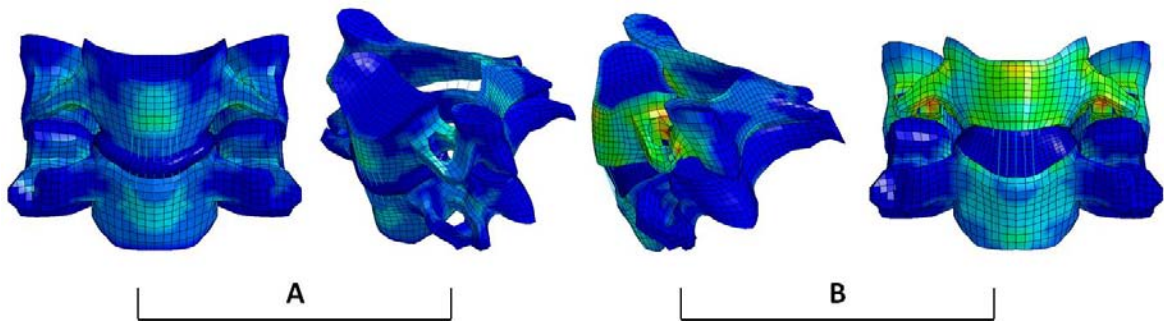
Figure 5 - 8: Stress Levels Before (A) and After (B) Observed Failure in Extension

Similar results were found in the compression case. Fracture initiated at the superior bony endplate of C6 where, again, the model showed high localized stress (Fig. 5-9) immediately before fracture onset.
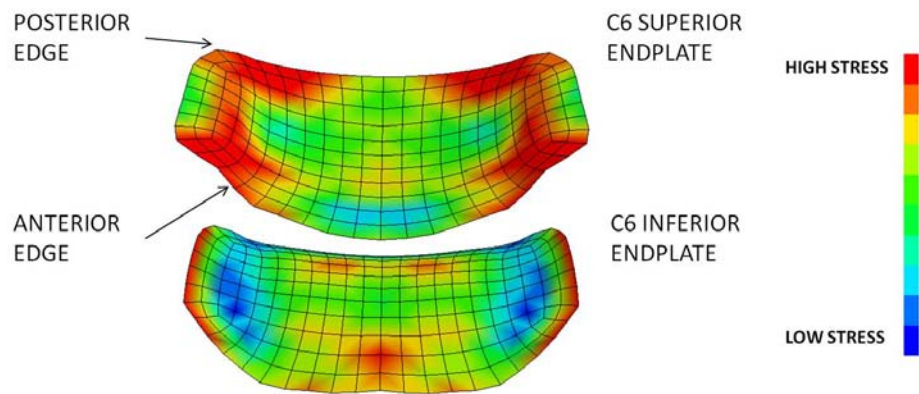
Figure 5 - 9: High Localized Stress on the Superior Bony Endplate

Compression fractures and burst fractures are the most frequent fracture observed in compression. Fracture onsets for these cases occur in various locations on the vertebral body (Fig. 5-10) and the stress composition before and after the endplate fracture show elevated stress in these locations (Fig. 5-11).
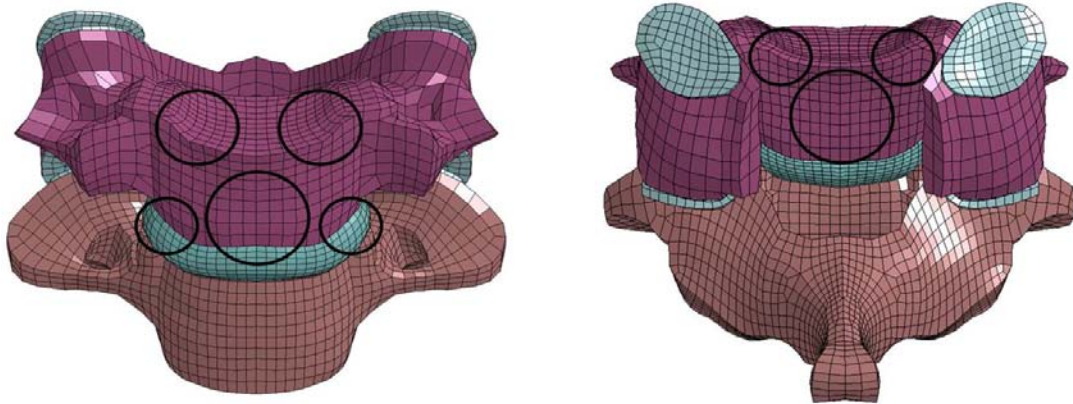
Figure 5 - 10: Fracture Locations for Compression and Burst Fractures (C5 vertebral body and C6 spinous process removed for clarity)
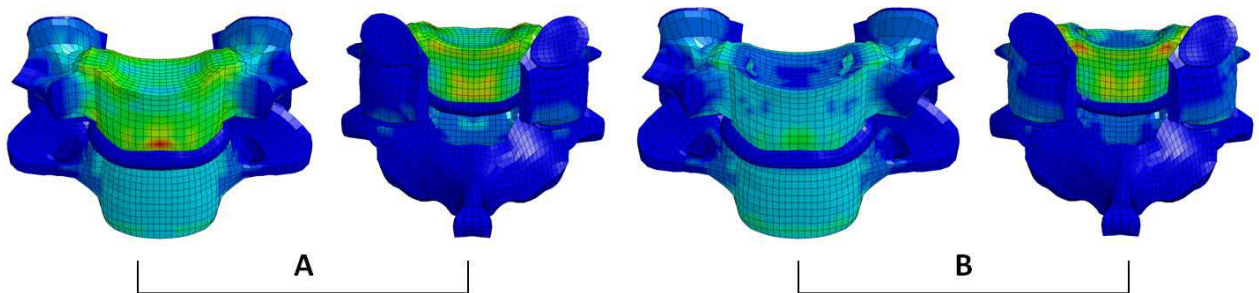
Figure 5 - 11: Stress Levels Before (A) and After (B) Observed Failure

5.3   Upper Cervical Spine Segment Validation

The simulation results for all four loading cases produced results that fell within the experimental corridors of the validation cases. Additionally, the tissue damage observed in the simulations matched well to the observed injuries in the experimental studies. Similar to the lower cervical spine, results are presented based on the applied load case with an additional section presenting the qualitative analysis.

5.3.1 Tension

The results for the failure simulation (Fig. 5-12) matched well to the experimental results from Dibb et al. (2009). The simulation approached the corridor and failed within the expected failure displacement but just above the corridor for failure force. Failure initiated with the soft tissues at the anterior of the segment; specifically the AAAM followed by the capsular ligaments between C1 and C2. As the segment continued to distract, the posterior elements began to fail (PAAM) as well as some of the ligaments inserting off the superior end of the odontoid (Apical, TM). There was no fracture during the simulation. Dibb et al. (2009) reported some Type III (base) fractures of the odontoid during testing. As discussed below, the simulation did show elevated stress in this area; however, the severe ligament damage agreed with the other injuries reported in Dibb et al. (2009).
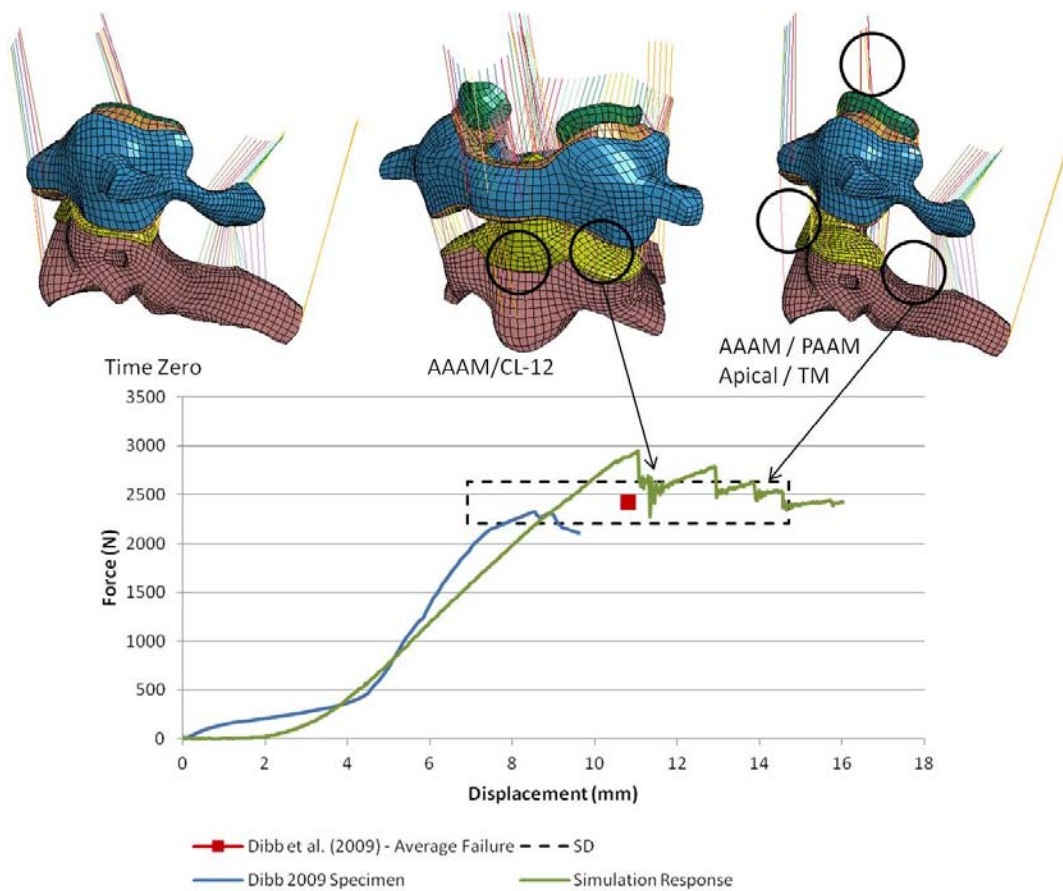
Figure 5 - 12: Simulated Results for C012 under Tensile Loading

5.3.2 Flexion and Extension

The simulated flexion case showed good agreement with the experimental averages, as well as the experimental test result from Nightingale et al. (2007) with comparable stiffness and ultimate failure (Fig. 5-13). There was an initial failure onset that fell within the corridors for rotational displacement with a slightly low failure moment, however; the results did show some failure within the experimental corridors. The failures initiated with the posterior soft tissues, first with minor tears to the PAAM, and then more serious tears to the PAAM and PAOM. The PAAM was torn completely and the PAOM had a severe tear just prior to ultimate failure when the segment fractured at the odontoid. These simulated injuries fall in line with the observed injuries reported in Nightingale et al. (2002, 2007).
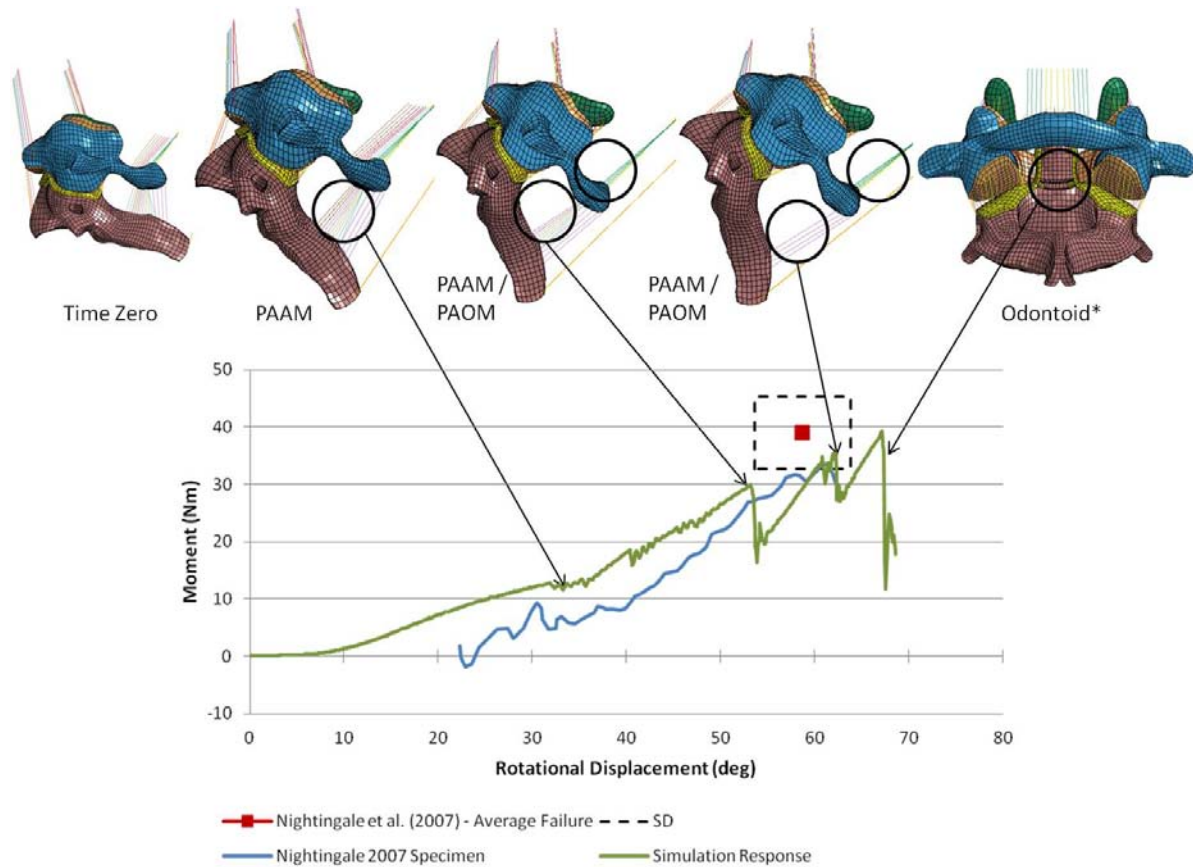
Figure 5 - 13: Simulated Results for C012 under Flexion Loading (*Some Ligaments Removed for Clarity)

The simulated results in extension showed reasonable agreement with the experimental averages reported by Nightingale et al. (2007) (Fig. 5-14). Failure occurred within the corridors for rotational displacement but did not reach the corridors for failure moment. The injuries produced in the simulation did not agree with those reported in the experimental tests but the simulation did show elevated levels of stress in reported fracture locations discussed further below. The observed injuries in the simulations included tearing of the AAAM and fracture of the C1 lamina. Interpretations of these injuries and why they occurred in the simulations are further discussed in the discussion section.
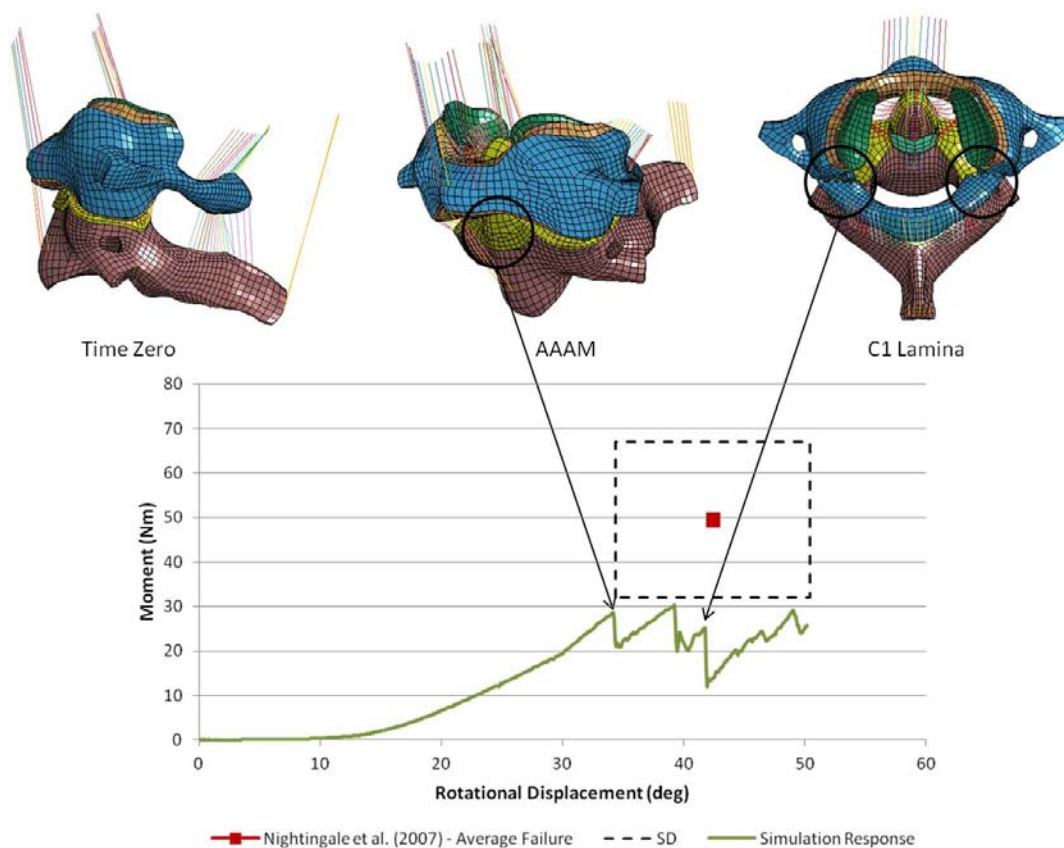
Figure 5 - 14: Simulated Results for C012 under Extension Loading

5.3.3 Axial Rotation

The simulated response in axial rotation showed good agreement with the experimental results from Goel et al. (1990). Although the ligaments engaged at an earlier rotational displacement, it matched the stiffness of the experimental results and failed with the

corridors for expected failure moment (Fig. 5-15). The injuries patterns observed in the simulation matched closely with the experimental injuries observed. Goel et al. (1990) reported rupture of the CL-12 and PAAM in all experimental cases, which is what the simulation produced. It should also be noted that the experimental data noted that in all cases, the TL, CL-01, AAOM, PAOM, apical and AAAM were intact in all case. This was also reflected in the simulated results. The simulation results for all four loading cases in comparison with their respective experimental studies are presented in Table 5-2
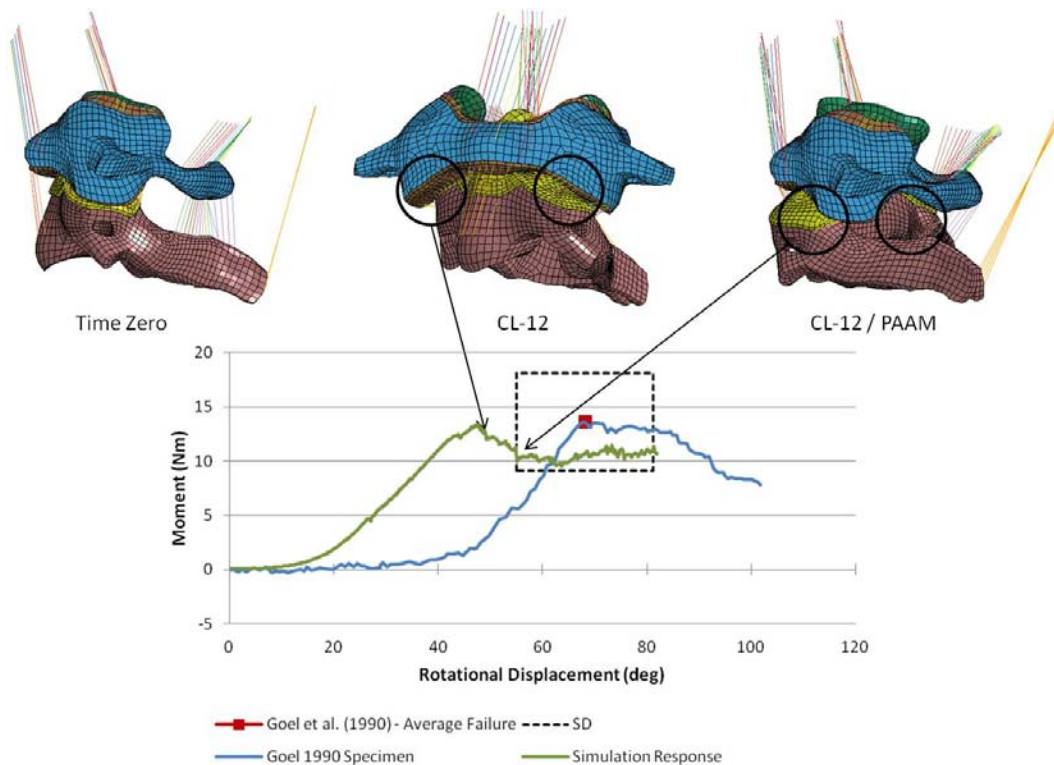
Figure 5 - 15: Simulated Response for C012 under Axial Rotation

Table 5 - 2: Summary of Upper Segment Results

Load Case	Experimental Study	Failure Details		Simulation Results
Tension	Dibb et al. (2009)	Force (N)	2417±215	2946
		Disp. (mm)	9.1±1.6 (major)	--
			10.8±3.9 (ultimate)	11.0 (ultimate)
Flexion	Nightingale et al. (2007)	Moment (Nm)	39.0±6.3	39.3
		Rotational Disp. (deg)	58.7±5.1	67.1
Extension	Nightingale et al. (2007)	Moment (Nm)	49.5±17.5	30.4
		Rotational Disp. (deg)	42.4±8.0	39.3
Axial Rotation	Goel et al. (1990)	Moment (Nm)	13.6±4.5	13.4
		Rotational Disp. (deg)	68.1±13.1	47.8

5.3.4 Qualitative Results – Upper Cervical Spine

Similar to the lower cervical spine segments, quantitative observations of higher stress levels can provide valuable insight into potential fracture locations. Based on experimental testing results from Dibb et al. (2009); Nightingale et al. (2002, 2007); and Van Ee et al. (2000), the majority of fractures to the upper cervical spine occur under tension and extension loading. There were also a few reported fractures in flexion reported by Nightingale et al. (2002, 2007) and in axial rotation as reported by Goel et al. (1990). The primary locations for fracture in the upper cervical spine are the odontoid (Type I, II and III), the C2 lamina and spinous process, and the C2 anterior pedicles (Hangman's fracture) (Fig. 5-16)
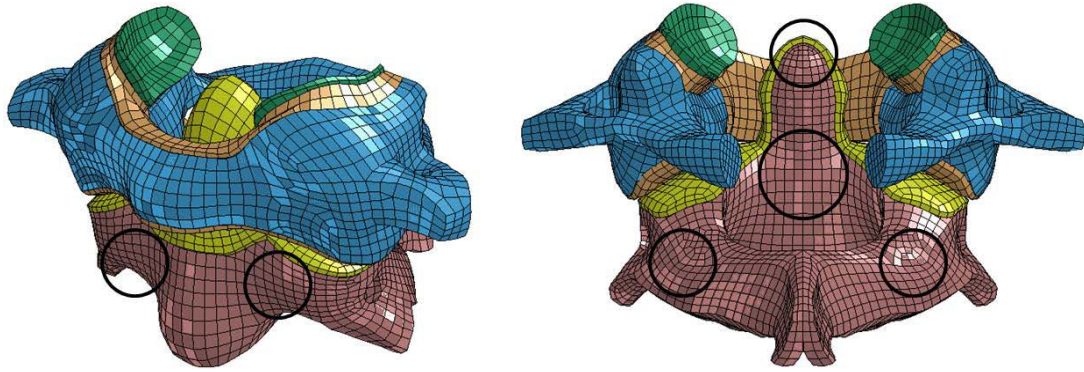
Figure 5 - 16: Primary Fracture Locations of the Upper Cervical Spine (Posterior Portion of C1 and Ligaments Removed for Clarity)

The simulated tension case showed elevated stress on the odontoid at the base as well as at the superior end (Fig. 5-17). These are areas associated with Type III odontoid fracture (base) and Type I odontoid fracture (superior end). The high stress at the superior end of the odontoid could also indicate the potential for an avulsion fracture at the insertion of the apical or TM ligament; an injury also observed under tensile loading.
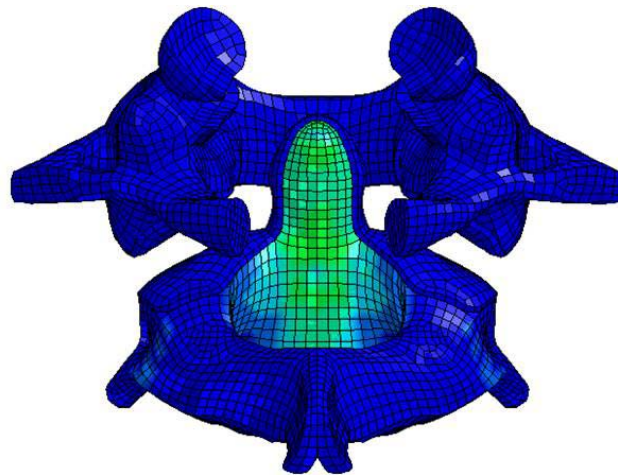
Figure 5 - 17: Areas of Elevated Stress in the Odontoid Under Tensile Loading

In the flexion tests by Nightingale et al. (2002, 2007) only three fractures were reported. In all cases, the fractures were reported as Type III odontoid fractures which agreed with the fracture observed in the simulation. As expected, the location of elevated stress levels in the odontoid prior to fracture was consistent with the location of this type of fracture (Fig. 5-18).
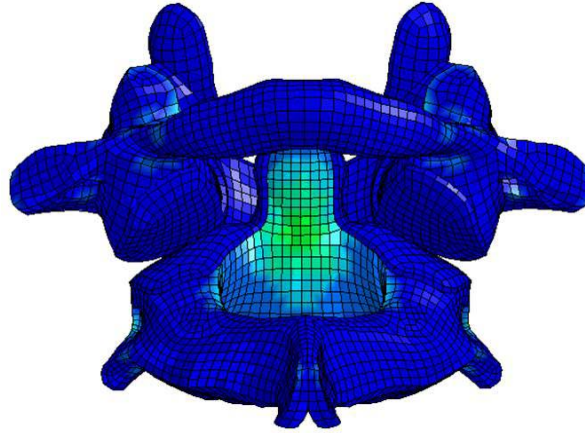
Figure 5 - 18: Areas of Elevated Stress in the Upper Cervical Spine under Flexion Loading (Ligaments Removed for Clarity)

The extension case also showed elevated stress at the base of the odontoid indicative of a Type III odontoid fracture (Fig. 5-19). Type III odontoid fractures were a commonly reported fracture in extension loading. There was additional stress elevation at the C2 lamina which was a reported fracture site in Nightingale et al. (2002). The majority of the stress concentration in the extension case was found at the C1 lamina which will be discussed further in the sections below.
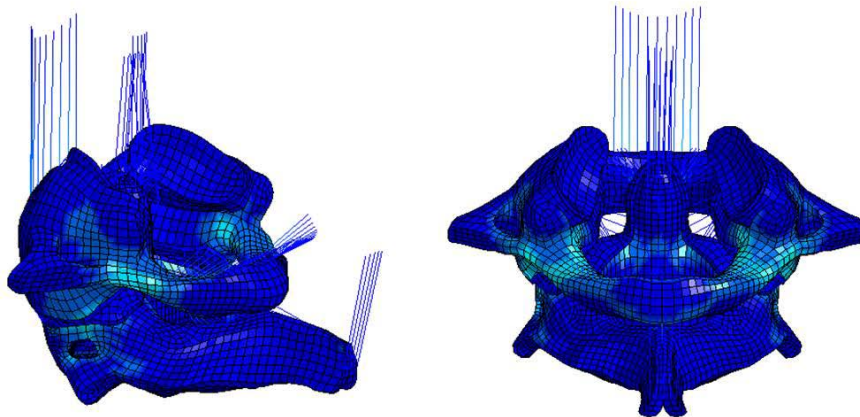
Figure 5 - 19: Areas of Elevated Stress in the Upper Cervical Spine under Extension Loading

In axial rotation, the simulation showed elevated stress where the odontoid extends from the vertebral body (Fig. 5-20). The experimental results from Goel et al. (1990) mentioned

97

that odontoid fracture occurred in four of their tests. In all four cases the fracture was associated with the odontoid with two out of four being Type II odontoid fractures (vertebral body/odontoid interface). The other two fractures were associated with ligament insertions near the tip of the odontoid and laterally at the alars insertion. There was some stress elevation at these locations, but not as prominent as the stress elevation in areas corresponding to the Type II and Type III odontoid fracture.
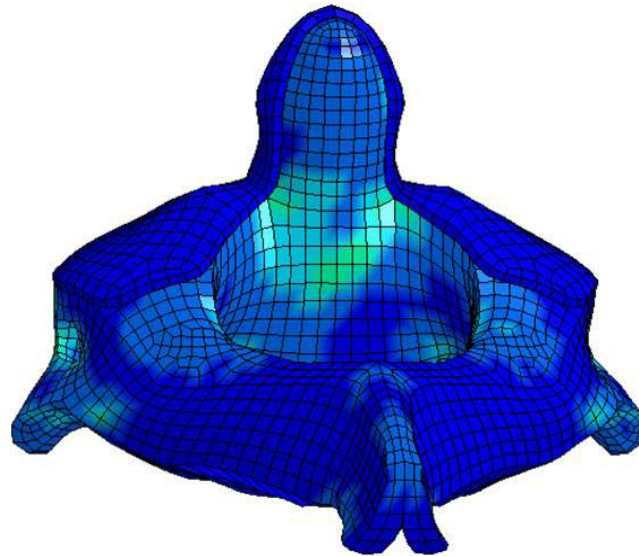
Figure 5 - 20: Areas of Elevated Stress in the Upper Cervical Spine under Axial Rotation Loading (C1 Vertebral Body and Ligaments removed for Clarity)

5.4 Discussion

5.4.1 Lower Cervical Spine – Tension

The injuries predicted in the tensile simulations were indicative of severe sprains to the ligaments, particularly the ALL and PLL. The order and location of failure agree with the observations in the clinical study by Argenson et al. (1997) that showed severe sprains to be the most common injury associated with tensile loading. It should also be noted that severe sprains were the second most severe injury observed under tensile loading (Argenson et al. 1997).

The simulation predicted failure to initiate at the disc, followed by the PLL and the ALL. The results from Dibb et al. (2009) did not indicate the failure sequence for the soft tissue but

only a final summation described as total joint disruption including ligament and disc tearing. This was well represented in the failures produced by the simulation. The boundary conditions for the experiment by Dibb et al. (2009) were duplicated in the simulation and likely had some influence on the sequence of tissue failure. The superior vertebral body was attached to the fixture using an eccentricity bracket to maintain the lordotic orientation of the C45 segment. For failure simulations, the upper vertebral body was held with a 'free cephalad' end condition. In the case of the lower cervical spine segments, this meant that the top of the eccentricity bracket was allowed to translate in the anterior-posterior direction and rotate in the sagittal plane. Because the segments were loaded aligned with the head center of gravity (CG), a small amount of extension was induced in the tension test leading to additional stresses to the anterior portion of the segment. In addition to the soft tissue damage reported by Dibb et al. (2009), a C4 body fracture was observed along with the complete joint disruption in 6 out of 20 cases, where four of the six fractures were associated with the fixation. This was consistent with the low incidence of fractures under pure tensile loading.

The simulation results predicted a failure force of 2639 N falling outside the corridors (1700 ± 199 N) presented in the experimental data from Dibb et al. (2009). The failure displacement of 3.9 mm produced in the simulation also fell just outside the reported corridors (7.7 ± 2.0 mm). The simulated response showed distinct failure peaks likely caused by the abrupt failure of the intervertebral discs. The tie-break contact results in an abrupt failure once a certain stress is attained which would account for the significant drop in the load. In reality, failure of the annulus fibrosus is not a catastrophic event, but more of a progressive failure similar to ligaments (Pezowicz et al. 2005). An initial tear occurs at the endplate but does not immediately propagate through the tissue as the load is redistributed among the remaining intact fibres (Pezowicz et al. 2005). Once a sufficient amount of damage is incurred, full separation occurs. There is also the possibility of shear failure between the AF layers and the AF ground substance (Fujita et al. 1997; Goel et al. 1995). Shear stresses result in delamination of the AF layers initiating the propagation of further disc damage (Iatridis et

al. 2005; Iatridis and ap Gwynn, 2004). If the disc was able to fail in a more progressive manner, the multiple failure peaks would likely be eliminated and be more representative of the major failures observed by Dibb et al. (2009) prior to ultimate failure. Dibb et al. (2009) defined major failure as a 10% decrease in the load, or a 20% decrease in the material stiffness. Additionally, a more progressive disc failure would delay the ultimate failure and improve the simulations predicted failure displacement.

5.4.2 Lower Cervical Spine – Flexion and Extension

The flexion and extension simulations predicted similar soft tissue injuries to those described in Nightingale et al. (2007). For the lower cervical spine segments, Nightingale reported complete disruption of the ligamentous structures between the vertebrae, as well as the disc. The extension simulations demonstrated fractures to the posterior pedicles near the facet joints while the flexion simulations produced no fractures. Nightingale et al. (2007) reported minor fractures of the spinous process, anterior body, or facets in 9 out of 26 segment failures where two of the nine fractures were associated with the fixation. It was not indicated whether the specific fractures resulted from the flexion or extension tests. As mentioned previously in the tension case, the simulation of failure associated with disc avulsion has some shortcomings. This could account for why anterior body fractures were not observed in the flexion simulation.

The flexion simulation predicted a failure moment of 20.9 Nm at a rotational displacement of 13.7 deg showing excellent agreement with the experimental averages in both failure moment (19.2 ± 2.8 Nm) and rotational displacement (13.1 ± 3.4 deg) from Nightingale et al. (2007). In addition to the excellent agreement with the experimental average, it was observed that, when plotted against a segment result from Nightingale et al. (2007), the simulation followed the experimental curve very well. The only notable difference was in the time to failure where the experimental segment had a more gradual failure compared to the simulation which resulted in a more abrupt failure. This difference could be attributed to the abrupt nature of the simulated disc failure in the current material model of the disc.

The extension simulation predicted a failure moment of 22.4 Nm at a rotational displacement of 19.6 deg also showing good agreement with the experimental results (15.6 ± 3.3 Nm, 13.0 ± 7.5 deg) from Nightingale et al. (2007). The failure moment predicted by the simulation in extension was on the upper edge of the experimental corridors. This could be attributed to how the fracture patterns propagate with the element erosion. In this case, fracture initiated at the posterior pedicles near the facets and elements in that area continued to erode as they reached the prescribed strain to failure. The erosion delayed the onset of the ligament and disc failure potentially leading to a higher moment at failure.

As noted previously, Nightingale et al. (2007) reported fractures in their experimental results. Although it was not indicated if the fractures occurred under flexion or extension, there are clinical studies that report that both flexion and extension loading can result in fractures (Argenson et al. 1997). While the extension simulation was the only case that produced an actual fracture, there were other results from the flexion and extension simulations that provided insight into potential fracture locations. By observing areas of elevated stress within the model, direct comparisons were made between these areas of elevated stress and locations of reported fractures. Specific to the flexion case, following the soft tissue failure, there was an increase in stress in the anterior body of C4, an area associated with fracture. It is possible that, due to the above mentioned limitations with the simulated disc failure, a fracture could have occurred at this location had the disc failed in a more gradual manner. Similar observations were made in the extension simulation. Initial observations showed elevated stress in all the reported fracture locations. After the fracture onset and immediately following the disc avulsion, observed stress levels at the facets had increased significantly while the spinous process only showed a small elevation. Both of these areas would be expected to carry additional load once the disc avulsed. A possible reason for the larger increase in stress near the facets as opposed to the spinous process could be related to how the elements erode. The erosion of elements caused an increased stress level in the immediate surrounding area whereas in an actual bone fracture, volume would not be eliminated in the same way resulting in a more even stress distribution.

101

5.4.3 Lower Cervical Spine – Compression

The experimental results from Carter et al. (2002) did not report observed injuries along with their failure values. To compare the injuries observed in the simulations, other clinical cases were considered. Injury locations predicted from the compression simulations showed good agreement with the injuries reported in clinical studies by Argenson et al. (1997), and Yoganandan et al. (1989b). The element erosion observed in the simulation indicated the onset of fracture at the superior bony endplate of C6. In a clinical study of over 400 spinal injuries conducted by Denis, (1983), it was noted that compression and burst fractures where among the most common vertebral fractures. A compression fracture is confirmed when only the mid to anterior portion of the vertebral body is fractured while a burst fracture also includes fractures to the posterior of the vertebral body and into the laminae. Denis, (1983), observed that 62.4% of the 256 compressive fracture cases initiated at the superior bony endplate and, for burst fractures specifically, 49.2% of fractures initiate at the superior endplate in the middle to anterior portion of the vertebral column. The locations of the elements eroded at failure showed good agreement with the fracture locations from clinical observations. This indicated that the simulation was able to predict the location of the onset of a compression fracture.

The failure force of 2971 N predicted in the simulations showed good agreement with the experimental results (3261 ± 708 N) from Carter et al. (2002). The final displacement to failure of 2.1 mm was somewhat lower than the observed experimental values (2.9 ± 0.48 mm) indicating that the simulation response was stiffer than desired. A possible explanation for this could be how the failure is modeled in the cancellous bone. Elements are eroded once they reach the prescribed strain to failure removing material from the model. This caused a sharp drop in the load resulting in a premature ultimate failure displacement. In reality, human cancellous bone is a porous material that when compressed to failure, micro-cracks form in the trabecular structures, progressively damaging the tissue until complete fracture (Yeh and Keaveny, 2001). Initiating fracture to this porous structure occurs quickly

but slows as the porosity is reduced with each additional fracture. Replicating this in the model would assist to delay the ultimate failure displacement.

Similar to the flexion and extension cases, a qualitative evaluation of the stress concentration was conducted for the compression case. The highest areas of stress concentration corresponded with the area where fracture initiated while areas of elevated stress corresponded to other areas prone to fracture in compression and burst fractures. Specific to burst fractures, there were areas of increased stress in the posterior vertebral body but not to the laminae. Again, this could be due to the element erosion affecting the stress distribution throughout the vertebral body.

5.4.4   Upper Cervical Spine – Tension

The injuries observed in the upper cervical spine under tensile loading included severe ligament disruption (posterior and capsular ligaments) as well as bone fracture (odontoid). Cusick and Yoganandan, (2002), reported distraction injuries to include disruption of posterior ligaments, odontoid fracture, Hangman's fracture, and occipital condyle dislocation.

The upper cervical spine simulation showed slightly different failure patterns than the lower cervical spine simulation. Due to the nature of the experimental boundary conditions set by Dibb et al. (2009), the segment experiences a small amount of extension at the beginning of the simulation causing failure to initiate with the AAAM and the anterior portion of the CL-12 ligaments. The extension load was induced by the end conditions imposed during the failure tests conducted by Dibb et al. (2009). The skull was held under 'free cephalad' conditions meaning that it was allowed to translate in an anterior-posterior direction, as well as rotate in the sagittal plane with the fixed point of rotation being the head center of gravity (CG). As the simulation continued, additional failures were observed at the PAAM, Apical and TM, along with the continued tearing of the AAAM. The observed soft tissue injuries during the simulation were similar to those reported by Dibb et al. (2009). Several of the experimental tests reported complete joint disruption at the C1-C2 level which

103

corresponds well to the simulated injuries. A number of injuries observed in the experimental testing were reported as odontoid fracture with C1-C2 complete joint disruption. Odontoid fracture was also observed to occur with O-C1 complete joint disruption. Although there was no fracture observed in the simulation, elevated levels of stress were found in all areas of the odontoid indicating the potential for fracture. It is expected there would be elevated stress levels in the odontoid under this type of loading as the majority of the strength in tensile loading comes from the ligaments attached between the occipital condyles and the odontoid. This would transmit a significant amount of stress to the odontoid bone, especially if there was some extension induced as it would effectively load the odontoid like a cantilevered beam. The inability of the simulation to produce an odontoid fracture could be attributed to the variability in the material properties of the bone specimens reported in literature. The failure strains in the bone material properties represent experimental averages within a range data. Small changes plus or minus the averages could have an effect on the simulation results. It is also possible the lack of fracture could be a result of the joint complexity. Although not pursued in these simulations, Dibb et al. (2002) observed significant difference in the number of major failures depending on if the applied load was centered over the head CG or over the occipital condyles. They reported that, for the upper cervical spine segment, there were major failures in 50% of the tested specimen loaded with head CG alignment. The number of major failures increased to 75% when the load was aligned over the occipital condyles. The occipital condyles are located posterior to the head CG and Dibb et al. (2009) noted that the tensile strength of the cervical spine increased with increased anterior eccentricity. Due to the fact that the simulations were loaded in line with the head CG it is probable that the simulation was less likely to produce an odontoid fracture. Additionally, this could also explain why the simulated ultimate failure value falls just above the experimental corridors.

The simulation predicted a failure force of 2946 N at 11.0 mm displacement which fell within the experimental corridors for displacement failure (10.8 ± 3.9 mm) and just above the corridors for failure force (2417 ± 215 N) reported by Dibb et al. (2009). As mentioned

104

previously, the higher than expected failure force could be attributed to the loading aligned with the head CG. Dibb et al. (2009) noted an increase in cervical spine strength as the loading alignment moved in the anterior direction. The response of the simulation followed closely with the experimental test specimen from Dibb et al. (2009) showing strong similarities in stiffness. There is a discrepancy in the shape of the curve where the experimental result shows two distinct slopes that are not captured by the simulation. It also appeared that there was no toe-region representing the ligament engagement in the experimental results presented by Dibb et al. (2009). This could be addressed in the simulation by applying laxity and pretension to different ligaments of the upper cervical spine segment but it was not observed experimentally what ligaments engaged first and what ligaments were delayed. Without knowledge of the engagement order and time to engagement, it is difficult to apply exactly representative laxity and pretension to the simulation. The current pretension and laxity were inferred based on literature reviews of segment and ligament behaviour as well as observation during ligament testing.

Qualitatively, it was observed that the area with the highest stress level was throughout the odontoid. Additional areas of elevated stress were observed near the pedicles of the C2 vertebral body. Each cervical spine segment is unique making it impossible for the simulation to accurately represent all injuries in a single simulation. In this simulation, the high stress throughout the odontoid specifically concentrated at the base showed a strong association with the location of Type III odontoid fracture; an injury observed in experimental and clinical cases under tensile loading. Although no fracture was observed at the C2 pedicles during the simulation, higher stress levels indicate the potential for a Hangman's fracture which agreed with the reported injuries under tensile loading. Dibb et al. (2009) also commented that Hangman's fracture is an injury commonly associated with tensile loading and speculated that the boundary conditions of their fixation limited their tests ability to accurately reproduce a Hangman's fracture. Combining the quantitative and qualitative results provided a more comprehensive depiction of the expected injuries for the cervical spine segment.

5.4.5 Upper Cervical Spine – Flexion and Extension

The expected injuries in the upper cervical spine under flexion and extension were somewhat different. In flexion, the majority of injuries reported in experimental studies by Nightingale et al. (2002, and 2007) were soft tissue injuries to the posterior ligaments with few reported fractures. In extension, the majority of reported injuries from Nightingale et al. (2002, 2007) were Type III odontoid fractures that initiated at the base of the odontoid into the vertebral body. In addition to the odontoid fractures, dislocation at C1-C2 was also observed, along with some instances of a Hangman's fracture.

The observed failure patterns in the simulated flexion response showed good agreement with the reported experimental injuries including tears of the PAAM and PAOM. Failure in the simulation initiated with the PAAM and then progressed to tearing in both the PAAM and the PAOM with ultimate failure occurring with the complete disruption of the PAAM, severe tearing of the PAOM and an odontoid fracture. The simulated response also produced a comparable stiffness to the experimental test specimen from Nightingale et al. (2007). There was an offset of 22 degrees on the plotted experimental result due to the weight of the apparatus prior to the failure load. The weight was not replicated during testing as it was accounted for in the initial portion of the simulation as the ligaments began to engage. In some experimental cases, a Type III odontoid fracture was observed similar to the fracture observed in the flexion simulation. In qualitative observation, there was an increased level of stress at the base of the odontoid throughout the majority of the simulation up until fracture was observed.

The failure values produced by the simulation were comparable to the failure values reported in Nightingale et al. (2007). The simulation produced a final moment of 39.3 Nm at 67.1 deg which fell into the corridor for failure moment (39.0 ± 6.3 Nm) but just outside for failure rotational displacement (58.7 ± 5.1 deg). The simulation produced three peak forces that could be considered for failure analysis as each peak corresponds to a fairly severe ligament tear or ligament tear with fracture. Of the three failure peaks, the second fell within the corridor on both moment and rotational displacement. The first fell just short on the

moment and the final was slightly over in rotational displacement. It is difficult to fully represent the gradual nature of the soft tissue failure in numerical models so it is not uncommon to have more abrupt failures as seen in this case. In this simulation, even though there are three failure peaks, each is representative of injury observed in the experimental testing and the failure values are close to the experimental averages.

The injuries produced during the extension simulation were not entirely representative of the injuries observed in the experimental tests conducted by Nightingale et al. (2002, 2007) who reported almost exclusively Type III odontoid fractures with a few Hangman's fractures and C2 lamina and spinous process fractures. Qualitatively, the simulation showed elevated stress in areas corresponding to the reported injuries but was unable to produce the associated fractures. This is likely explained due to the high accumulation of stress at the C1 lamina where the simulation actually produced a fracture. Eliminating the initial fracture at the C1 lamina would likely result in fractures more representative of the experimental results. The C1 lamina is an area in the bone between the bulky facet articular surface and the spinous process where the bone transitions from quite thick to relatively thin. Areas that transition from thick to thin over a short distance are challenging to represent in numerical models and are often associated as areas at risk for elevated stress concentration. In this case, where the model is designed to fail at high stresses to represent injury it is not surprising that the model initiated fracture at this location. It is possible that further refinement to the geometry of this area could help alleviate some of the stress concentrations. Additionally, future investigation into mesh refinements could also aid in reducing the stress concentrations but would have to be carefully considered as further reduction in mesh size could dramatically affect the simulation time. The simulation also produced tears in the AAAM which was not reported experimentally. The AAAM tearing is likely a result of the limited resources describing the initial laxity of the upper cervical spine ligaments. The laxities imposed on the simulation were based on literature reviews of the segment response as well as reported range of motion studies. The results of the other simulations and their associated results were also considered when the values were chosen.

This offered a best case overall for all simulations which did not allow for individual cases to be run with different ligament laxities and pretensions. It is also possible that had a fracture occurred at the odontoid as expected the AAAM would not have been extended to the point of failure.

The failure values produced by the simulations were close to the reported values from Nightingale et al. (2007). The simulation failed at a rotational displacement of 39.3 deg that fell within the experimental corridors of 42.4 ± 8.0 deg and the peak moment of 30.4 Nm was just below the experimental corridors of 49.5 ± 17.5 Nm.

5.4.6   Upper Cervical Spine – Axial Rotation

Injuries reported in axial rotation reported by Goel et al. (1990) were primarily soft tissue injuries. In all tests, injuries to the CL-12, and PAAM were identified. There was some isolated stretching and attenuation of the apical and AAAM in a single specimen. Of the twelve specimens tested only five produced fractures. In the five observed fractures, two were classified as Type II odontoid fractures; one was a Type I fracture at the superior end of the odontoid. Another fracture was classified as an avulsion type fracture of the alar ligament at its insertion at the occipital condyles, and the last was a spiral fracture on the odontoid normal to the direction of the left alar ligament.

The injuries produced in the simulation matched well with the reported injuries in Goel et al. (1990). The simulation was able to produce tears of both the CL-12 and the PAAM which were reported in all experimental tests. Additionally, the experimental results reported that the TL, CL-01, AAOM, PAOM, apical and AAAM were not damaged in any of the tests. The simulation showed no damage to any of these ligaments in good agreement with the experimental results. The simulation did not predict any fractures but the qualitative observations did show elevated stress levels near the superior end and the base of the odontoid where it extends from the vertebral body. These areas of elevated stress correspond well to the reported fracture locations.

The simulation resulted in failure moment values that showed good agreement with the experimental results reported by Goel et al. (1990). The peak moment produced was 13.4 Nm falling well within the experimental corridors (13.6 ± 4.5 Nm), while the rotational displacement at failure of 47.8 deg was outside the corridors (68.1 ± 13.1 deg). When compared directly with the experimental test specimen from Goel et al. (1990), the simulation showed a comparable shape and stiffness. The obvious discrepancy between the two curves was the initial ligament engagement which occurs at a rotational displacement approximately 25 degrees prior to the experimental result. If a 25 degree offset was applied to the simulated results it is noted that the simulation and experimental test match almost exactly. The early engagement of the ligaments in the simulation was likely due to limitations in the model to accurately represent the laxity in the ligaments of the upper cervical spine. Based on the anatomy of the joint, the majority of the rotation should occur between the C1 and C2 vertebral bodies. In previous range of motion studies by Goel et al. (1988a), the average relative rotation between C1 and C2 was approximately 23 degrees under very small loads. This indicated that the ligaments joining these two bones should have a certain amount of laxity to allow for this range of motion. Some investigation into increasing the laxity at this level was attempted and a certain amount of delayed ligament engagement was achieved but limitations in the ligament implementations induced some non-physiological responses in the model making it undesirable to proceed with the modified values. If ligament laxities were modified based on their specific load case without guidance from experimental data, it would diminish the integrity of the model and its ability to accurately simulate injury.

5.5   Model Limitations

The lower cervical spine model is unable to accurately represent the progressive failure of the tissue under tensile loading with the current AF fibre constitutive model. The existing model was selected for its ability to represent stresses along the fibre direction, which was essential when modeling the layers of the AF. Further investigation into composite material models is underway to incorporate inter-layer shear stresses as well as the stress along the

fibres. This would allow for a more biofidelic representation of the progressive tissue failure in the disc. This should improve the response of the tension case specifically where there appeared to be not enough compliance in the current disc model leading to higher than expected failure forces at earlier displacements.

Specific to the upper cervical spine model, further investigation into the initial conditions of the ligaments prior to loading is required to accurately represent ligament engagement times. Due to the complex nature of this joint, it is difficult to deduce the values for pretension and laxity the same way it was done for the lower cervical spine segment by Fice (2010), who used the reaction force of the disc to calculate the ligament pretensions. To gain a better understanding of the initial state of the ligaments, experimental testing must be carried out to determine how much initial laxity or pretension each ligament has when the spine segment is held in a lordotic orientation representing in-vivo conditions. This would allow the model to have a more biofidelic representation of the initial properties and position prior to loading. Improvements to the laxity and pretensions in the upper cervical spine ligaments would likely improve the results of the axial rotation case and potentially the flexion and extension case.

Another limitation affecting both segment models is their limited ability to accurately represent post fracture response of the bone under compressive loading as it would be observed in an actual fracture of a human specimen. The current method of element erosion only indicated the initialization of a compressive fracture revealing only the location at which it could occur. In reality, a fracture would propagate through the cancellous bone, gradually reducing the porosity of the bone, in turn slowing the propagation of the fracture. Future studies into damage-based material models will allow for post-fracture response to be predicted which could improve the models ability to predict fracture under compression loading. By modeling the crack propagation, more information can be gathered about the exact type of fracture that can be simulated leading to more concise and focused injury prediction.

Chapter 6

Summary and Recommendations

6.1 Summary

Motor vehicle accidents remain a leading cause of traumatic spinal cord injury. Injury severities in the cervical spine range from minor to fatal, where severe injuries may include spinal cord damage, and are often associated with multiple failures to both hard and soft tissue. Minor injuries would include whiplash, as well as singular soft or hard tissue damage to isolated areas of the cervical spine. Research into injury prevention and occupant protection are an ongoing area of development in the automotive industry with the goal of improving safety and reducing injury.

Current methods of injury prediction for automotive safety use anthropometric test dummies (ATD) and numerical models of ATD's. ATD's and their numerical equivalents rely on global kinematic indicators that have been correlated to occupant injury but are unable to predict injury at the tissue level. The goal of this research was to develop a cervical spine segment model with the capacity to predict injury at the segment level. The segment models developed in this study were used to evaluate severe cervical spine trauma with the intent of future implementation into a full cervical spine model to predict cervical spine injury. From a full body model development perspective, it is important that each area of the body be sufficiently accurate and have the ability to predict injuries that could occur at that location.

The segment models used in this work were developed from a full cervical spine model representative of a 50th percentile male developed at the University of Waterloo using detailed geometric data and available material property data from the literature. The segment model included detailed representations of the intervertebral discs and facet joints,

111

rate-dependent ligaments, and vertebral bodies capable of representing failure at a given stress level. It is important to note that the material properties and failure criteria implemented were all based on existing data from the literature and were not calibrated to the validation cases used in this research. For the segment level models, the musculature of the cervical spine was not included. It is understood that the musculature plays an important role in the stabilization of the cervical spine, but to match the experimental studies which were conducted using ligamentous cervical spine segments, the musculature was omitted.

The segment models had been previously verified and validated under a variety of physiological range of motion cases including tension, compression, flexion, extension, lateral bending, anterior shear and axial rotation. This study expanded upon the range of motion validation to include validation under failure conditions. The lower cervical spine segment was evaluated against experimental studies that loaded specimens to failure under tension, compression, flexion and extension loading, while the upper cervical spine segment was evaluated against experimental studies loading specimens to failure under tension, flexion, extension, and axial rotation. For each case, the segment was loaded based on the boundary conditions described in the experimental studies. In general, one end of the segment was fixed while the load was applied to the opposite end. Load-displacement data was recorded for each simulation and then compared against the respective experimental case to access the response of the model. Also taken into consideration was the tissue failure type and sequence to compare with the reported injuries in each case. Progressive failure of ligaments, modeled using discrete beam elements, provided a representative, computationally efficient, and numerically stable method of predicting response and failure. The advancements using progressive failure in the ligaments to produce a more biofidelic failure response and sequence, as well as predicting injury location, represent an area not previously investigated in great detail. This method of predicting ligament injury was particularly important in the upper cervical spine segment as there is no disc so the ligaments are the primary soft tissue damaged. The ligament response in tension, flexion

and axial rotation provided a good overall representation of the soft tissue injuries expected. In addition to progressive ligament failure, the lower segment model required a method for disc failure. Tensile failure of the disc was represented as disc avulsion modeled by a tied contact failure between the endplate cartilage and AF lamina interface. This failure method provided a good prediction of overall failure force in tension, flexion, and extension. Compressive failure was predicted to initiate in the vertebral body endplates, in agreement with the literature, and the predicted loads were in good agreement with the experimental validation cases. Similarly, in extension failure, fracture initiated at the posterior pedicle of the facets which was a reported fracture site in the literature. Often the experimental studies reported multiple types of injuries. This is not unexpected due to the inherent difference of properties between human specimens. A qualitative observation of areas of elevated stress concentration in the models was used to extrapolate addition injury potential, specifically areas of potential fracture that were not explicitly produced in the simulation.

Simulations of loading conditions causing failure in tension, flexion, extension and compression modes of loading have provided a solid basis for future studies related to cervical spine injury simulation. The ability to predict injury in automotive collision scenarios at the tissue level represents a new development in this area. Validating injurious loading conditions at the segment level will lead to improved simulations for predicting injury in full cervical spine models to evaluate injurious loading scenarios and potential mitigation strategies.

6.2   Recommendations

Developing a cervical spine segment model capable of predicting injury at the tissue level had a number of challenges. One of the primary challenges was the sensitivity to boundary conditions and material properties where small changes had the potential to affect the simulation outcome. Additionally, modifications to the material failure properties within the experimental ranges could change the model outcome from no injury observed to severe fracture. While this variability is a challenge from a modeling perspective, it is not that unlike the variability seen within experimental tests. It was not unusual to see a large range

in the failure loads and displacements of the experimental data used in this research. The variance was likely attributed to differences within the sample populations including age, gender, and physical condition among other aspects. This addresses the importance of having large sample sizes when conducting experimental tests to increase the statistical significance of the reported averages.

The variance among the experimental data also had an effect on how the model response was evaluated. As part of the assessment, the model was compared to the experimental average plus or minus one standard deviation presented in the experimental results. In some instances, where the model fell just outside these experimental corridors, it was difficult to assess whether there was an issue in the model response or was the result of a small sample size within the experiment. This emphasized the importance of evaluating the model response against the reported injuries as well as the experimental averages.

Despite these challenges, this study was able to produce a cervical spine segment model that predicted injuries under tension, compression, flexion, extension, and axial rotation. These results provide an excellent base for future studies in injury prediction using numerical models. Some of the next steps would include further investigation into tissue failure modeling, specifically in the disc and bone. The current failure implementation in the disc shows an abrupt failure that, while representative of disc avulsion, does not have the ability to predict shear failure between the AF fibre layers and the AF ground substance. Implementing failure within the AF fibres and ground substance would introduce a more progressive failure in the disc more representative of soft tissue failure. Specific to bone failure response, the current implementation provided a good representation of fractures under a tensile load but lacked the ability to predict the post-failure response under a compressive load. Element erosion removes material from the model limiting the model to only predict the onset of fracture under compressive loads. Further research into different material models used to model crack propagation could improve the level of detail in compressive fracture prediction. Accurate demonstration of the post-failure response would allow for a more precise representation of specific compressive fractures that are defined

based on their propagation through the bone allowing for a broad spectrum of fractures to be represented during the simulations.

To address these next steps, continued work in experimental testing is necessary. Experimental tests involving the response of the disc under different modes of loading would provide additional insight into specific failure mechanisms and values. Another area that would benefit from additional experimental testing is the upper cervical spine segment. It is a very complex joint and much still needs to be learned regarding the intricate interactions between the various components. More investigation into how the ligaments react under higher loads would improve the constitutive properties used in the ligament models. Specifically, additional information regarding the laxity before the ligaments engage, as well as potential initial pretensions would improve the response of the upper cervical spine segment. While it is understood that the majority of joint stability at that location comes from the associated musculature, it is still important to accurately represent the response of the ligaments when predicting injury.

 Finally, the goal of this research was to predict injury at the segment level with the intention to implement in a full cervical spine model for injury prediction. This work has succeeded in developing segment level models capable predicting injury under several modes of loading. Future development in this area can expand beyond simulated crash scenarios to applications in sports injury, protective equipment and biomedical research.

References

Argenson, C., de Peretti, F., Ghabris, A., Eude, P., Lovet, J., and Hovorka, I., 1997. Classification of Lower Cervical Spine Injuries. *European Journal of Orthopaedic Surgery and Traumatology* 7(4), 215 – 229.

Bass, E.C., Ashford, F.A., Segal, M.R., and Lotz, J.C., 2004. Biaxial Testing of Human Annulus Fibrosus and its Implications for a constitutive Formulation. *Annals of Biomedical Engineering* 32(9), 1231 – 1242.

Blacksin, M. F., 1993. Patterns of Fracture After Air Bag Deployment, *Journal of Trauma* 35(6), 840–843.

Bogduk, N., and Mercer, S., 2000. Biomechanics of the Cervical Spine I: Normal Kinematics. *Clinical Biomechanics* 15, 633 – 648.

Burney, R.E., Maio, R.F., Maynard, F., and Karunas, R. 1993. Incidence, Characteristics, and Outcome of Spinal Cord Injury at Trauma Centers in North America. *Archives of Surgery* 128(5), 596 – 599.

Carter, D.R., and Hayes, W.C., 1977. The Compressive Behaviour of Bone as a Two-Phase Porous Structure. *Journal of Bone and Joint Surgery* 59A, 954 – 962.

Carter, J.W., 2002. Compressive Cervical Spine Injury: The Effect of Injury Mechanisms on Structural Injury Pattern and Neurologic Injury Potential. PhD Thesis, University of Washington.

Carter, J.W., Ku, G.S., Nuckley, D.J., and Ching, R.P., 2002. Tolerance of the Cervical Spine to Eccentric Axial Compression. *Stapp Car Crash Journal* 46, 441 – 459.

Cassidy, J.J., Hiltner, A., and Baer, E., 1989. Hierarchical Structure of the Intervertebral Disc. *ConnectiveTissue Research* 23(1), 75 – 88.

Chazal, J., Tanguy, A., Bourges, M., Gaurel, G., Escande, G., Guillot, M., and Vanneuville, G., 1985. Biomechanical Properties of Spinal Ligaments and a Histological Study of the Supraspinal Ligament in Traction. *Journal of Biomechanics* 18(3), 167 – 176.

Clausen, J.D., Goel, V.K., Traynelis, V.C., and Scifert, J., 1997. Unicinate Process and Luschka Joints Influence the Biomechanics of the Cervical Spine: Quantification Using a Finite Element Model of the C5-C6 Segment. *Journal of Orthopaedic Research* 15, 342 – 347.

Cowin, S.C., 2001. *Bone Mechanics Handbook* 2nd Ed. CRC Press LLC., Boca Raton, Florida.

Cross, N., 2003. The Ligamentum Nuchae. *Massage Today* 3.

Cusick, J.F., and Yoganandan, N., 2002. Biomechanics of the Cervical Spine 4: Major Injuries. *Clinical Biomechanics* 17, 1 – 20.

Daffner, R.H., Sciulli, R.L., Rodriguez, A., and Protech, J., 2006. Imaging for Evaluation of Suspected Cervical Spine Trauma: A 2-Year Analysis. *Injury, International Journal of the Care of the Injured* 37(7), 652-658.

Deng, Y.C., Li, X., and Liu, Y., 1999. Modeling of the Human Cervical Spine Using Finite Element Techniques. *Proceedings from the 43rd Stapp Car Crash Conference.* SAE 1999-01-1310.

Denis, F., 1983. The Three Column Spine and Its Significance in the Classification of Acute Thorocolumbar Spinal Injuries. *Spine* 8(8). 817 – 831.

Denoziere, G., and Ku, D.N., 2006. Biomechanical Comparison Between Fusion of Two Vertebrae and Implantation of an Artificial Intervertebral Disc. *Journal of Biomechanics* 39(4), 766 – 775.

Dibb, A.T., Nightingale, R.W., Luck, J.F., Chancey, V.C., Fronheiser, L.E., and Myers, B.S., 2009. Tension and Combined Tension-Extension Structural Response and Tolerance Properties of the Human Male Ligamentous Cervical Spine. *Journal of Biomechanical Engineering* 131, 1 – 10.

Dvorak, J., and Panjabi, M.M., 1987. Functional Anatomy of the Alar Ligaments. *Spine* 12, 183 – 189.

Eppinger, R., Sun, E., Bandak, F., Haffner, M., Khaewpong, N., Maltese, M., Kuppa, S., Nguyen, T., Takhounts, E., Tannous, R., Zhang, A., and Saul, R., 1999. *Development of Improved Injury Criteria for the Assessment of Advanced Automotive Restraint Systems II.* National Highway Traffic Safety Administration, Docket No. 1999-6407-5.

Farry, A., and Baxter, D., 2010. *The Incidence and Prevalence of Spinal Cord Injury in Canada.* Joint Publication of the Rick Hansen Institute and Urban Futures, Vancouver, BC.

Fice, J.B., 2010. Numerical Modeling of Whiplash Injury. MASc Thesis, University of Waterloo.

Fice, J.B., Cronin, D.S., Panzer, M.B., 2011. Cervical Spine Model to Predict Capsular Ligament Response in Rear Impact. *Annals of Biomedical Engineering.* 39(8), 2152-2162.

Fujita, Y., Duncan, N.A., and Lotz, J.C., 1997. Radial Tensile Properties of the Lumbar Annulus Fibrosus are Site and Degeneration Dependent. *Journal of Orthopaedic Research* 15, 814 – 819.

Fung, Y.C., 1993. *Biomechanics: Mechanical Properties of Living Tissue* 2nd Ed. Springer, New York, NY.

Gilad, I., and Nissan, M., 1986. A Study of Vertebra and Disc Geometric Relations of the Human Cervical and Lumbar Spine. *Spine* 11(2), 154 – 157.

Goel, V.K., Clark, C.R., McGowan, D., and Goyal, S., 1984. An In-Vitro Study of the Kinematics of the Normal, Injured and Stabilized Cervical Spine. *Journal of Biomechanics* 17(5), 363 – 376.

Goel, V.K., Clark, C.R., Gallaes, K., and Liu, Y.K., 1988a. Moment-Rotation Relationships of the Ligamentous Occipito-Atlanto-Axial Complex. *Journal of Biomechanics* 21, 673 – 680.

Goel, V.K., Clark, C.R., Harris, K.G., and Schulte, K.R., 1988b. Kinematics of the Cervical Spine: Effects of Multiple Total Laminectomy and Facet Wiring. *Journal of Orthopaedic Research* 6, 611 – 619.

Goel, V.K., Winterbottom, J.M., Schulte, K.R., Chang, H., Gilbertson, L.G., Pudgil, A.G., and Gwon, J.K., 1990. Ligamentous Laxity Across C0-C1-C2 Complex: Axial Torque-Rotation Characteristics Until Failure. *Spine* 15(10), 990 – 996.

Goel, V.K., Monroe, B.T., Gilbertson, L.G., and Brinkmann, P., 1995. Interlaminar Shear Stresses and Laminae Separation in a Disc. *Spine* 20(6), 689 – 698.

Goel, V.K., and Clausen, J.D., 1998. Prediction of Load Sharing Among Spinal Components of a C5-C6 Motion Segment Using the Finite Element Approach. *Spine* 23(6), 684 – 691.

Gray, H., 1918. *Anatomy of the Human Body*. Lea & Febiger, Philadelphia; Bartleby.com, 2000.

Halldin, P.H., Brolin, K., Kleiven, S., von Holst, H., Jakobsson, L., and Palmertz, C., 2000. Investigation ofConditions that Affect Neck Compression-Flexion Injuries Using Numerical Techniques. *Proceedings from the 44th Stapp Car Crash Conference*. SAE 2000-01-SC10.

Heuer, F., Schmidt, H., Klezl, Z., Claes, L., & Wilke, H., 2007. Stepwise reduction of functional spinal structures increase range of motion and change lordosis angle. *Journal of Biomechanics,* 40(2), 271-80.

Holzapfel, G.A., Schulze-Bauer, C.A.J., Feigl, G., and Regitnig, P., 2005. Single Lamellar Mechanics of the Human Lumbar Annulus Fibrosus. *Biomechanics and Modeling in Mechanobiology* 3, 125 – 140.

Iatridis, J.C., Weidenbaum, M., Setton, L.A., and Mow, V.C., 1996. Is the Nucleus Pulposus a Solid or a Fluid? Mechanical Behaviours of the Nucleus Pulposus of the Human Intervertebral Disc. *Spine* 21, 1174 – 1184.

Iatridis, J.C., Setton, L.A., Foster, R.J., Rawlins, B.A., Weidenbaum, M., and Mow, V.C., 1998. Degeneration Affects the Anisotropic and Nonlinear Behaviours of Human Anulus Fibrosus in Compression. *Journal of Biomechanics* 31, 535 – 544.

Iatridis, J.C., Kumar, S., Foster, R.J., Weidenbaum, M., and Mow, V.C., 1999. Shear Mechanical Properties of Human Lumbar Annulus Fibrosus. *Journal of Orthopaedic Research* 17, 732 – 737.

Iatridis, J.C., and ap Gwynn, I., 2004. Mechanisms for Mechanical Damage in the Intervertebral Disc Annulus Fibrosus. *Journal of Biomechanics* 31, 535 – 544.

Iatridis, J.C., MacLean, J.J., and Ryan, D.A., 2005. Mechanical Damage to the Intervertebral Disc Annulus Fibrosus Subjected to Tensile Loading. *Journal of Biomechanics* 38, 557 – 565.

Kasra, M., Parnianpour, M., Shirazi-Adl, A., Wang, J.L., and Grynpas, M.D., 2004. Effect of Strain Rate on Tensile Properties of Sheep Disc Annulus Fibrosus. *Technology and Health Care* 12, 333 – 342.

Keaveny, T.M., Morgan, E.F., Niebur, G.L., and Yeh, O.C., 2001. Biomechanics of Trabecular Bone. *Annual Review of Biomedical Engineering* 3, 307 – 333.

Kleinberger, M., and Summers, L., 1997. Mechanism of Injuries for Adults and Children Resulting From Airbag Interaction, *41st Annual Meeting of the Association for the Advancement of Automotive Medicine* 405–420.

Klisch, S.M. and Lotz, J.C., 1999. Application of a Fiber-Reinforced Continuum Theory to Multiple Deformations of the Annulus Fibrosus. *Journal of Biomechanics* 32, 1027 – 1036.

Kopperdahl, D.L., and Keaveny, T.M., 1998. Yield Strain Behaviour of Trabecular Bone. *Journal of Biomechanics* 31, 601 – 608.

Kumaresan, S., Yoganandan, N., Pintar, F.A., Voo, L.M., Cusick, J.F., and Larson, S.J., 1997. Finite Element Modeling of Cervical Laminectomy with Graded Facetectomy. *Journal of Spinal Disorders* 10(1), 40 – 46.

Kumaresan, S., Yoganandan, N., Pintar, F.A., and Maiman, D.J., 1999. Finite Element Modeling of the Cervical Spine: Role of Intervertebral Disc Under Axial and Eccentric Loads. *Medical Engineering and Physics* 21, 689 – 700.

Lindahl, O., 1976. Mechanical Properties of Dried Defatted Spongy Bone. *Acta Orthopaedica Scandinavica* 47, 11 – 19.

Marchand, F., and Ahmed, A.M., 1990. Investigation of the Laminate Structure of the Lumbar Disc Anulus Fibrosus. *Spine* 15(5), 402 – 410.

Mattucci, S., 2011. Strain Rate Dependent Properties of Younger Human Cervical Spine Ligaments. MASc Thesis, University of Waterloo.

McElhaney, J.H., 1966. Dynamic Response of Bone and Muscle Tissue. *Journal of Applied Physiology* 21, 1231 – 1236.

Meakin, J.R., Reid, J.E., and Hukins, D.W.L., 2001. Replacing the Nucleus Pulposus of the Intervertebral Disc. *Clinical Biomechanics* 16, 560 – 565.

Meyer, F., Bourdet, N., Deck, C., Willinger, R., and Raul, J.S., 2004. Human Neck Finite Element Model Development and Validation Against Original Experimental Data. *Proceedings from the 48th Stapp Car Crash Conference*, 177 – 206. SAE 2004-22-0008.

Mosekilde, Li., Mosekilde, Le., and Danielsen, C.C., 1987. Biomechanical Competence of Vertebral Trabecular Bone in Relation to Ash Density and Age in Normal Individuals. *Bone* 8, 79 – 85.

Myers, B.S., and Winkelstein, B.A., 1995. Epidiemiology, Classification, Mechanism, and Tolerance of Human Cervical Spine Injuries. *Critical Reviews in Biomedical Engineering* 23(5&6), 307 – 409.

Myklebust, J.B., Pintar, F.A., Yoganandan, N., Cusick, J.F., Maiman, D., Myers, T.J., and Sances, A., 1988. Tensile Strength of Spinal Ligaments, *Spine* 13, 526 – 531.

Natarajan, R.N., Chen, B.H., An, H.S., and Andersson, G.B.J., 2000. Anterior Cervical Fusion: A Finite Element Model Study on Motion Segment Stability Including the Effect of Osteoporosis. *Spine* 25(8), 955 – 961.

Nightingale, R.W., Winkelstein, B.A., Knaub, K.E., Richardson, W.J., Luck, J.F., and Myers, B.S., 2002. Comparative Strengths and Structural Properties of the Upper and Lower Cervical Spine in Flexion and Extension. *Journal of Biomechanics* 35(6), 725 – 732.

Nightingale, R.W., Chancey, V.C., Ottaviano, D., Luck, J.F., Tran, L., Prange, M., and Myers, B.S., 2007. Flexion and Extension Structural Properties and Strengths for Male Cervical Spine Segments. *Journal of Biomechanics* 40(3), 535 – 542.

Ng, H.W., and Teo, E.C., 2001. Nonlinear Finite-Element Analysis of the Lower Cervical Spine (C4-C6) Under Axial Loading. *Journal of Spinal Disorders* 14(3), 201 – 210.

Ng, H.W., Teo, E.C., and Lee, V.S., 2004. Statistical Factorial Analysis on the Material Property Sensitivity of the Mechanical Response of the C4-C6 Under Compression, Anterior and Posterior Shear. *Journal of Biomechanics* 37, 771 – 777.

Pal, G.P., Routal, R.V., and Saggu, S.K., 2001. The Orientation of the Articular Facets of the Zygapophyseal Joints at the Cervical and Thoracic Region. *Journal of Anatomy* 198, 431 – 441.

Panjabi, M.M., Summers, D.J., Pelker, R.R., Videman, T., Friedlaender, G.E., and Southwick, W.O., 1986. Three-Dimensional Load-Displacement Curves Due to Forces on the Cervical Spine. *Journal of Orthopaedic Research* 4, 152 – 161.

Panjabi, M.M., Dvorak, J., Duranceau, J., Yamamoto, I., Gerber, M., Rauschining, W., and Bueff, H.U., 1988. Three-Dimensional Movements of the Upper Cervical Spine. *Spine* 13(7), 726 – 730.

Panjabi, M.M., Dvorak, J., Crisco, J.J., Oda, T., Wang, P., and Grob, D., 1991a. Effects of Alar Ligament Transection on Upper Cervical Spine Rotation. *Journal of Orthopaedic Research* 9, 584 – 593.

Panjabi, M.M., Duranceau, J., Goel, V., Oxland, T., and Takata, K., 1991b. Cervical Human Vertebrae: Quantitative Three-Dimensional Anatomy of the Middle and Lower Regions. *Spine* 16(8), 7 – 12.

Panjabi, M.M., Dvorak, J., Crisco, J.J., Oda, T., Hilibrand, A., and Grob, D., 1991c. Flexion, Extension, and Lateral Bending of the Upper Cervical Spine in Response to Alara Ligament Transections. *Journal of Spinal Disorders* 4(2), 157 – 167.

Panjabi, M.M., Oxland, T., Takata, K., Goel, V., Duranceau, J., and Krag, M., 1993. Articular Facets of the Human Spine: Quantitative Three-Dimensional Anatomy. *Spine* 18(10), 1298 – 1310.

Panjabi, M.M., 1998. Cervical Spine Models for Biomechanical Research. *Spine,* 23(24), 2684 – 2699.

Panjabi, M.M., Crisco, J.J., Lydon, C., and Dvorak, J., 1998. The Mechanical Properties of Human Alar and Transverse Ligaments at Slow and Fast Extension Rates. *Clinical Biomechanics* 13(2), 112 – 120.

Panjabi, M.M., Chen, N.C., Shin, E.K., and Wang, J-L., 2001a. The Cortical Shell Architecture of Human Cervical Vertebral Bodies. *Spine* 26(22), 2478 – 2484.

Panjabi, M.M., Crisco, J.J., Vasavada, A., Oda, T., Cholewicki, J., Nibu, K., and Shin, E., 2001b. Mechnical Properties of the Human Cervical Spine as Shown by Three-Dimensional Load-Displacement Curves. *Spine* 26(24), 2692 – 2700.

Panzer, M.B., 2006. Numerical Modelling of the Human Cervical Spine in Frontal Impact. MASc Thesis, University of Waterloo.

Panzer, M.B., and Cronin, D.S., 2009. C4-C5 Segment Finite Element Model Development, Validation, and Load Sharing Investigation. *Journal of Biomechanics* 42, 480 – 490.

Panzer, M.B., Fice, J.B., Cronin, D.S., 2011. Cervical Spine Response in Frontal Crash. *Medical Engineering & Physics* 33(9), 1147-59.

Pezowicz, C.A., Roberston, P.A., and Broom, N.D., 2005. Intralamellar Relationships within the Collagenous Architecture of the Annulus Fibrosus Imaged in its Fully Hydrated State. *Journal of Anatomy* 207, 299 – 312.

Quapp, K.M., and Weiss, J.A., 1998. Material Characterization of Human Medial Collateral Ligament. *Journal of Biomechanical Engineering* 120, 757 – 763.

Riggins, R.S, and Kraus, J.F., 1977. The Risk of Neurologic Damage with Fractures to the Vertebrae. *Journal of Trauma* 17(2), 126 – 133.

Robbins, D.H., 1983. *Anthropometric Specifications for Mid-Sized Male Dummy, Volume 2*. University of Michigan Transportation Research Institute, UMTRI-83-53-2.

Robertson, A., Branfoot, T., Barlow, I.F., and Giannoudies, P.V., 2002. Spinal Injury Patterns Resulting From Car and Motorcycle Accidents. *Spine* 27(24), 2825 – 2830.

Rockoff, S.D., Sweet, E., and Bleustein, J., 1969. The Relative Contribution of Trabecular and Cortical Bone to the Strength of Human Lumbar Vertebrae. *Calcified Tissue Research* 3, 163.

Sato, Y., Ohshima, T., and Kondo, T., 2002. Air Bag Injuries – A Literature Review in Consideration of Demands in Forensic Autopsies. *Forensic Science International* 128(3), 162–167.

Skaggs, D.L., Weidenbaum, M., Iatridis, J.C., Ratcliffe, A., and Mow, V.C., 1994. Regional Variation in Tensile Properties and Biochemical Composition of the Human Lumbar Annulus Fibrosus. *Spine* 19(12), 1310 – 1319.

Shea, M., Edwards, W.T., White, A.A., and Hayes, W.C., 1991. Variations of Stiffness and Strength along the Human Cervical Spine. *Journal of Biomechanics* 24(2), 95 – 107.

Setton, L.A., Zhu, W., Weidenbaum, M., Ratcliffe, A., and Mow, V.C., 1993b. Compressive Properties of the Cartilaginous End-Plate of the Baboon Lumbar Spine. *Journal of Orthopaedic Research* 11, 228 – 239.

Traynelis, V. C., and Gold, M., 1993. Cervical Spine Injury in an Air-Bag-Equipped Vehicle, *Journal of Spinal Disorders* 6(1) 60–61.

Teo, E.C., and Ng, H.W., 2001. Evaluation of the Role of Ligaments, Facets and Disc Nucleus in Lower Cervical Spine Under Compression and Sagittal Moments Using Finite Element Method. *Medical Engineering and Physics* 23, 155 – 164.

Van Ee, C.A., Nightingale, R.W., Camacho, D.L.A., Chancey, V.C., Knaub, K.E., Sun, E.A., and Myers, B.S., 2000. Tensile Properties of the Human Muscular and Ligamentous Cervical Spine. *Proceedings from the 44th Stapp Car Crash Conference*. SAE 2000-01-SC07.

Viano, D.C., King, A.I., Melvin, J.W., and Weber, K., 1989. Injury Biomechanics Research: An Essential Element in the Prevention of Trauma. *Journal of Biomechanics* 22(5), 403 – 417.

Wagner, D.R., and Lotz, J.C., 2004. Theoretical Model and Experimental Results for the Nonlinear Elastic Behaviour of Human Annulus Fibrosus. *Journal of Orthopaedic Research* 22, 901 – 909.

Walker, L.B., Harris, E.H., and Pontius, U.R., 1973. Mass, Volume, Center of Mass, and Mass Moment of Inertia of Head and Head and Neck of Human Body. *Proceedings from the 17th Stapp Car Crash Conference*. SAE 730985.

White, A.A., and Panjabi, M.M., 1990. *Clinical Biomechanics of the Spine. 2nd Ed*. J.B. Lippincott Co., Philadelphia.

Yeh, O.C., and Keaveny, T.M., 2001. Relative Roles of Microdamage and Microfracture in the Mechanical Behaviour of Trabecular Bone. *Journal of Orthopaedic Research* 19, 1001 – 1007.

Yoganandan, N., Pintar, F., Butler, J., Reinartz, J., Sances, A., and Larson, S.J., 1989a. Dynamic Response of Human Cervical Spine Ligaments. *Spine* 14(10), 1102 – 1110.

Yoganandan, N., Pintar, F., Haffner, M., Jentzen, J., Mainma, D.J., Weinshel, S.S., Larson, S.J., Nichols, H., and Sances, A., 1989b. Epidemiology and Injury Biomechanics of Motor

Vehicle Related Trauma to the Human Spine. *Proceedings from the 33rd Stapp Car Crash Conference*, 223 – 242. SAE 892438.

Yoganandan, N., Kumaresan, S., Voo, L., and Pintar, F.A., 1996. Finite Element Applications in Cervical Spine Modeling. *Spine* 21(15), 1824 – 1834.

Yoganandan, N., Kumaresan, S., and Pintar, FA., 2001. Biomechanics of the Cervical Spine Part 2: Cervical Spine Soft Tissue Responses and Biomechanical Modeling. *Clinical Biomechanics* 16, 1 – 27.